University of Alberta

Study of the hydrogenation of Mg alloy thin film multilayers by Neutron Refraction

by

Christopher Harrower

A thesis submitted to the Faculty of Graduate Studies and Research
in partial fulfillment of the requirements for the degree of

Doctor of Philosophy
in
Microsystems & Nanodevices

Electrical and Computer Engineering

Spring 2014
Edmonton, Alberta

I. Abstract

Magnesium is a promising material for solid state hydrogen storage applications owing to its high theoretical capacity of 8.2 wt% (H/Mg). Unfavourable thermodynamics coupled with poor kinetics leads to unacceptably slow sorption rates at modest temperatures and pressures. Approaches to increasing the sorption rates include using various formulations of catalytic additions on magnesium surface or using alloy additions within magnesium. The aim of these additions is to increase the kinetics while altering the thermodynamics by making the hydride less stable relative to the metal phase. In this thesis magnetron co-sputtering and sequential sputtering are used to introduce the destabilizing or nanocrystalline catalytic phases. In particular, this thesis shows the hydrogen sorption stages of several binary surface catalysts with particular attention to the superior sorption behaviour of a Pd-Ta binary surface catalyst. The results show that the addition of a Ta layer between the Pd and Mg layers lowers the required sorption pressure by a factor of 10 as compared to a simple Pd-catalysed sample. The sorption behaviour is compared to other bi-layer catalysts that also show promise for increased sorption. (e.g. Pd-Ti bilayer catalyst).

Next, the sorption behaviour of the Mg-Al samples is compared to the sorption behaviour of a pure Mg sample. The result show that Mg-Al tends to absorb homogenously throughout the thin film whereas pure Mg sample tends to absorb from the surface downwards (in a core-shell type of absorption).

Finally, absorption kinetics are increased through catalytic additions within the Mg bulk alloy. This increased sorption behaviour and absorption character is observed through

neutron reflectometry measurements of multilayer thin film multilayer structures. The results show that the absorption occurs within the catalysts layers prior to absorption within the Mg layers; however this observation is not widely seen due to typical instrumentation limitations.

II. Table of Contents

I. Abstract II

II. Table of Contents IV

III. List of Figures VII

1 Introduction 1

1.1. The Role of Metal Hydrides 2

1.1.1. Hydride pathway 3

1.1.2. Metal Hydride Thermodynamics 5

1.1.3. Integration with a Fuel Cell 8

1.1.4. Mg Hydride 9

1.1.5. Mg Alloy Systems 10

2. Experimental Techniques 12

2.1. Introduction 12

2.2. Synthesis of Thin Film Materials by Sputter Deposition 13

2.3. X-ray Diffraction, X-Ray Reflectometry Measurements 15

2.4. Volumetric Measurements (Modified Sievert's Apparatus) 16

2.4.1. Buoyancy Correction 21

3. Neutron and X-ray Reflectometry Theory 23

3.1. Introduction 23

3.2. Theory 25

3.3. Abeles Matrix Formulation 27

3.4. Critical Edge Measurement 30

3.5. Hydrogen versus Deuterium 31

3.6. Determination of Hydrogen Concentration 33

3.7. Potential Pitfalls of Neutron Reflectivity 35

4. Results and Discussion 37

4.1. Introduction 37

4.2. Preliminary Sorption on Catalytic Layers 37

4.3. Mg thin film - Volumetric Absorption 40

4.4. Mg – 30 at% Al thin film - Volumetric Absorption 45

4.5. Mg-Al X-ray Diffraction 49

4.5.1. Volumetric Absorption Conclusions 52

5. Neutron Reflectometry Study of Surface Catalysts 55

5.1. Mg – Pd 56

5.2. Pd Catalysed Mg-x at % Al at Elevated Temperatures 64

5.3. Conclusions about a Simple Pd-Catalysed Mg-x Al System 71

6. Binary Catalysts 73

6.1. Mg-30 at % Al with a Pd/Ta Bi-layer Catalyst 74

6.2. Mg-30 at% Al with a Pd/Ti Bi-layer Catalyst 85
6.3. Mg-30 at% Al with a Pd/Ni Bi-layer Catalyst 93
6.4. Mg – 30 at% Al with a Ni/Ta Bi-layer Catalyst 98
6.5. Conclusions about Binary Surface Catalysts 101
7. Magnesium Absorption Process 103
7.1. Pd/Ta Catalysed Mg – 30 at% Al sample 103
7.2. Pd/Ta Catalysed Mg Thin Film 108
7.3. Discussion 112
8. Neutron Reflectometry Multilayer 114
8.1. FeTi-Mg Multilayer 115
8.2. Mg-Al-Ti Multilayer 121
8.3. Multilayer Conclusions 131
9. Conclusions and Future Work 132
9.1. Future Work 132
9.1.1. Optical Mirrors 133
9.1.2. Hydrogen Storage Material 134
10. Bibliography 136

III. List of Figures

Figure 1-1 Storage weight capacity versus hydrogen storage density of select metal hydride materials. Hydrogen concentrations for metal hydrides and compressed hydrogen are calculated from [10] and [11] respectively. 3

Figure 1-2 Schematic of the potential energy curve of hydrogen, from far away from a metal surface to deep within a metal. The energy landscape corresponds to a typical metal that easily takes up hydrogen gas (sorption). Each part of the landscape corresponds to (i) physisorption for both activated and nonactivated surfaces, (ii) dissociation and surface chemisorption, (iii) chemisorption on subsurface sites, and (iv) diffusion within the metal lattice. The dashed line corresponds to molecular hydrogen whereas the solid line corresponds to elemental hydrogen (H). Figure is adapted from[13] 4

Figure 1-3: Pressure composition isotherm (PCI) (a) of an arbitrary metal hydride and a corresponding van't Hoff plot and (b) used to extract the heat of hydride formation 6

Figure 2-1 – Operation of a physical vapour deposition (PVD) system known as sputtering. 13

Figure 2-2 Structure of the samples used in this thesis. (a) One of the bulk samples used in the volumetric sorption measurements with an SEM micrograph, illustrating the release film. (b) A sample used in the neutron reflectometry measurements 14

Figure 2-3: Basic Sievert's type apparatus (volumetric). The instrument used in this thesis uses these basic blocks but is much more complex. Figure adapted from[42] 16

Figure 2-4: Compressibility factor versus pressure at T=500K. (a) Measured [49] and calculated using an SRK equation [48] and a polynomial equation for a pressure of 0 to 200 atm. (b) and an exploded view of a pressure range from 0 to 20 atm. 20

Figure 2-5: Compressibility factor versus pressure at T=300K. (a)Measured [49] and calculated using an SRK equation [48] and a polynomial equation for a pressure of 0 to 200 atm (b) An expanded view of a pressure range from 0 to 20 atm. ... 21

Figure 3-1 X-ray (Cu Kα radiation or λ = 1.54 Å) and neutron scattering length (λ = 1.798 Å) of several elements based upon experimental data [51]. 24

Figure 3-2 Reflection of an arbitrary small layer within a structure of n layers. To the far right is the substrate, as indicated, which is assumed to be large enough such that there are no backward travelling waves in medium k + 1 (i.e., yk+1 = 0) 29

Figure 3-3 Average SLD of film deduced by critical-edge measurement. 31

Figure 4-1: Hydrogen sorption character of Mg - 30 at %Al. (a) Absorption at 125 °C and 30 bar hydrogen. (b) Desorption in a thermal gradient analyzer (TGA) at 100°C with 20 sccm of argon flow through the cell 39

Figure 4-2 Hydrogen absorption measurements of a 1 µm-thick Mg thin film catalysed by a 7.5/7.5 nm Pd/Ta-catalysed layer deposited on the surface. Measurements are performed with a modified Sieverts apparatus at 250°C and 30 bar. The high temperature and pressures are chosen to reproduce conditions required for a hydrogen sorption application (i.e., a hydrogen car fuel tank) 41

Figure 4-3 Hydrogen absorption time to 5 wt% as a function of cycle number for a 1 µm-thick Mg sample catalysed by a Pd/Ta bilayer catalyst deposited on the surface. 42

Figure 4-4 Hydrogen desorption measurements of 1 µm-thick Mg thin film catalysed by a Pd/Ta bilayer catalyst deposited on surface of film. Measurements are performed with a modified Sieverts apparatus at 250°C and 0.1 bar. The high temperature and pressures are chosen to reproduce conditions that would be required for a hydrogen sorption application (i.e., a hydrogen car fuel tank). The hydrogen wt% is relative to the weight of the metal (in this case Mg) and not the hydride to allow a direct comparison with the amount of absorption..... 44

Figure 4-5 Hydrogen desorption time to 5 wt% as a function of cycle number for a 1µm-thick Mg sample catalysed by a Pd/Ta bilayer catalyst deposited on surface..... 45

Figure 4-6 6 Hydrogen absorption measurements of a 1 µm-thick Mg-30 at %Al thin film catalysed by 7.5/7.5 nm Pd/Ta layers deposited on surface. Measurements are performed with a modified Sieverts apparatus at 250°C and 30 bar. 46

Figure 4-7 Hydrogen absorption time to 1 wt% as a function of cycle number of a 1µm-thick Mg-30 at %Al sample catalysed by Pd/Ta bilayer catalyst deposited on surface. 47

Figure 4-8 Hydrogen desoprtion measurements of a 1 µm-thick Mg-30 at %Al thin film catalysed by a 7.5/7.5 nm Pd/Ta catalysed layer deposited on surface. Measurements are performed with a modified Sieverts apparatus at 250°C and 30 bar. Desorption measurements are relative to the weight of the metal (Mg Al) and not the hydride..... 48

Figure 4-9 Hydrogen desorption time to 1 wt% as a function of cycle number for a 1µm-thick Mg-30 at %Al sample catalysed by a Pd/Ta bilayer catalyst deposited on surface 49
Figure 4-10 X-ray diffraction pattern of Mg- 30 at% Al at the first, third and 10th absorption, and the third desorption 51
Figure 5-1 Illustration of the Pd catlayzed Mg thin film deposited on a Ta (10 nm)-coated (100) silicon wafer 57
Figure 5-2 Neutron reflectometry measurements of a Pd (10nm)-capped Mg-30 at %Al (50nm) thin film deposited on a Ta (10nm)-covered (100) Si substrate (see Figure 5-1). (a) As-sputtered state. (b) D_2 = 20 mbar. (c) D_2=1310 mbar t = 0 hr. (d) D_2 = 1310 mbar, t = 10 hr. Absorption experiments are performed in situ to neutron reflectometry measurements and performed at room temperature (20°C). The sample was held at 20mbar for ~30minutes before reflectometry measurements taken. The history of the pressure is indicated in Figure 5-3. 59
Figure 5-3 Neutron reflectometry critical-edge measurements of a Pd (10nm)-catalysed Mg-30 at %Al thin film deposited on a 10nm Ta-coated (100) Si wafer (see Figure 5-1) and performed under a deuterium atmosphere as indicated. Measurements are taken after reaching a quasi-steady state. The samples was held at each pressure for ~1.5 hours before increase the pressure again. i.e. 30 minutes to reach equilibrium and 1 hour to take the full reflectometry measurements. 60
Figure 5-4 Neutron reflectivity critical-edge measurements (low q) of a Pd-catalysed Mg-30 at %Al thin film deposited on a Ta (10 nm)-coated (100) silicon wafer (see

Figure 5-1). Measurements are taken at room temperature at 1309 mbar after a slow increase in the deuterium pressure as presented in Figure 5-2. 61
Figure 5-5 Hydrogen concentration profile of a Pd (10nm)-catalysed Mg-30 at %Al thin film deposited on a Ta (10nm)-coated (100) Si substrate. The thin film structure being investigated is illustrated in Figure 5-1. 62
Figure 5-6 - Structure used to study the sorption behaviour of a Pd-catalysed Mg-40 at %Al thin film. The film consists of a Pd (10nm)-covered Mg-40 at %Al (50nm) native oxide (~1nm) silicon (100) wafer..... 64
Figure 5-7 Neutron reflectometry measurements of a Pd-covered (10nm) Mg-40 at %Al thin film on a (100) Si substrate (see Figure 4 16). (a) Hydrogenated at 125°C and 30 bar and measured ex situ in an inert atmosphere at room temperature. (b) Measured at 200°C in an inert atmosphere. (c) Measured at room temperature in an inert atmosphere after annealing at 200°C for 24 hours. This figure is published in[87] and reproduced without alteration. 66
Figure 5-8 Neutron reflectometry measurements of a Pd-covered (10nm) Mg-40 at %Al thin film on a (100) Si substrate (see Figure 4 16). (a) As prepared film in an inert atmosphere. (b) Measured at room temperature in an inert atmosphere after being annealed at 200°C for 24 hours. Note the silicon substrate native oxide is not removed prior to deposition and can be easily seen in the scattering length density profile. This figure is published in [87] and reproduced without alteration here. 68
Figure 5-9 Structure used to illustrate the sorption behaviour of Pd-catalysed Mg-40 at %Al thin film 69

Figure 5-10 Neutron reflectometry measurements of Pd (10nm)-covered Mg-30 at %Al (50nm) thin film on a (100) oriented Si substrate. (a) After 1 hour annealing at 200°C. (b) After 3 hours at 200°C. (c) After 9 hours annealing at 200°C. Experiments are performed in air at room temperature ex situ to sorption experiments. This figure is published in [87] and reproduced here without alteration. 70

Figure 6-1 Pd/Ta (5nm/5nm)-catalysed Mg-30 at %Al thin film deposited on a Ta (10nm)-coated (100) silicon wafer. Note the native oxide is removed prior to Ta deposition by an in situ back sputtering method motivated by a reduction in complexity. 74

Figure 6-2 2 Neutron reflectometry measurements of Pd/Ta (5 nm/5nm)-catalysed Mg-30 at% Al thin film deposited on a Ta (10nm)-coated (100) Si substrate (see Figure 6-1) (a) As-sputtered state. (b) D_2 = 6.66 mbar. (c) D_2=133 mbar, t = 1 hr. (d) D_2=133 mbar, t = 12 hr. Absorption experiments are performed in situ to neutron reflectometry measurements and performed at room temperature (20°C). The sample was held at 6.66mbar for a total of 5 hours and 133mbar for 14 hours. The time indicated above is the time the sample was at the indicated pressure before the measurement was taken. 75

Figure 6-3 Neutron reflectometry critical-edge measurements of Pd/Ta (5nm/5nm)-catalysed Mg-30 at %Al thin film deposited on a 10nm Ta-coated (100) Si wafer (see Figure 6-1). Measurements are performed at room temperature in situ to deuterium absorption at a deuterium pressure of 133 mbar 77

Figure 6-4 Hydrogen concentration profile of a Pd/Ta (5nm/5nm)-catalysed Mg-30 at %Al thin film deposited on a Ta (10nm)-coated (100) Si substrate (see Figure 6-1). 78

Figure 6-5 Neutron reflectometry measurements of Pd/Ta (5nm/5nm)-catalysed Mg-30 at %Al thin film deposited on a Ta (10nm)-coated (100) silicon wafer (see Figure 5 1a). (b) After hydrogen is absorbed by the thin film for 24 hours at 125°C and 40 bar hydrogen (measurements performed under an inert argon atmosphere at room temperature). (c) Desorption measurements are performed in situ in the sample cell equipped with a heater. The sample is kept at the described temperature for at least 1 hour before neutron reflectometry measurements commence..... 80

Figure 6-6 – A comparison of the equilibrium hydrogen concentration at several temperatures of Pd/Ta (5nm/5nm) and Pd (10nm)-catalysed Mg-30 at %Al thin film structure depicted in Figure 5-9 and Figure 6-1 respectively. 82

Figure 6-7 - X-ray diffraction measurements of Pd/Ta (5nm/5nm)-coated Mg-30 at %Al thin film deposited on a Ta (10nm)-coated (100) silicon wafer (see Figure 6-1). 83

Figure 6-8 Pd/Ti (5nm/5nm)-catalysed Mg (50 nm) thin film deposited on a Ta (10nm)-coated (100) silicon substrate 85

Figure 6-9 Neutron reflectometry measurements of Pd/Ti (5nm/5nm)-catalysed Mg-30 at %Al thin film deposited on a Ta (10nm)-coated (100) Si wafer. (a) As-sputtered state. (b) D_2 = 1.1 mbar for 0.5 hours (c) D_2 = 10.2 mbar for a total 3 hours. D2=2-mbar for a total of 0.75 hours (not shown) (d) D_2 = 50 mbar for a total of ~1 hour. (e) D_2 = 100 mbar for a total 9 hours. (f) D_2 = 1000 mbar for a total of 4 hours.

Absorption experiments are performed at 20°C and in situ to NR measurements. The time stated above is the time at which the scan was initiated..... 87

Figure 6-10 Neutron reflectometry critical-edge measurements of Pd/Ti (5nm/5nm)-catalysed Mg-30 at % Al thin film deposited on a 10nm Ta (100)-coated silicon wafer 90

Figure 6-11 - Neutron reflectometry critical-edge measurements of Pd/Ti (5nm/5nm)-catalysed Mg-30 at %Al thin film deposited on a Ta (10nm)-coated (100) silicon wafer (see Figure 6-8). Measurements are performed in situ either in vacuo (as-prepared), at D_2 = 10 mbar, at D_2 = 50 mbar, and at D_2 = 100 mbar, all at room temperature. The sample was immersed in the deuterium at 10 mbar for 2 h and 29 minutes, then at 50 mbar for 41 minutes, and then at 100 mbar for 7 hours and 28 minutes. 91

Figure 6-12 – Hydrogen concentration distribution of a Pd/Ti (5nm/5nm) catalysed Mg-30 at% Al thin film deposited on a Ta (10nm) coated (100) silicon wafer (see Figure 6-8). 92

Figure 6-13 Illustration of the Pd/Ni catalyzed Mg-30at%Al thin film deposited on a Ta (10nm) coated (100) silicon wafer. 93

Figure 6-14 Neutron reflectometry measurements of Pd/Ni (5nm/5nm)-catalysed Mg-30 at % Al thin film coated on a Ta (10nm)-coated (100) silicon wafer (see Figure 6-13)) . (a) As-deposited state. (b) D_2 = 20 mbar. (c) D_2 = 100 mbar. (d) D_2 = 500 mbar. (e) D_2 = 1000 mbar. The time indicated is the time at the commencement of the scan. The sample remained at 20 mbar, 100 mbar, 500 mbar and 1000 mbar for 1 hour, ~30minutes, 30minutes, 1 hour respectively. 94

Figure 6-15 Neutron reflectometry critical-edge measurements of a Pd/Ni (5nm/5nm)-catalysed Mg-30 at % Al thin film deposited on a Ta (10nm)-coated (100) Si wafer (see Figure 6-13), measured at room temperature in situ to the deuterium atmosphere. 96
Figure 6-16 Hydrogen concentration distribution of Pd/Ni (5nm/5nm)-catalysed Mg-30 at % Al thin film deposited on a Ta (10nm)-coated (100) silicon wafer. The structure being examined is illustrated in Figure 6-13. 97
Figure 6-17 Ni/Ta (5nm/5nm)-catalysed Mg-30 at % Al thin film (50 nm) deposited on a Ta (10nm)-coated (100) silicon wafer 98
Figure 6-18 Neutron reflectometry measurements of Ni/Ta (5nm/5nm)-catalysed Mg-30 at % Al thin film deposited on Ta (10nm)-coated (100) silicon wafer 99
Figure 6-19 Neutron reflectometry measurements of Ni/Ta (5nm/5nm)-catalysed Mg-30 at % Al thin film deposited on a Ta (10nm)-covered (100) silicon substrate (a) in vacuum at room temperature and as-prepared and (b) immersed in an 8-bar deuterium environment at room temperature for 34 minutes. The structure being investigated is illustrated inFigure 6-17. The reflectivity curves presented here are the same as that presented in Figure 6-18 but with the fitted SLD curve to the measured data. 100
Figure 7-1 Pd/Ta-catalysed Mg-30 at % Al thin film deposited on a Ta (10nm)-coated silicon wafer used in the measurement of the absorption process of the Mg-30 at % Al alloy. This sample is similar to that presented in Figure 6-1 but the following experiments were performed on a different sample. 103
Figure 7-2 Neutron reflectometry measurements of Pd/Ta (5nm/5nm)-catalysed Mg - 30 at% Al thin film deposited on a Ta (10nm)-covered (100) Si substrate. (a) As-

sputtered state. (b) D_2 = 20 mbar. (c) D_2 = 50 mbar. (d) D_2 = 100 mbar. (e) D_2 = 1000 mbar. Absorption experiments are performed in situ to neutron reflectometry measurements and performed at room temperature (20°C). Times indicated above are the times at which the measurement was taken. Therefore, the sample was at 20 mbar, 50 mbar, 100 mbar, and 1000 mbar for 4.75 hours, 2 hours, 19.75 hours, 3.5 hours respectively. 104

Figure 7-3 Neutron reflectometry critical-edge measurements of Pd/Ta-catalysed Mg thin film at a deuterium pressure of 100 mbar..... 106

Figure 7-4 Hydrogen concentration distribution of Pd/Ta (5nm/5nm)-catalysed Mg-Al thin film deposited on a Ta (10nm)-coated (100) silicon wafer..... 107

Figure 7-5 Neutron reflectometry measurements of Pd/Ta (5nm/5nm)-catalysed Mg thin film deposited on a Ta (10nm)-covered (100) silicon substrate at room temperature. (a) As-prepared. (b) 20 mbar, (c) 50 mbar. (d) 100 mbar. (e) 1000 mbar. The loss of the catalysts' contrast in (e) is due to the surface roughness resulting from deuterium absorption in the Mg layer and not due to the experimental procedure or other noise sources. The times indicated above are the times at which the measurement was taken. Therefore, the sample was at 20 mbar, 50 mbar, 100 mbar and 1000 mbar for 4 hours, 2 hours, 1.5 hours, and 4 hours respectively. 110

Figure 7-6 Hydrogen concentration profile of Pd/Ta (5nm/5nm)-catalysed Mg thin film deposited on a Ta (10nm)-covered (100) silicon substrate 112

Figure 8-1 Neutron reflectivity critical edge measurements of FeTi catalysed Mg thin film structure, (see Figure 8-Multilayer structure used to measure the influence of FeTi catalyst on hydrogen absorption characteristics of nanoscale Mg thin film.

The bottom Ta layer is to prevent formation of Mg-Si intermetallic mixtures and act as a reflectometry measurement contrast agent). 117
Figure 8-2 Neutron reflectivity measurements of a thin film multilayer consisting of an alternating stack of Mg and FeTi (see Figure 8-Multilayer structure used to measure the influence of FeTi catalyst on hydrogen absorption characteristics of nanoscale Mg thin film. The bottom Ta layer is to prevent formation of Mg-Si intermetallic mixtures and act as a reflectometry measurement contrast agent). The time indicated is the time at which the measurements were taken. Since each measurement required only 1 hour, the sample was at 10 mbar, 100 mbar and 1000 mbar for 11 hours, 15 hours, and 5 hours, respectively before the measurements were taken. 118
Figure 8-3 – Calculated hydrogen concentration profile of the Mg/FeTi multilayer structure at a deuterium pressure of 10, 100, and 1000 mbar. These profiles are compiled from the neutron reflectivity measurements of the multilayer structure illustrated in Figure 8-1. 120
Figure 8-4 Multilayer structure used to measure the influence of an Al-Ti catalyst on the hydrogen absorption characteristic of a nanoscale Mg thin film. The bottom Ta layer is to prevent the formation of Mg-Si intermetallic mixture and also acts as a neutron reflectometry measurement contrast agent..... 123
Figure 8-5 Neutron reflectometry critical-edge measurements of the Al-Ti catalysed Mg thin film structure as illustrated in Figure 8-4..... 124
Figure 8-6 Neutron reflectivity measurements of a thin film multilayer consisting of an alternating stack of Mg and Al-Ti (Figure 8-4 Reflectometry measurements are represented on the left with the real-space representation of the scattering

length on the right. Measurements are taken in situ in a deuterium environment at (a) vacuum, (b) 10 mbar, (c) 100 mbar, and (d) 1,000 mbar. Each scan required ~1 hour to complete. Therefore, the sample was at 10mbar, 100mbar, and 1000 mbar for 13 hours, 4 hours, and 5 hours respectively before the measurements were taken. 125

Figure 8-7 Hydrogen concentration profile at deuterium pressures of 10, 100, and 1,000 mbar of the Al-Ti-catalysed Mg thin film structure illustrated in Figure 8-4 127

Figure 8-8 Neutron reflectivity measurements of a thin film multilayer consisting of an alternating stack of Mg and Al-Ti (see Figure 8-4). Reflectometry measurements are represented on the left with the real-space representation of the scattering length on the right. Measurements are taken in situ in a deuterium environment at (a) vacuum, (b) 0.5 mbar, (c) 1 mbar, (d) 2 mbar, and (e) 5.6 mbar. These measurements are used to complement the measurements taken previously at higher pressures. The time above is the time at which the measurements were taken. Since each measurement takes ~1 hour, the sample was at 0.5 mbar, 1 mbar, 2 mbar, and 5.6 mbar for 1 hour, 1 hour, 1 hour, and 2 hours respectively before the measurements were taken. 129

1 Introduction

Greenhouse gas production - the use of hydrocarbons for energy generation - has reached unprecedented levels and has resulted in dramatic changes to the ecosystem. It is imperative to find an alternative energy system that produces little or no pollution. Hydrogen is considered the best alternative energy carrier, unlike hydrocarbons. Hydrogen is very abundant, easily produced and does not inherently produce pollution. Hydrogen production is straightforward because it can be created from [1] electrolysis, [2] photocatalytic water splitting, [3] biochemical reactions, and [4] from steam reforming of natural gas. Currently, steam reforming of natural gas is the most widely used method of producing hydrogen but has the disadvantage of producing large quantities of CO_2 (a greenhouse gas). This means that producing hydrogen through steam reforming negates the greenhouse gas emission advantage gained from using hydrogen. The other methods have the distinct disadvantage of not being efficient and therefore not feasible for large scale production. Great strides have been made to increase the conversion efficiency, but the current commercial technology has failed to achieve the necessary efficiency Therefore the cost remains too high, for wide spread acceptance. However, several ingenious plans have been proposed to mass-produce hydrogen even in light of inefficiencies and relatively high costs [5],[6]. One example is the large-scale solar hydrogen production facility currently operating in Spain named Hydrosol 2 [7]. Eventually it may be feasible to produce hydrogen without producing significant amounts of greenhouse gases, namely, CO_2.

1.1.The Role of Metal Hydrides

One of the obstacles that prevent the wide-spread use of hydrogen as an energy carrier is the relative difficulty storing it. Hydrogen is a light, volatile substance that is difficult to store at high gravimetric and volumetric densities. Storage in gaseous or liquid form requires an extremely high pressure or extremely low temperatures, which in turn limits overall energy efficiency. One promising medium for storing hydrogen is within metal hydride. Metal hydrides have significantly higher storage densities than hydrogen stored in a liquid or gas state and, in principle, can operate at room temperature and atmospheric pressure. On the surface, the final storage vessel would consist of a hydrogen gas vessel filled with a metal hydride powder. Filling the vessel would be achieved through connecting the storage vessel to a pressurized hydrogen source and filling the storage vessel to just over atmospheric pressure. Currently, filling a 0.7 litre storage vessel with a commercially available metal hydride is capable of storing an equivalent of 370 litres of hydrogen gas (room temperature, 1 bar)[8]. A storage vessel without the metal hydride would require the hydrogen to be compressed to approximately 530 bar to create a comparable volumetric capacity; such a level of compression is currently viable but not practical.

Figure 1-1 shows a comparison of the gravimetric and volumetric densities of several hydrogen storage media. This comparison does not account for the storage vessel or storage system that would need to be used for the proper storage of the material. For instance, storage of hydrogen gas would require a storage container that could contain the corresponding hydrogen without leakage [9]. Moreover, hydrogen storage through a metal hydride requires the transfer of heat to load and unload the hydrogen from the storage medium, as discussed later in this chapter. These required container and energy

transfer systems increase the overall weight of the hydrogen storage vessel, thus decreasing the resulting system gravimetric capacity (hydrogen weight over system weight).

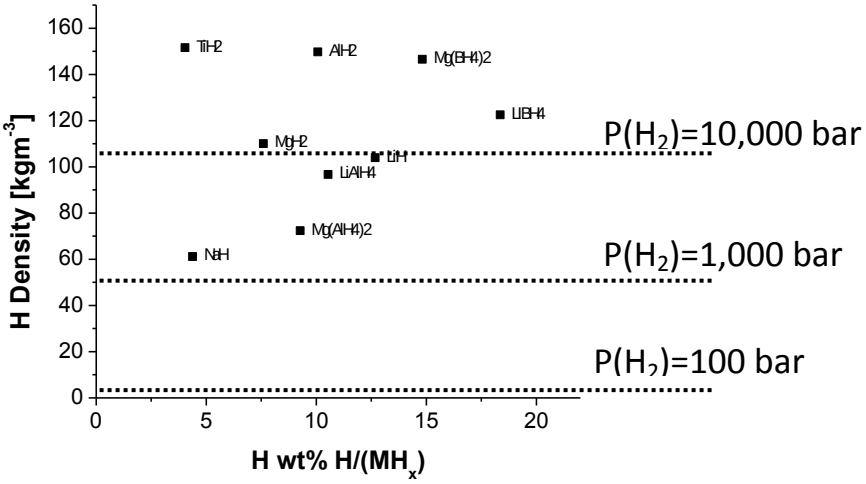

Figure 1-1 Storage weight capacity versus hydrogen storage density of select metal hydride materials. Hydrogen concentrations for metal hydrides and compressed hydrogen are calculated from [10] and [11] respectively.

1.1.1. Hydride pathway

The reaction pathway of hydrogen absorption into a metal consists of several steps, which are schematically represented in Figure 1-2. Molecular hydrogen physically adheres to the surface of the metal without the formation of a chemical bond (adsorption or physisorption). Adsorption is characterized by a reversible process that strongly depends on the temperature and pressure of the hydrogen gas [12].

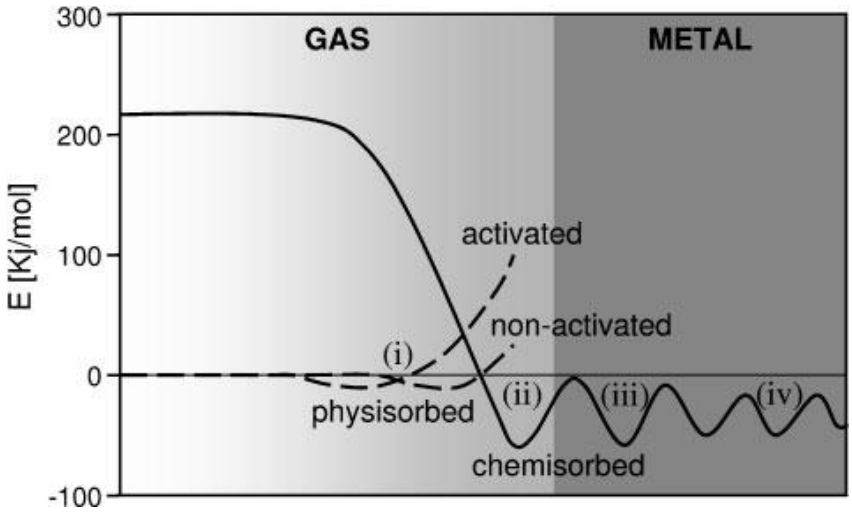

Figure 1-2 Schematic of the potential energy curve of hydrogen, from far away from a metal surface to deep within a metal. The energy landscape corresponds to a typical metal that easily takes up hydrogen gas (sorption). Each part of the landscape corresponds to (i) physisorption for both activated and nonactivated surfaces, (ii) dissociation and surface chemisorption, (iii) chemisorption on subsurface sites, and (iv) diffusion within the metal lattice. The dashed line corresponds to molecular hydrogen whereas the solid line corresponds to elemental hydrogen (H). Figure is adapted from[13]

If the temperature and pressure are sufficient, then hydrogen will dissociate on the metal surface and be chemisorbed into the base metal. Typically chemisorption of hydrogen is reversible but often the chemical reaction favours the formation of the metal hydride. Moreover, significant changes occur in the host metal arrangements, atomic spacing, and electron density, to name a few. Understanding these interactions is central to understanding the sorption process. Unfortunately, measurements of the hydrogen interaction with the metal solute are not easily performed and the hydrogen absorption pathway from the surface to the bulk material (from gas phase to metal) is not well understood.

After surface chemisorption, the hydrogen diffuses through the surface to subsurface sites (see Figure 1-2[iii]). Subsurface sites may vary more than bulk material in terms of hydrogen concentration and association energy At least for palladium, in the subsurface

region, hydrogen concentration increases locally and is characterized by lower association energy than the bulk material [14].

It has been theorized that these subsurface sites are responsible for Pd acting as an exceptional hydrogen catalyst, which has been confirmed by several investigations [15, 16]. One possible explanation is that the observed lattice expansion of the outermost lattice planes of Pd (110) corresponds to an increase in hydrogen concentration [17]. Accurate isothermal measurements [18], coupled with theoretical calculations [19], have also confirmed the existence of sub-surface sites in the Pd lattice. These sub-surface sites, depending on the crystal orientation, extend from one to 10 atomic layers deep into the Pd lattice. They are also characterized by a low enthalpy and do not contribute to increased hydrogen sorption kinetics above 50°C; therefore they do not appear in most sorption measurements [20]. In summary, low-energy sub surface sites have been observed in Pd but, to this author's knowledge, this phenomenon has not been seen in other metal hydride systems.

1.1.2. Metal Hydride Thermodynamics

After diffusion through the subsurface layer, hydrogen enters into the bulk of the material. At low concentrations, the H atoms remain and diffuse through interstitial positions, leading to a solid solution wherein the metal lattice expands proportionally to the hydrogen concentration. At greater concentrations, the lattice expansion induces a sufficient amount of strain in the material to cause the nucleation of a new crystallographic phase. This new phase is characterized by a large volumetric expansion (~30% v/v) and drastic changes in the electronic and physical properties of the material.

The thermodynamics of the hydrogen process can be calculated from a pressure composition isotherm such that at constant temperature, the logarithm of the pressure is plotted against the hydrogen concentration. In each isotherm there are three distinct regions of interest: the solid solution region, the alpha to beta transformation regions, and the saturation region; indicated as 1, 2, and 3, respectively in Figure 1-3.

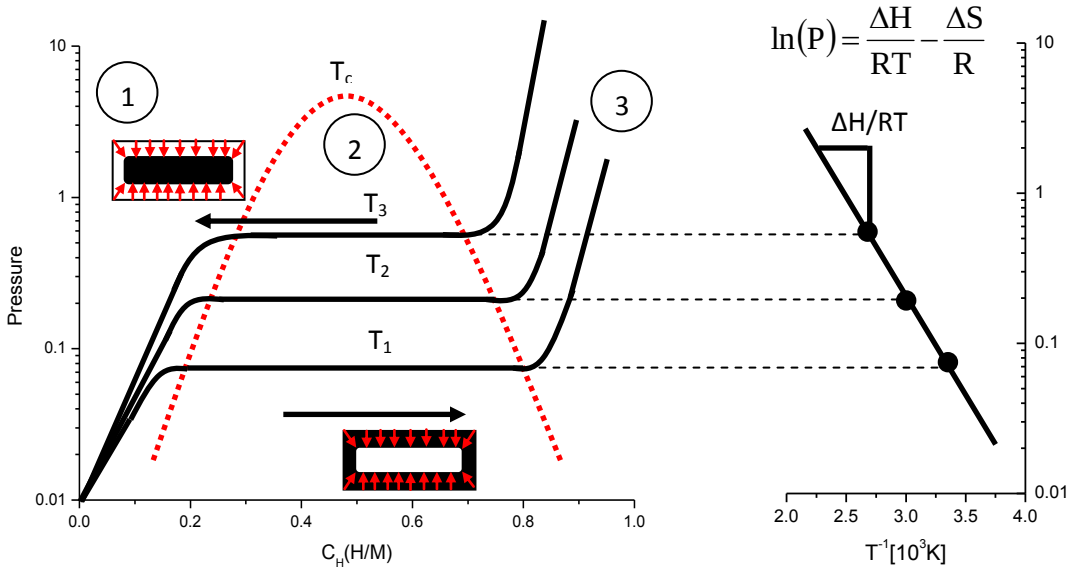

Figure 1-3: Pressure composition isotherm (PCI) (a) of an arbitrary metal hydride and a corresponding van't Hoff plot and (b) used to extract the heat of hydride formation

In the first region - the solid solution region and often the low concentration region_ the hydrogen exists in the interstitial positions of the host metal lattice. In the second region, the plateau region, the solid solution and the alpha phase coexist until all of the solid solution phase is consumed. The plateau pressure and temperature are related through the van't Hoff equation:

$$\ln\left(\frac{P}{P_0}\right) = \frac{\Delta H}{RT} - \frac{\Delta S}{R} \qquad \text{1-1}$$

where R is the gas constant, ΔH is the heat of hydride formation, and ΔS is the entropy difference between the hydrogen in the gas state and condensed in the hydride. The entropy term (ΔS) is dominated by the transition of molecular hydrogen to atomic hydrogen from the gas phase to the metal phase and is therefore similar for all metals. For most metal-hydride systems the entropy is estimated as -130.8 J/mol K. Of course this value can be calculated, along with the heat of hydride formation from a plot of each plateau pressure (ln(P)) versus 1/T graph. A straight line passing through the data points can be used to calculate the thermodynamics quantities (enthalpy and entropy).

From the van't Hoff equation the thermodynamics of the ideal hydrogen storage metal hydride can be calculated. Assuming, as suggested previously, the ideal system operates at 1 bar and 20°C, it is necessary to create a metal hydride with an enthalpy of hydride formation of -38.3 kJ/mol. More realistically, the hydrogen storage medium would operate at 100°C and 5 bar, corresponding to a metal hydride with an enthalpy of -43.8 kJ/mol. A third possible operating temperature to consider is 200°C, corresponding to an enthalpy of hydride formation of -55 kJ/mol.

One important aspect that is ignored in solid-state hydrogen storage is the heat of absorption, which is is necessary to dissipate during the absorption process. This point is best illustrated with an example of a practical storage medium used in a mobile application. First, it is assumed it is possible to absorb hydrogen in a pure Mg sample to the maximum 8.2wt% (H/Mg). Second, if a driving range of 500 km is assumed and the Honda FCX Clarity driving range of 95 km/kg[1] of hydrogen is used, then a hydrogen storage capacity of ~5.26kg is necessary. For an ideal system operating at 200°C with a

[1] http://automobiles.honda.com/fcx-clarity/refueling.aspx

heat of hydride formation of -76kJ/(mol H_2), the hydrogen storage system would have to dissipate ~200 mega joules of heat energy during absorption (fuelling) and provide the ~200 mega joules on desorption (usage). The large energy transfer required for hydrogen sorption necessitates additional components of a hydrogen storage vessel; therefore the overall gravimetric and volumetric storage capacity is reduced. Therefore, a reduction in enthalpy of hydrogen formation might remove a design constraint from the overall system (i.e. by decreasing the amount of energy transfer). In this thesis the main storage material and not the design of the final storage system (e.g. container, the heat dissipation/source, etc.) is considered. The final system constraints are noted as a motivation for lowering the enthalpy for hydride formation and increasing the material kinetics.

1.1.3. Integration with a Fuel Cell

If the stored hydrogen were used for locomotion or electrical grid stabilization (electrical energy storage), one technique would be to couple the hydrogen storage system with a hydrogen fuel cell. Each hydrogen fuel cell has a particular operating temperature and pressure, which ideally should be consistent with the hydrogen storage medium. There are two main fuel cells that seem well suited for the temperature and pressures investigated in this thesis: the proton exchange membrane (PEM) fuel cell and the phosphoric acid fuel cell (PAFC).

There are many types of fuel cells with varying operating conditions being developed. The most prominent commercial fuel cell is the PEM fuel cell due to its low cost (it is easily constructed) and relatively long lifetime. Advances in PEM fuel cells have achieved

operating temperatures of up to 100°C [21], which is quite low for several metal hydrides that typically operate at 200°C.

Another more advanced hydrogen fuel cell is the PAFC. The PAFC operates between 150° and 200°C but it has the main disadvantage of typically being relatively heavier (in terms of the amount of power produced per unit of system weight g/w) than PEM fuel cells. This increased operating temperature could result in fuel cells with increased conversion efficiency and therefore allow for improved overall system operational energy density (volumetric and gravimetric).

1.1.4. Mg Hydride

Mg hydride is a promising material for hydrogen storage due to its high hydrogen storage capacity (8.2wt% H/M) and low cost. The main disadvantages are the high temperature required for hydrogen discharge, slow kinetics, and high reactivity to oxygen [22]. The high operating temperature is too high for several applications; and therefore several studies have been performed with the aim of reducing this temperature.

Approached to increasing hydrogen absorption kinetics include mechanically milling the samples smaller (ball milling) [23], synthesizing thin films [24], and producing powders through a plasma spray process [25]. The aim of all these techniques is to produce microparticles [23] that are also nanocrystalline [26]. These small particles reduce the diffusion distance and thus decreases the amount of time required for full hydrogenation. Also nanocrystalline Mg has been shown to take up hydrogen more easily, but the mechanism remains debated [26, 22].

1.1.5. Mg Alloy Systems

Recent research has focused on decreasing the enthalpy of hydrogenation of metal hydrides through elemental additions to the Mg. The prominent alloys (Mg-Al, Mg-Cu, Mg-Ni, and to a lesser extent Mg-Ti alloys) have gained a substantial amount of attention due to their promising behaviour. For instance Mg-Cu is shown to have reduced enthalpy (-17 kJ/mol) [27] of hydride formation but at the expense of reduced kinetics. Even though decreased enthalpy results in sorption at desirable temperatures, the reduced kinetics dictates an increase in the practical sorption temperature.

Mg-Ni is also a promising hydrogen storage alloy [28, 29, 30, 31]. Due to its acceptable hydrogen sorption characteristics, this material – also known as MA200 - has been used as a commercial hydrogen storage material. At ~300C the material can absorb and desorb hydrogen at appreciable rates - at 5 atm and 2.5 atm respectively – suggesting an enthalpy of -19 kJ/mol. The main drawback of this material is a low overall gravimetric hydrogen capacity of 3.76 wt % (H/M) which has been deemed too low for several commercial applications. The agreed upon [32] target for commercial metal hydrides is at minimum ~6 wt% [H/system] (the system weight of the storage container plus material) or an approximate 12.0wt% (H/M) gravimetric capacity.

Another hydrogen storage material is the Mg-Ti alloy. This alloy is shown to have increased storage capacity with good sorption characteristics but at the expense of cycling behaviour, (i.e. the material degrades quickly on cycling) [33]. Theoretically, the Ti remains in a solid solution with the Mg and helps to dissociate and transport the hydrogen through the magnesium matrix [33]. Theoretically, the alloy should be more stable than pure Mg as Ti tends to form a stable hydride, even more so than pure Mg

[34]. The leading theory is that the Ti in the Mg matrix introduces stress and strain within the Mg, thereby destabilizing the Mg hydride, as opposed to other alloys that thermodynamically destabilize the material.

A fourth hydrogen storage material considered here is the Mg-Al alloy [35, 36, 37, 38, 39]. Similar to the Mg-Ti counterpart, the Al in the Mg matrix increases the hydrogen kinetic rates by introducing stress and strain within the Mg matrix. The main difference with Mg-Al alloys is that the Al tends to precipitate out as nano-sized precipitates (the size of the precipitates depends on the starting Al concentration). These Al precipitates only participate by increasing the hydrogen kinetics, doing little to decrease the enthalpy of hydride formation. In fact, the measured hydrogenation enthalpy of Mg-Al is -78 kJ/mol, a value corresponding to formation of Mg-H_2 rather than the Mg-Al-H_x alloy.

2. Experimental Techniques

2.1.Introduction

The first technique examined is X-ray diffraction. In these experiments the crystal structure is deduced from a scattered x-ray beam. This technique has the main advantage of being easily performed and the information gathered can be used to assess hydrogen absorption kinetics, hydrogen absorption thermodynamics and crystal phases. The typical instruments used for this technique are limited to a crystal structure spatial resolution from several hundred micrometers to millimeters. State of the art x-ray diffraction instruments have only achieved a spatial resolution of 200 nm. [40, 41] Even so, the x-ray diffraction technique provides a vast wealth of information.

The second experimental technique is volumetric hydrogen absorption. This technique indirectly measures the hydrogen uptake and release in a well-controlled environment. It also can be performed with relative ease and can be used to deduce the thermodynamics of a system.

The third-and the main experimental technique used in this thesis, is neutron reflectivity. A neutron reflectivity measurement provides a wealth of information on the structure of stratified layers. This technique is used to measure the hydrogen distribution within the stratified layers and can also be used in conjunction with in-situ hydrogenation experiments. With further work, an instrument could be used to measure the hydrogen total amount of hydrogen uptake during measurements of the hydrogen concentration profile. Due to time limitations, only the hydrogen profile was measured and not the total amount of hydrogen uptake into the sample.

2.2.Synthesis of Thin Film Materials by Sputter Deposition

Samples used for the investigation in this thesis are synthesized through a physical vapour deposition process known as sputtering. In this process, samples are loaded into an ultra-high vacuum chamber that is subsequently backfilled with argon gas to a pressure of $2x10^{-6}$ bar where the sputtering process takes place. The starting materials have a purity of no less than 99.999% to eliminate spurious results due to impurities in the starting materials. All samples are synthesized using a custom designed AJA Orion 5 sputtering system from AJA International.

In order to study the volumetric absorption of the magnesium alloys, thin films are deposited on a photoresist-covered silicon wafer. The photoresist is thoroughly baked at relatively high temperatures to ensure that no water content remained and therefore no out gassing occurs during sputtering. Each layer of the sample is sputtered sequentially, without interruption with a 5 nm Pd, 5 nm Ta, and 1µm of either Mg or Mg Al, and with subsequent deposition of 5 nm Pd and 5 nm Ta, as illustrated in Figure 2-1. Upon completion of sputter deposition, the samples are immersed in acetone in order to

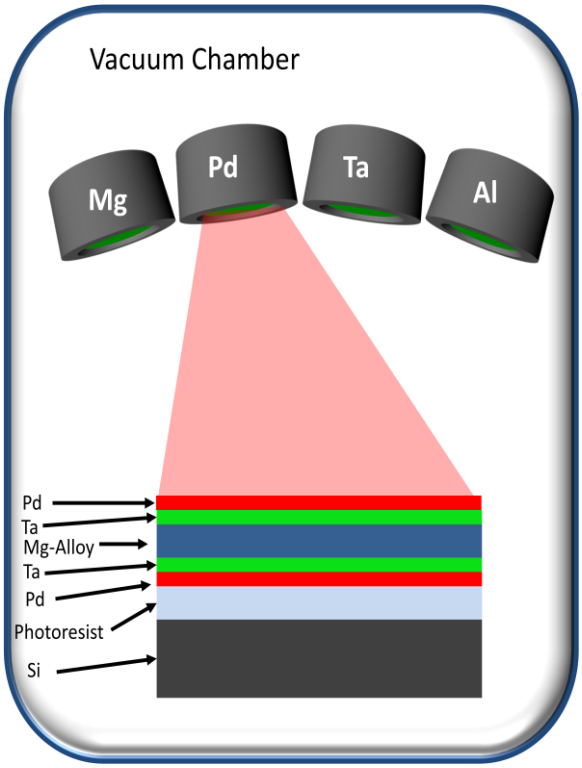

Figure 2-1 – Operation of a physical vapour deposition (PVD) system known as sputtering.

dissolve the photoresist layer and thus effectively release the samples from the silicon layer (see Figure 2-2a for an SEM micrograph of the resulting material). After the film is fully released in the acetone solution, the films are washed several times in fresh acetone and subsequently in isopropyl alcohol to remove the acetone residue. Upon completion of the cleaning procedure, the samples are placed in a rough vacuum overnight to allow the water or isopropyl alcohol to evaporate from the samples.

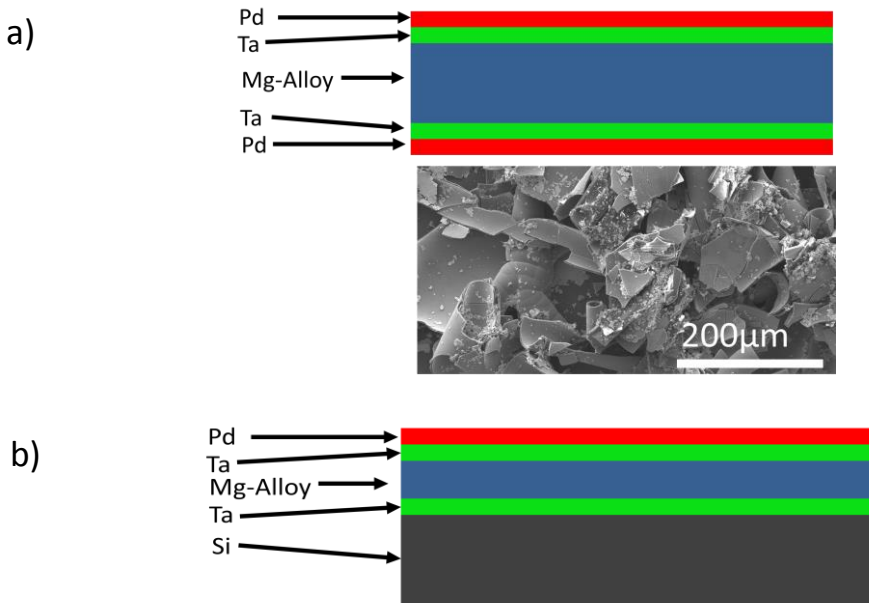

Figure 2-2 Structure of the samples used in this thesis. (a) One of the bulk samples used in the volumetric sorption measurements with an SEM micrograph, illustrating the release film. (b) A sample used in the neutron reflectometry measurements

Samples used for neutron reflectivity measurements are deposited onto an in-situ clean, or a native oxide, (100) silicon wafer. Cleaning of the silicon wafer was achieved within the sputtering chamber by RF (13.5 MHz) sputtering of the silicon wafer prior to thin film deposition. This sputtering process eliminates the native oxide layer normally present on the wafers, reducing the amount of composite layers and thus complexity. All of the thin-film structures were deposited sequentially, without interruption, with

the thickness and deposited material dependent on the desired sample. A sample structure used in neutron reflectivity measurements is illustrated in Figure 2-2b.

2.3.X-ray Diffraction, X-Ray Reflectometry Measurements

Two experimental techniques that are complementary to each other and provide information on the crystal structure of stratified layers are x-ray diffraction (XRD) and x-ray reflectometry (XRR). In XRD the X-ray and the electrons interact in a manner that causes the reflected beam to diffract. The angle and intensity of the diffracted beam are correlated to the periodicity of the electron density within the sample and therefore only suggest a crystal structure.

The other, alternative, x-ray technique which measures the stratified distribution of the sample is x-ray reflectometry (XRR). In XRR, the stratified electron density within the sample is deduced from the intensity and angle of the diffracted x-ray beam. Further explanation of the deduction of the stratified electron density within the material is presented in section 3.2.

In this thesis the XRD experiments are performed on a Bruker AXS diffractometer (Bruker Discover 8) using a copper $K\alpha_1$radiation source (λ=1.5406 Å) that is monochromized using a single Göbel mirror. The system uses parallel beam geometry with a general area two dimensional detection system (GADDs). Further XRD and XRR are performed on a commercial Rigaku Ultima III X-ray diffractometer, which is also monochromized with a single Göbel mirror and used the $K\alpha_1$ wavelength of 1.5406 Å.

2.4.Volumetric Measurements (Modified Sievert's Apparatus)

An important step in understanding the hydrogen interaction with a metal matrix is accurately determining the sorption behaviour. The hydrogen sorption data obtained through a modified Sievert's apparatus are much more accurate as compared to thermogravimetric measurements, especially for low-density samples. Gravimetric analysis relies on the accuracy of the particular scale used, and great strides have been made in achieving a very sensitive mass scale for this purpose. In so doing, the instrument becomes quite complex and therefore is prone to calibration error, error due to oxidation and warping of components. Volumetric analysis requires only a simple inert container with a highly accurate pressure measurement device. Pressure sensors are typically calibrated easily and maintain their calibration for an extended period of time. In addition, the pressure sensor is not required for the sample cell, alleviating the typical drift in measurements from temperature cycling.

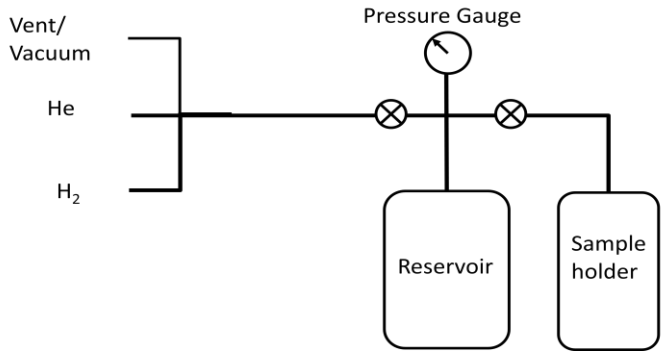

Figure 2-3: Basic Sievert's type apparatus (volumetric). The instrument used in this thesis uses these basic blocks but is much more complex. Figure adapted from[42]

A basic diagram of a simple Sievert's apparatus is depicted in Figure 2-3, an apparatus thoroughly examined and qualified by Lee.[42] The Sievert's apparatus employs a system with many valves and tubes to facilitate an array of gas phase experiments but the basic operation remains the same. At first the whole system is purged of residual air

by pumping to a vacuum (~10^{-3} bar), pressurizing with an inert gas (~2 bar), and once again pumped to a vacuum. This purging process is cycled three times to reduce the amount of residual air in the system. Once the purge cycle is complete, a determination of the sample holder volume is carried out by pressurizing the reservoir, expanding the gas into the sample holder held under a vacuum, and monitoring the drop in reservoir pressure. With prior determination of the reservoir volume, one can calculate the effective sample holder volume also known as free volume, within an adequate degree of certainty. Several gas expansion measurements can be performed to eliminate issues due to temperature or pressure gauge drift. One key issue with the volumetric technique is the free volume measurement as the inert gas may interact with the sample. For instance, He, the typical volume measurement gas, adsorbs onto zeolites, activated carbon, and carbon nanotubes at cryogenic temperatures [43]. Furthermore, He is a slightly smaller atom than the H_2 molecule and may diffuse into smaller pores than H_2 can [44]. Therefore, this would lead to a slightly larger measurement of the free volume [45, 46]. This apparently larger volume would result in greater hydrogen content in both the absorption and desorption measurements. The samples used in this thesis are assumed to not adsorb helium. A study by Emery [47] illustrated that helium effectively boils off of magnesium at temperature greater than 20°C. This study suggested that helium-magnesium interaction only occurred at temperatures where liquid helium is present. Therefore, since the temperatures used here are well away from the liquid helium temperatures, helium is assumed not to interact with magnesium and is assumed to remain an inert gas. Inaccuracies in the pressure, temperature, and initial mass measurements dominate the total error in determining the total amount of hydrogen absorption and desorption.

The experimental procedure for measuring hydrogen absorption using the volumetric measurement technique is relatively simple and straightforward once the free volume of the sample holder is known. Using the simple volumetric measurement apparatus illustrated in Figure 2-3, the absorption procedure is as follows: First the sample holder is evacuated of all residual gas. Secondly, the reservoir is pressurized to a pressure given by $P_I = \frac{V_r+V_s}{V_r} P_f$, where V_r and V_s are the reservoir and sample volume, respectively, and P_f is the final desired sample test pressure. Once the reservoir is pressurized to the desired pressure, the valve isolating the sample holder is opened, the pressure is continually monitored, and the change in pressure is logged as a function of time.

Similarly, the experimental procedure during desorption measurements is quite similar to the absorption measurements except for the differences in pressure of the sample holder and reservoir. Before the desorption experiments, the sample holder is pressurized and the reservoir pressure is reduced to $P_I = \frac{V_s}{V_s+V_r} P_f$, where P_f is the desired final pressure and P_I is the initial pressure of the reservoir. Again, upon completion of the reservoir pressure adjustments, the valve isolating the sample holder is opened, and the pressure is monitored and logged as a function of time.

Using the above pressure measurements, the total amount of hydrogen being absorbed or desorbed is calculated as follows:

$$\Delta n_H^k = \left(\frac{P_r^{k-1}}{Z(P_r,T_r)RT_r} - \frac{P_r^k}{Z(P_r,T_r)RT_r}\right)V_r + \left(\frac{P_s^{k-1}}{Z(P_s,T_s)RT_s} - \frac{P_s^k}{Z(P_s,T_s)RT_s}\right)V_s \quad \textbf{2-1}$$

where P_r, P_s are the pressure of the reservoir, sample container respectively. Also, T_r and T_s are the temperature of the reservoir and sample respectively, Z the compressibility factor as a function of pressure and temperature, and R is Boltzmann's constant. The total amount of hydrogen is calculated at discrete steps (k) and therefore the total amount of hydrogen is the sum over all k, namely, $n_H = \sum_k \Delta n_H^k$.

The calculation of the hydrogen sorption includes the compressibility factor Z of hydrogen, which for an ideal gas is 1 but differs for a real gas. (i.e. Z is recalculated for each data sample taken and is dependent on pressure and temperature). The sample is typically heated to a higher temperature than the reservoir; therefore a different compressibility factor is used. The commercial software included with the HyEnergy PCTPro2000, which is used in this investigation, utilizes a third order polynomial in the calculation of the compressibility factor, Z, namely,

$$Z = \mathrm{K}_0 + \mathrm{K}_1\mathrm{P} + \mathrm{K}_2\mathrm{P}^2 + \mathrm{K}_3\mathrm{P}^3 \text{ where}$$

$$K_0 = 0.9946, K_1 = 0.00060692, K_2 = 8.6617x10^{-8}, \quad \textbf{2-2}$$

$$K_3 = -5.7372\mathrm{x}10^{-11}$$

Another form of the compressibility factor suggested by Zhou[48] called the Soave-Redlich-Kwong SRK equation, takes the following form:

$$Z^3 - Z^2 + Z(A - B - B^2) - AB = 0$$

where

$$A = 0.4278\alpha \frac{P/P_c}{(T/T_c)^2} \qquad \text{2-3}$$

$$B = 0.0867 \frac{P/P_c}{T/T_c}$$

$$\alpha = 1 + m\,(1 - T_r^{0.5}) = 0.5429 \text{ (for hydrogen)}$$

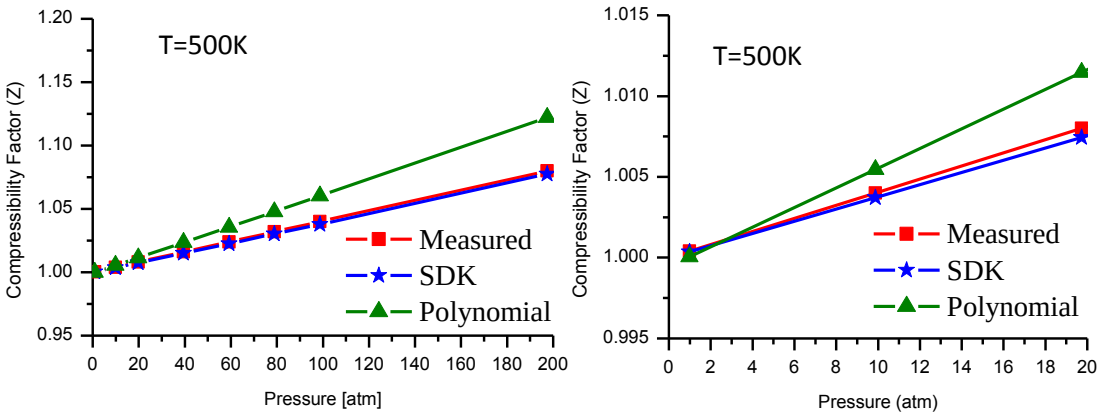

Figure 2-4: Compressibility factor versus pressure at T=500K. (a) Measured [49] and calculated using an SRK equation [48] and a polynomial equation for a pressure of 0 to 200 atm. (b) and an exploded view of a pressure range from 0 to 20 atm.

A comparison between the compressibility factor of the polynomial equation and the well-known SRK equation can be made against the measured compressibility factor, as illustrated in Figure 2-4 and Figure 2-5. As illustrated in Figure 2-4, the difference between the polynomial and actual data is significant, leading to an error of 5% at 200 atm and 500K. This is in contrast to room temperature measurements where the difference in the above methods is minimal and no adjustment need be made (see

Figure 2-5). The computational penalty of using the SRK equation is minimal for the expected operational range, and given its higher accuracy, it will be used for the calculation of volumetric absorption measurements.

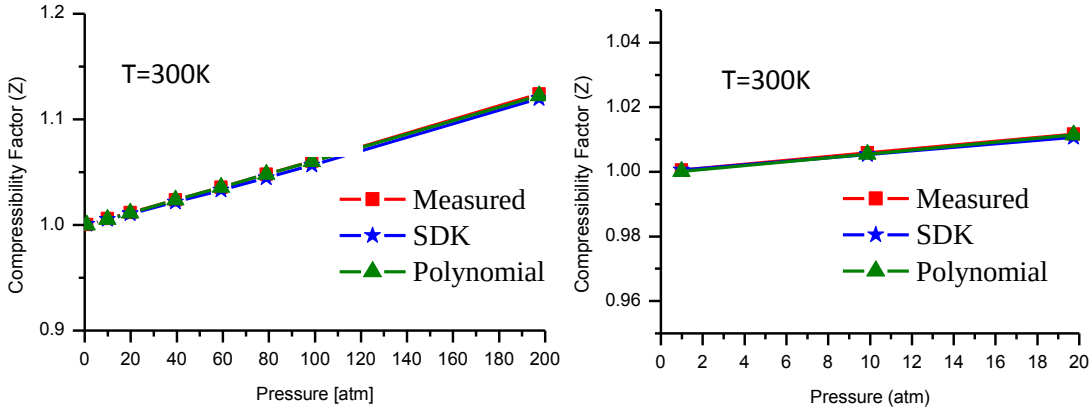

Figure 2-5: Compressibility factor versus pressure at T=300K. (a)Measured [49] and calculated using an SRK equation [48] and a polynomial equation for a pressure of 0 to 200 atm (b) An expanded view of a pressure range from 0 to 20 atm.

2.4.1. Buoyancy Correction

It has been well established that buoyancy plays a significant role in the hydrogen absorption measurements obtained through thermogravimetric means. However it is not widely known that if the same buoyancy problems (e.g. changes in material density) contribute to uncertainty in the volumetric absorption of hydrogen in low-density metals. Blach and Gray [50] outlined the system restrictions and measurement uncertainty for hydrogenation measurements of light weight low-density alloys, noting that significant sample volume changes during sorption measurements can introduce significant errors if a system was not well designed. One error can be introduced by expansion or contraction of the sample, thereby decreasing or increasing the free volume (volume occupied by the gas V_s). Equation 2-1, which calculates the total hydrogen being absorbed, assumes the sample cell volume (V_s) remains constant

throughout the volumetric measurement. There is no easy way to determine the amount the sample has expanded or contracted during the volumetric experiment and therefore a degree of uncertainty in the measurements.

Blach and Gray [50] outlined the importance of keeping the measured P,T, and volume errors well below 0.1% for accurate hydrogenation measurements. In this study, the thin film volume is 0.02ml while the sample cell and reservoir are approximately 8 ml and 10ml respectively. Therefore, if it is assumed that the sample has expanded by 30%[2], the error introduced is 0.03%- well below the acceptable 0.1% error.

[2] Magnesium expands by an approximate 30% when hydrogenated[137]. As illustrated later on, this is the largest amount the film will expand when hydrogenated.

3. Neutron and X-ray Reflectometry Theory

3.1.Introduction

NR and XRR are ideal candidates for measuring the variation in the scattering length density (SLD) as a function of depth from the surface of a thin film sample. This SLD profile then can be used to deduce the structure of the thin film to a high degree. In this instance it is most important to determine of the hydrogen concentration within the film and XRR and NR are complementary methods in this case.

Neutron reflectometry (NR) is the ideal probe to investigate the hydrogen absorption/desorption character of thin film materials owing to its high sensitivity to hydrogen. Other, complementary, experimental techniques used in hydrogen storage interrogations often provide limited data. For example, the hydrogen sorption kinetics obtained by volumetric means provide the total amount absorbed but do not give the hydrogen distribution or individual layer absorption kinetics – although the kinetics can be deduced through several experiments.

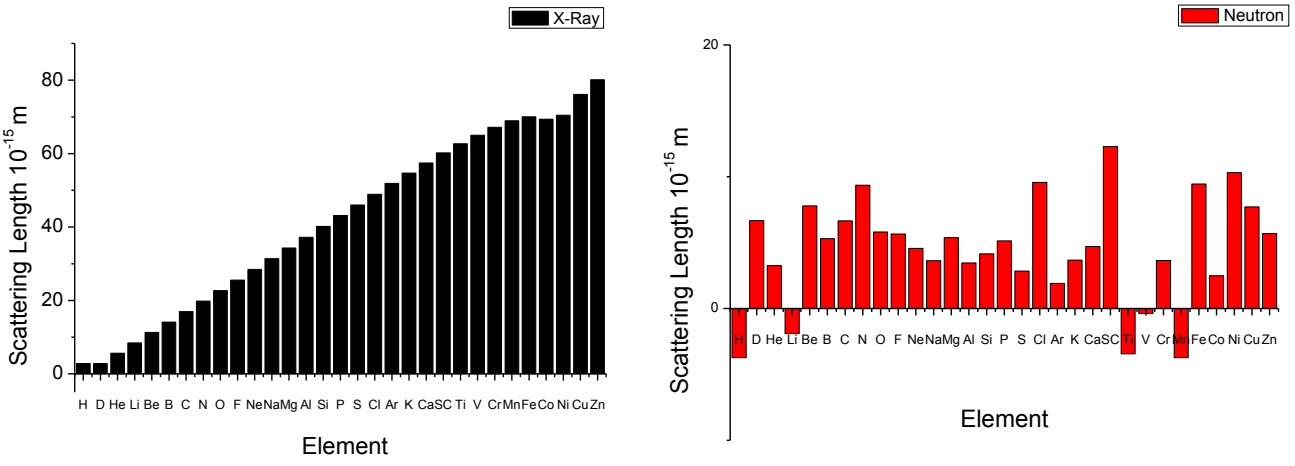

Figure 3-1 X-ray (Cu Kα radiation or λ = 1.54 Å) and neutron scattering length (λ = 1.798 Å) of several elements based upon experimental data [51].

NR is a well established technique that compares to x-ray reflectivity measurements. On the surface one would question the wisdom of using neutron over x-ray for reflectivity measurements. For instance x-ray sources are easily acquired and have higher beam intensity with smaller deviation in wavelength.

Neutron diffraction measurements have the advantage of being relatively more sensitive to lighter elements than XRD experiments (see Figure 3-1). Most notably, neutrons have a relatively strong interaction with hydrogen atoms; therefore they can help to accurately discern the location of the hydrogen atoms [52]. Furthermore, the neutrons interaction with hydrogen and deuterium (an isotope of hydrogen) is substantially different and this difference can be used to elucidate more information about the sample. For instance, the scattered neutron wavefunction from a hydrogen atom is out of phase with respect to the incident neutron wavefunction and is denoted by a negative scattering length. Sensitivity to different isotopes allows one to execute two experiments with a different ratio of isotopes, which can be used to support the

hydrogen concentration measurements. The methodology of this procedure is explained in further later. It is important to understand that contrast enhancement can be achieved using different isotopes of hydrogen.

3.2.Theory

Scattering of a neutron by a free nucleus can be through in terms of cross sections or effective nuclear areas. A free nucleus can be considered to have a cross section to a passing neutron. If the neutron hits this area, the neutron scatters isotropically. The scattering is isotropic because the effective cross section is much smaller than the neutron wavelength and the nucleus appears as a point scatterer.

If we assume that a free nucleus is a point scatterer for neutrons, the interaction may be described by the Fermi pseudopotential [53]:

$$\mathrm{V_F}(r) = b(\frac{2\pi\hbar^2}{\mathrm{m}})\delta(r) \qquad \textbf{3-1}$$

Where $\partial(r)$ is the Dirac delta function centered at r=0 (center of mass of the nucleus) m is the mass, $\hbar$ is plancks constant divided by 2 π.The term (b), a unit of length, is a measure of the strength of interaction between the neutrons and nucleus. The effective nucleus area (σ) is related to the scattering length (b) by $\sigma = 4\pi b^2$. In general b is considered a complex number ($\mathrm{b} = \dot{\mathrm{b}} + i\ddot{\mathrm{b}}$) in order to take into account neutron absorption within the atom instead of scattering. Scattering lengths are provided for most atoms in the periodic table and this thesis refers to the work by Sears [51] for such data.

For a system of many nuclei and for reflectometry measurements, the interaction of the neutrons with the film can be reduced to a one-dimensional problem. The reflectivity can be described by a one-dimensional Fermi pseudopotential as follows:

$$\mathrm{V} = \frac{1}{\mathrm{v}}\int_{\mathrm{v}} \mathrm{V_F}(r)\partial^3\mathrm{r} = \frac{2\pi\hbar^2}{\mathrm{m}}\mathrm{b}\rho \qquad \textbf{3-2}$$

where b and ρ are the scattering length and atomic density, respectively. Therefore, the term $\mathrm{b}\rho$ is the scattering length density (SLD) of the material.

The SLD of several materials has been published previously in [51]. The SLD of a mixture (alloy) with elements A and B is given by the following:

$$SLD = \ pb = \frac{\sum_{i=1}^{n} b_i}{v_m} \qquad \textbf{3-3}$$

where b is the coherent scattering length of all elements i located within a volume v_m In our case we add all the elements within the unit cell and use the unit cell volume (v_m).

Since the interaction of neutrons and the nucleus is described by V(r), the steady state wave function $(\psi)$of the neutron-nucleus interaction is described by the Schrodinger as follows:

$$\frac{\partial^2\psi}{\partial\mathrm{r}^2} + \mathrm{k}^2\psi = 0 \ \text{ where } \ \mathrm{k}^2 = \frac{2\mathrm{m}}{\hbar^2}[\mathrm{E} - V] \qquad \textbf{3-4}$$

where $\hbar$ is Planck's constant divided by 2π, E and m are the neutron energy and mass respectively. As can be seen, this equation is similar in form to the Hemlholtz propagation equation and in fact there are analogies to optical reflections. An analogy can be made if an optical index (n) of the material as follows:

$$n^2 = \frac{k^2}{k_0^2} = 1 - \frac{\lambda^2}{\pi}\rho b$$

$$n \approx 1 - \frac{\lambda^2}{2\pi}\rho b \qquad \textbf{3-5}$$

where λ is the neutron wavelength.

This result suggests that, analogous to optics of visible light, a critical angle is described by Snells law $n_1 \sin\theta_1 = n_2 \sin\theta_2$, giving a critical angle of reflection as

$$\sin(\theta_c) = (\frac{n_2}{n_1}) \qquad \textbf{3-6}$$

where n_2 is the optical lower refractive index.

As in Snells law, the critical angle can be approximated as follows:

$$q_c \approx 4\sqrt{\pi\rho b} \qquad \textbf{3-7}$$

where q is the scattering vector, which is, typically used in neutron reflectivity measurements and is calculated as follows:

$$q = \frac{4\pi}{\lambda}\sin(\theta) \qquad \textbf{3-8}$$

where λ is the neutron wavelength.

3.3.Abeles Matrix Formulation

The Abeles matrix formulation is a computational efficient method to calculate the total reflectivity of a surface consisting of several homogenous stratified layers. In particular the formulation calculates the SLD of the homogenous stratified layers oriented perpendicular to the surface. Although a real surface does not consist of sharply contrasted stratified layers, and therefore there are smooth changes in scattering length

density, the structure can be approximated by a larger set of discrete, homogeneous, slabs.

The analysis of determining the neutron reflectance and transmission at each surface as follows:

[54]:

$$R = \frac{k_1 - k_2}{k_1 + k_2}$$
$$T = \frac{2k_1}{k_1 + k_2} \quad \textbf{3-9}$$

where R is the reflectance and T the transmission amplitude of the neutron beam for each wavevector (k). For a non-perfect interface, an interface with roughness, Nevot and Croce [55] suggest a correction factor for the reflectivity:

$$R = \frac{k_1 - k_2}{k_1 + k_2} e^{\left(-2k_n k_{n+1} \sigma_{n,n+1}^2\right)} \quad \textbf{3-10}$$

where σ is the root mean squared roughness between layers n and n+1.

This logic can be extended to consider the effects of multiple interfaces simultaneously, an interface indicated in Figure 3-2.

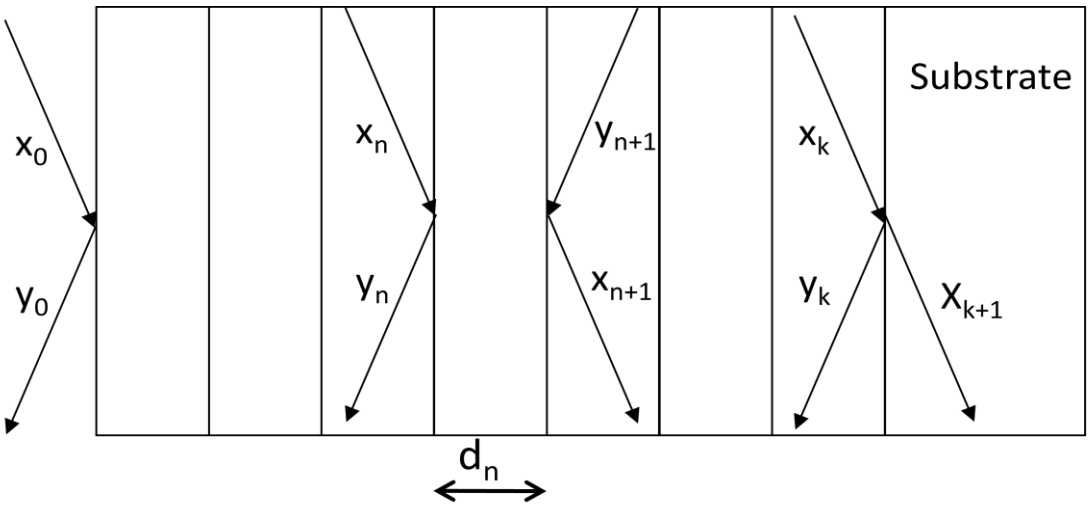

Figure 3-2 Reflection of an arbitrary small layer within a structure of n layers. To the far right is the substrate, as indicated, which is assumed to be large enough such that there are no backward travelling waves in medium k + 1 (i.e., yk+1 = 0)

At each interface the reflectivity can be written as a recursive statement:

$$\begin{bmatrix} x_n \\ y_n \end{bmatrix} = M_n \begin{bmatrix} x_{n+1} \\ y_{n+1} \end{bmatrix} \quad \textbf{3-11}$$

$$\text{where } M_n = \begin{bmatrix} e^{(\beta_n)} & r_n e^{(\beta_n)} \\ r_n e^{(-\beta_n)} & e^{(-\beta_n)} \end{bmatrix} \quad \textbf{3-12}$$

$$\text{and } \beta_n = k_n d_n \text{ and } r_n = \frac{k_n - k_{n,n+1}}{k_n + k_{n,n+1}} e^{\left(-2k_n k_{n+1} \sigma_{n,n+1}^2\right)} \quad \textbf{3-13}$$

The total surface reflectivity is therefore written as follows:

$$\begin{bmatrix} x_n \\ y_n \end{bmatrix} = \sum_n M_n \begin{bmatrix} x_{n+1} \\ y_{n+1} \end{bmatrix} \quad \textbf{3-14}$$

where n is the total layers on a substrate denoted as n+1.

As previously stated, the wavevector k in medium n is given by $k_n = \sqrt{k_z^2 - 4\pi(S_n - S_0)}$

where S is the SLD of the medium and k_z is the free space wavevector.

The resulting reflectivity can therefore be calculated assuming the x_{n+1} slab is the substrate and the term y_n is zero. Therefore, the total resulting reflectometry at any point q,

is $$R = \left|\frac{M_{10}}{M_{00}}\right|^2 \text{ where } M = \prod_0^n M_n \quad \textbf{3-15)}$$

written

as follows:

and M_{00} and M_{10} are entries in the matrix M as: $M = \begin{bmatrix} M_{00} & M_{10} \\ M_{01} & M_{11} \end{bmatrix}$

3.4.Critical Edge Measurement

The smallest angle, or wavevector (q) at which the reflectance transitions from perfect to partial reflectance is called the critical edge. An approximation can be made such that the average of all the layers relates to the critical edge given as follows:

$$q_c = 4(\pi\Delta\rho)^{1/2} \quad \textbf{3-16)}$$

where Δρ is the difference in SLD of air (background) and the average SLD of the deposited surface layers.

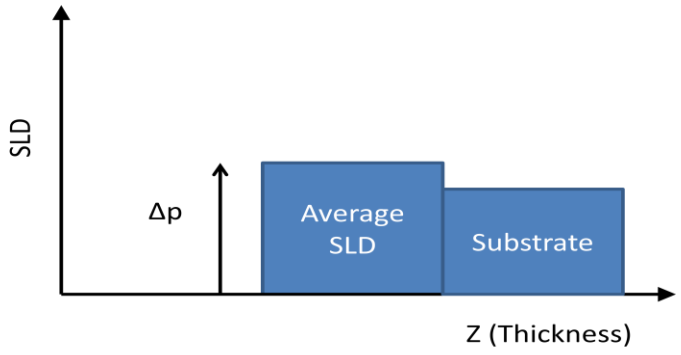

Figure 3-3 Average SLD of film deduced by critical-edge measurement.

Critical-edge measurements provide sufficient, albeit limited, information to suggest a change in the SLD of the film. In this thesis it is shown that critical-edge measurements can be obtained quickly and used as an adequate tool for determining the equilibrium of the hydrogen uptake within the film. Measurements can be taken in-situ during hydrogenation of the metallic films. Acquiring data relatively quickly in order to determine a quasi-stable point in the hydrogen uptake is important.

3.5.Hydrogen versus Deuterium

As briefly mentioned in section 3.1, the scattering length of hydrogen varies widely as the scattering lengths for hydrogen and deuterium are -3.76×10^{-15} and 6.671×10^{-15} meter respectively [51]. In NR experiments differences in the SLD have dramatic effects on the resulting SLD of the film. For instance, hydrogen introduction into a metal thin film reduces the SLD whereas deuterium increases the SLD. Moreover, the SLD of a film can also decrease if certain defects are introduced during hydrogenation. These defects may look similar to hydrogen uptake and increases the measurement error. By contrast, deuterium absorption increases the SLD of a film, and differences in the measurements of the hydrogenation sample or the deuterium absorbed sample can indicate the level of defects. Further details about calculating the hydrogen concentration from a SLD profile are given in the next section.

Hydrogen and deuterium diffuse through metals at different rates and react with metals differently but this difference is not very substantive. For instance, Powell and Kirkpatrick conclude that there is only a 13% difference in the diffusion constant for hydrogen and deuterium in palladium [56]. Bhati and Sholl [57] conclude that an

increase in temperature reduces the difference in activation energy, and therefore the diffusion constant, between hydrogen and deuterium in palladium. Moreover, Lasser [58] noted that Pd-H had a -19 kJ/mol enthalpy of formation whereas Pd-D had a -15.8 kJ/mol enthalpy of formation at 50°C, a difference of ~16%. This difference in enthalpy of formation would result in a lower solubility of deuterium in palladium than hydrogen in palladium, i.e. a lower concentration of deuterium in Palladium than hydrogen in palladium at the same pressure and temperature. The author is not aware of a published comparison of the enthalpy of formation of hydrogen and deuterium in other metals (e.g. magnesium). Differences in the enthalpy of formation of the other metals used and hydrogen and deuterium are not anticipated to be significant enough to drastically alter the system thermodynamics. In conclusion, it should be noted that there is a small, but noticeable, difference in the enthalpy of formation and the diffusion constant of hydrogen and deuterium in metals.

Critical edge measurements are taken very rapidly, as compared to a longer detailed scan, and are therefore useful in qualitatively determining if changes in the film have occurred. The observed critical edge may be that of the substrate if the film critical edge is lower than that of the substrate. Whereas if the film is sufficiently thick and the film critical edge is greater than that of the substrate, the observed critical edge may be larger than that of the substrate (in this case silicon). Hydrogen absorption in the films tends to decrease the critical edge of the film, resulting in the observed critical edge transitioning from that of the film to that of the substrate. Deuterium absorption in thin films may increase the critical edge, resulting in the observed critical edge remain that of the film instead that of the substrate. In conclusion, critical edge measurements can be

used to provide qualitative information when deuterium absorption has occurred in thin films.

3.6.Determination of Hydrogen Concentration

The hydrogen concentration of each stratified layer can be deduced through changes in the layers' SLD and thickness, a procedure first illustrated by Rehm et al [59]. Measurements of SLD and the thickness of the film before and after hydrogenation are used in the determination of hydrogen concentration.

First, it is assumed that the inevitable defects introduced by hydrogenation are smaller than the coherence of the neutron wave. For thin films, hydrogenation introduces interstitial, point, and microcracking defects that are very small and are assumed to be less than 2000 Å. Rauch *et al* [60] measured the neutron coherence length as 100 Å and 50,000 Å in the longitudinal and transverse directions respectively. Therefore the hydrogenation defects do not introduce error into the reflectometry measurements and may manifest as an apparent decrease in SLD.

A film that has undergone hydrogenation limited to expansion in the z direction due to substrate clamping. As such the film can be thought of as being strained in the z direction with hydrogen atoms placed in the spaces. Therefore, the total SLD is:

$$S_{M+H} = S_M(p_H) + S_H(p_H) \qquad \textbf{3-17}$$

where S_M and S_H are the SLD of the metal and of hydrogen respectively. Also, p_H denotes the SLD at a particular hydrogen pressure greater than zero. The SLD can be calculated using the volumetric density and scattering length of the metal and hydrogen as follows:1

$$S_M(p_H) = N_M(p_H)b_{Nb} \quad \textbf{3-18}$$

$$S_H(p_H) = N_H(p_H)b_H \quad \textbf{3-19}$$

where $b_{M,}$ b_H are the scattering length of the metal and hydrogen and N_M and N_H are the volumetric atomic density of the metal and hydrogen respectively.

The purpose of this procedure is to determine the ratio of hydrogen concentration against metal atoms and is usually stated as the percentage of metal atoms:

$$c_H(p_H) = \frac{N_H(p_H)}{N_M(p_H)} \quad \textbf{3-20}$$

The expansion of metallic film by hydrogen ingress is assumed to only occur in the z with no expansion in the plane of the substrate (i.e. no expansion in the x or y directions). This means the contribution to the SLD of the metal atoms at P=0 and P=p_H is:

$$N_M(p_H)t_{M+H}(p_H) = N_M(p_H = 0)t_M(p_H = 0) \quad \textbf{3-21}$$

Hydrogen has a widely varying scattering length depending upon the isotope used. For instance the scattering length of deuterium (hydrogen with an extra neutron) is positive whereas hydrogen has a negative scattering length. This peculiar negative SLD is only seen in very few atoms, one of which is hydrogen. A negative scattering length means the scattered neutron wave is out of phase with respect to the incident neutron wave.

For this thesis the neutron reflectivity measurements of the hydrogen absorption and desorption of the sample are taken in situ. One would expect that if measurements were taken during absorption, the absorption would continue while the measurements were taken. Therefore, steps have been taken to remove artefacts generated from hydrogen absorption during a scan. The approach was to: a) take short duration

measurement at each pressure until no noticeable changes are observed over a period of 20 minutes: b) Perform a longer, more detailed, measurement of the sample; and c) repeat the short duration measurement from step 1 to confirm that no changes occur. It is expected that some changes might occur in the sample during the measurements. However, this procedure greatly reduces the amount of error introduced while the measurements are taken. Therefore, these measurements are considered quasi-stable as it cannot be absolutely confirmed that they do not contain artefacts from hydrogen absorption during the measurement period.

3.7.Potential Pitfalls of Neutron Reflectivity

Several potential pitfalls may be made in calculating the hydrogen concentration within each stratified layer. These pitfalls must be addressed to lead to an understanding of the limitations of the NR results.

The first pitfall, is that the average coherent scattering length (b_M) of the starting material is the same as that of bulk material reported previously in the literature. At the onset of each experiment, the as-synthesized material SLD is determined through a thorough NR measurement and is compared against the expected results from bulk material.

The second pitfall is that the sample must be uniform in the xy plane when viewed by the neutron beam coherence length. If the sample is not xy uniform, the results would be similar to multiple samples within the neutron beam. Fitting of the reflectivity curves would be impossible and probably incorrect. X-ray diffraction measurements taken at multiple points across the surface were taken to confirm composition uniformity. Also,

SEM micrographs of the as-sputtered and hydrogenated samples confirm that no major cracking occurred with these thin samples.

The third pitfall is that the constituent concentration of the alloy is known prior to taking the NR measurements. In this study great care is taken to have a known the composition prior to taking the NR measurements by employing a careful fabrication procedure and independent confirmation by EDS and X-ray scattering measurements.

The fourth pitfall is that the film expansion due to hydrogenation is exclusively along the z-direction with effectively no expansion in the plane of the material (x ory direction). A material was chosen as an adhesion layer to cause the film to remain adhered to the substrate. This strong substrate film interaction limits the in-plane expansion and forces the film to expand in the z-direction. Since Mg tends to expand by ~30% (v/v), one would visually see a 30% in-plane expansion on an approximate 100 mm^2 sample. In all of the experiments there was no evidence of expansion other than along the z direction due to hydrogenation.

In conclusion, the above four pitfalls were avoided by careful fabrication of the samples through sputtering and independent measurements of the created material. These pitfalls are noted here to illustrate the care that was taken to avoid these potential pitfalls.

4. Results and Discussion

4.1.Introduction

The main drawback to using magnesium as hydrogen storage medium, as suggested in section 1.1, is the high operating temperature (~300°C) typically required to obtain reasonably fast hydrogen sorption kinetics. Reduction in operating temperature is accomplished through a combination of surface catalysts addition, nanostructuring, or bulk catalysts additions. Usually one cannot examine the kinetics and thermodynamics in isolation. Therefore measurements of data with kinetics and thermodynamics may be misleading which may bring about erroneous conclusions.

Hydrogenation is usually described in two mode: (a) a nucleation and growth model wherein the hydride grains may encroach before the whole magnesium particle becomes a hydride and (b) three-dimensional diffusion controlled shrinking core model, where a continuous layer of magnesium hydride forms immediately on the surface and this hydride stops the remaining magnesium from hydriding by reducing the effective hydrogen diffusion..[61] The addition of the catalysts may significantly alter the hydrating kinetics by lowering the hydrogen dissociation and surface diffusion barriers [62] or lowering the energy required to transform the Mg particle to MgH_2 [63]. To investigate these effects, thin films are used as a model system for deducing the hydrogen distribution within the structure using NR. – a non-destructive experimental procedure.

4.2.Preliminary Sorption on Catalytic Layers

Magnesium and magnesium oxide are well known to be inactive toward hydrogen dissociation. As such, catalysts films are generally deposited on fresh magnesium

surfaces. Several researchers have used thin film structures to examine the role of catalysts in hydrogen sorption, but several questions remain. In this study the catalytic sorption process of palladium and palladium bi-layer catalysts -namely, MgTi, MgNb, MgTa, and several others – are examined

Palladium catalysts are used extensively to increase sorption kinetics and have been shown to degrade easily. One drawback is the formation of a Mg_6Pd inter-metallic such that at temperatures above 200°C the Pd diffuses into Mg, destroying the catalytic advantage of the palladium. [3] Discovery of this palladium diffusion process has lead to the discovery of a Pd/Ta bi-layer catalyst that is stable at elevated temperatures while allowing hydrogen sorption to occur. Research has further shown that hydrogen desorption of the Ta/Pd catalyst is possible even at room temperature, a property not possible with a simple palladium catalyst layer.

Further investigation of the role of the bi-layer catalyst is required as it was not anticipated to be so catalytically active at room temperature.

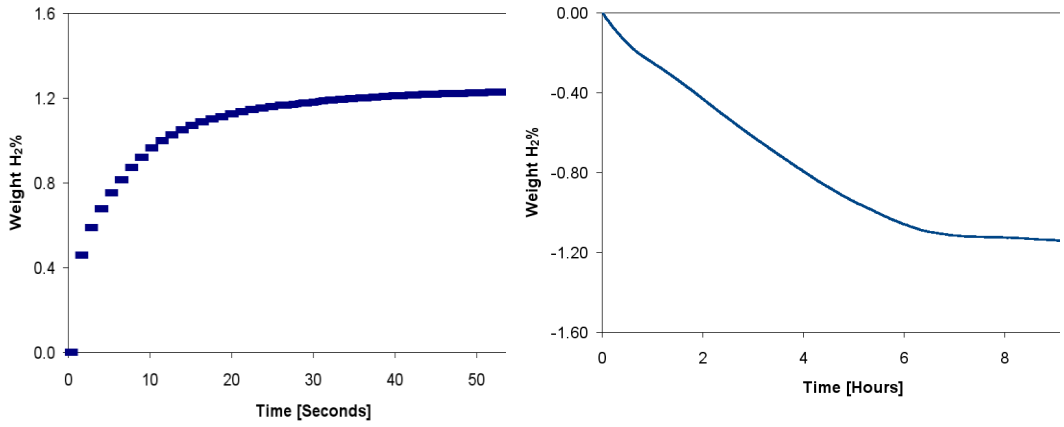

Figure 4-1: Hydrogen sorption character of Mg - 30 at %Al. (a) Absorption at 125 °C and 30 bar hydrogen. (b) Desorption in a thermal gradient analyzer (TGA) at 100°C with 20 sccm of argon flow through the cell

Preliminary measurements (shown in Figure 4-1) clearly show hydrogen sorption of Mg-30at%Al catalysed with a Pd/Ta bilayer catalyst at 100°C. The aim of this thesis is to describe the sorption processes of the above sample and try to elucidate the role of these catalyst layers.

4.3.Mg thin film - Volumetric Absorption

The investigation of hydrogen sorption on thin-film metal hydrides begins with measurement of a standard magnesium thin film sample in order to compare to results from the literature. A Pd/Ta catalyst layer is added to the sample to facilitate increased sorption rates without degradation Hydrogen sorption measurements are taken from a 1 micron thick magensium sample catalysed by a Pd/Ta bilayer using a modified Sievert's apparatus. Absorption measurements are taken at 250°C and 30 bar whereas desorption occurs at ~0.1 bar and 250°C. Hydrogen sorption of pure magnesium has been studied by many researchers and therefore it is a good subject for comparison.

The type and thickness of the catalyst layer are chosen with care to alleviate any catalyst degradation and degradation due to surface oxidation while maintaining a degree of catalyst hydrogen dissociation. In this thesis the role of the catalysts is explained in further detail (see Section 5). However, because study of optimal thickness was performed by J. Haagsma, it is not explored in more depth in this thesis.

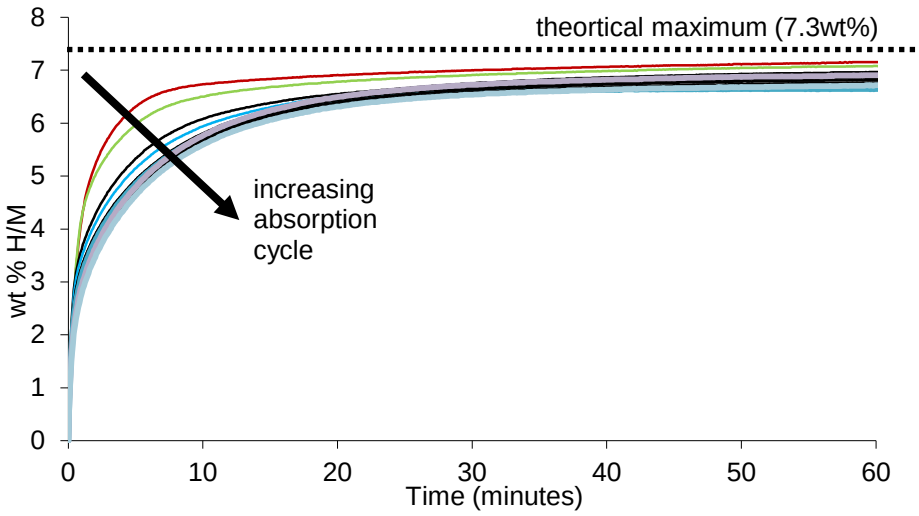

Figure 4-2 Hydrogen absorption measurements of a 1 µm-thick Mg thin film catalysed by a 7.5/7.5 nm Pd/Ta-catalysed layer deposited on the surface. Measurements are performed with a modified Sieverts apparatus at 250°C and 30 bar. The high temperature and pressures are chosen to reproduce conditions required for a hydrogen sorption application (i.e., a hydrogen car fuel tank)

Hydrogen absorption measurements are taken of a 1 micron-thick magnesium thin film catalysed with a 7.5 nm/7.5 nm thick catalyst layers deposited on the surface. These thin films are first deposited on a silicon wafer but subsequently removed and placed in the volumetric (Sievert's) apparatus. The detailed measurement procedure is outlined in section 2.4

As can be seen in the sorption measurements in Figure 4-2, the magnesium sample quickly absorbs hydrogen at 250°C with little or no initial impediment to MgH_2 nucleation. There is no barrier for hydrogen absorption for the experimental conditions as the activation energy is sufficiently low. One would expect that the hydrogen uptake would show a sigmoidal character if a large barrier existed for the experimental conditions. In other words, the hydrogen uptake would be initially slow followed by a

period of high (probably linear) hydrogen uptake and ending with a slow, progression to the final hydrogen uptake weight.

An attempt has been made to fit the data to the well-known Johnson-Mehl-Avrami-Kolmagrov equation (JMAK), which describes the kinetics and thermodynamics of crystallisation [64, 65, 66]. The lack of fit suggests that the hydrogen absorption is not analogous to a simple phase transformation form- for example, from Mg to MgH_2Indeed the JMAK equation encompasses several phase transformation forms but fundamentally assumes the phase transformation proceeds in a single step rather than a multi-step process. The lack of fit does not sufficient justification for conclusions about the absorption process. The lack of JMAK equation fit may elude that a simple absorption process may not have occurred. A conclusion of a complex absorption process may be similar to an observation by Borgshulte et al. that hydrogenation of magnesium does not follow a simple single rate-limiting model [67].

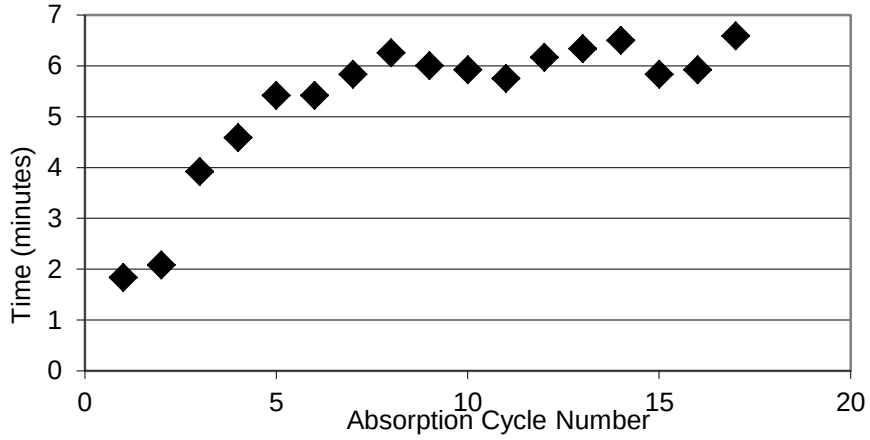

Figure 4-3 Hydrogen absorption time to 5 wt% as a function of cycle number for a 1 µm-thick Mg sample catalysed by a Pd/Ta bilayer catalyst deposited on the surface.

The first and second absorption measurements progress quite rapidly due to defects within the magnesium structure introduced by the synthesis methods. (e.g. the large

amount of interstitial defects, vertically oriented grain boundaries, and coherent catalyst layers across the surface). Any advantage due to sputtering the thin film instead of using other techniques is likely eliminated by repeated absorption/desorption recycling.

After the fifth absorption cycle, the material reaches steady-state equilibrium for absorption/desorption recycling such that the amount absorbed and desorbed and the rate of absorption are similar. This result is unexpected as there typically is degradation of the catalyst layers, which results in the degradation of the total level of hydrogen uptake. Moreover, degradation of hydrogen uptake usually occurs when a coherent layer of magnesium hydride on the magnesium surface inhibits further hydrogen uptake into the bulk of the magnesium. The outermost layer of magnesium is usually responsible for the recycling while the bulk of the material becomes inactive.

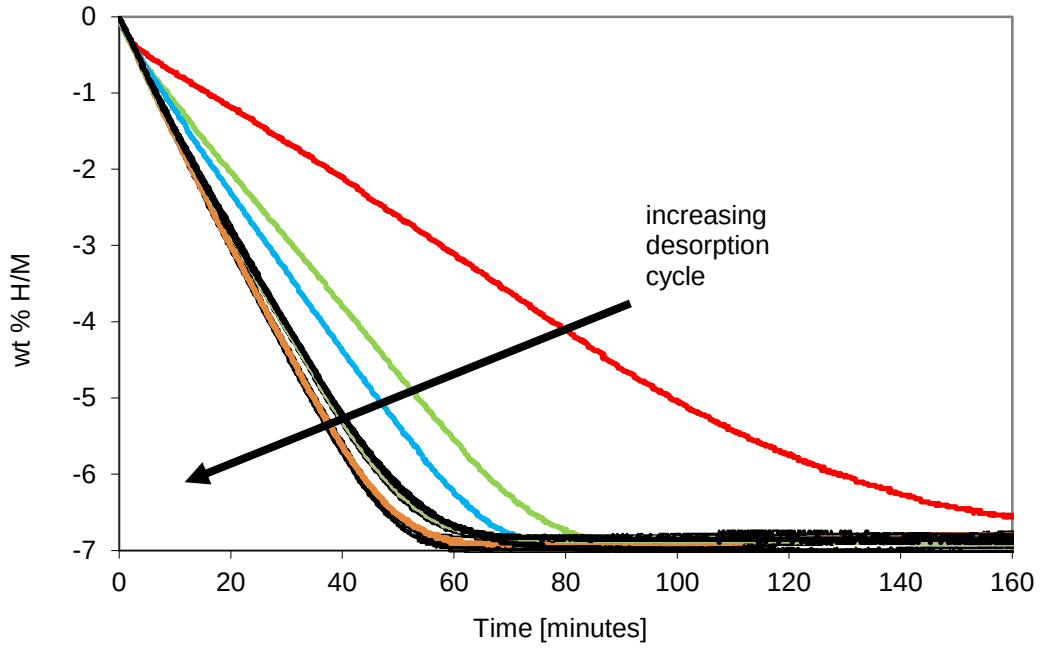

Figure 4-4 Hydrogen desorption measurements of 1 µm-thick Mg thin film catalysed by a Pd/Ta bilayer catalyst deposited on surface of film. Measurements are performed with a modified Sieverts apparatus at 250°C and 0.1 bar. The high temperature and pressures are chosen to reproduce conditions that would be required for a hydrogen sorption application (i.e., a hydrogen car fuel tank). The hydrogen wt% is relative to the weight of the metal (in this case Mg) and not the hydride to allow a direct comparison with the amount of absorption.

Hydrogen desorption (hydrogen release) of the Pd/Ta catalysed Mg layers proceeds with the first and second recycling cycles occurring at a much slower rate than the later cycles. During desorption, the hydrogen release rate seems linear with time and therefore seems to be rate limited by hydrogen diffusion through the magnesium layers. One would expect a sigmoidal curve if an activation process is limiting the desorption rate. Again, the data could not be fit to a JMAK equation and therefore does not seem to follow a simple sorption process.

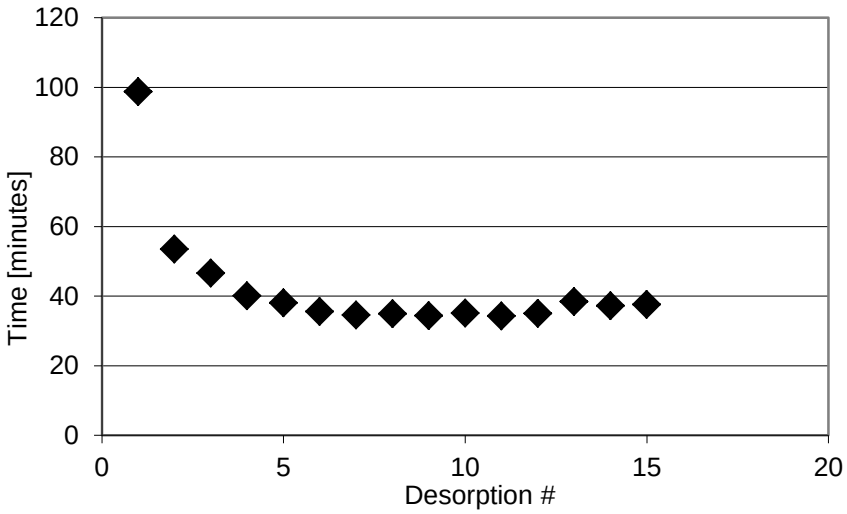

Figure 4-5 Hydrogen desorption time to 5 wt% as a function of cycle number for a 1µm-thick Mg sample catalysed by a Pd/Ta bilayer catalyst deposited on surface

In the first desorption cycle, the hydrogen release is quite slow requiring ~160 minutes for complete desorption. This behaviour is opposite to the absorption process where the first few absorptions step occur quite rapidly but there is a subsequent increase in the amount of time required. After only the second desorption does the system appear to behave in a exhibit steady-state and continue to require the same amount of desorption.

4.4.Mg – 30 at% Al thin film - Volumetric Absorption

The next part of the investigation of hydrogen sorption on thin-film metal hydrides consists of measuring a Mg-30 at % Al sample. Again, as with the magnesium sample, a Pd/Ta catalyst layer is added to allow an increased sorption rate without degradation. Hydrogen sorption measurements are taken of a 1 µm thick Mg-30at%Al sample catalysed by a Pd/Ta bilayer catalyst using a modified Sievert's apparatus. Absorption measurements are taken at 250°C and 30 bar whereas desorption occurred at ~0.1 bar

and 250°C. Experimental conditions are the same as those used for the measurements of the magnesium sample in order to make a direct comparison

The type and thickness of the catalyst layer are chosen with care as to alleviate any catalyst degradation or degradation due to surface oxidation while maintaining a degree of catalytic hydrogen dissociation. This thesis investigates the role of catalysts in further detail, using the neutron refraction technique discussed in section 5.

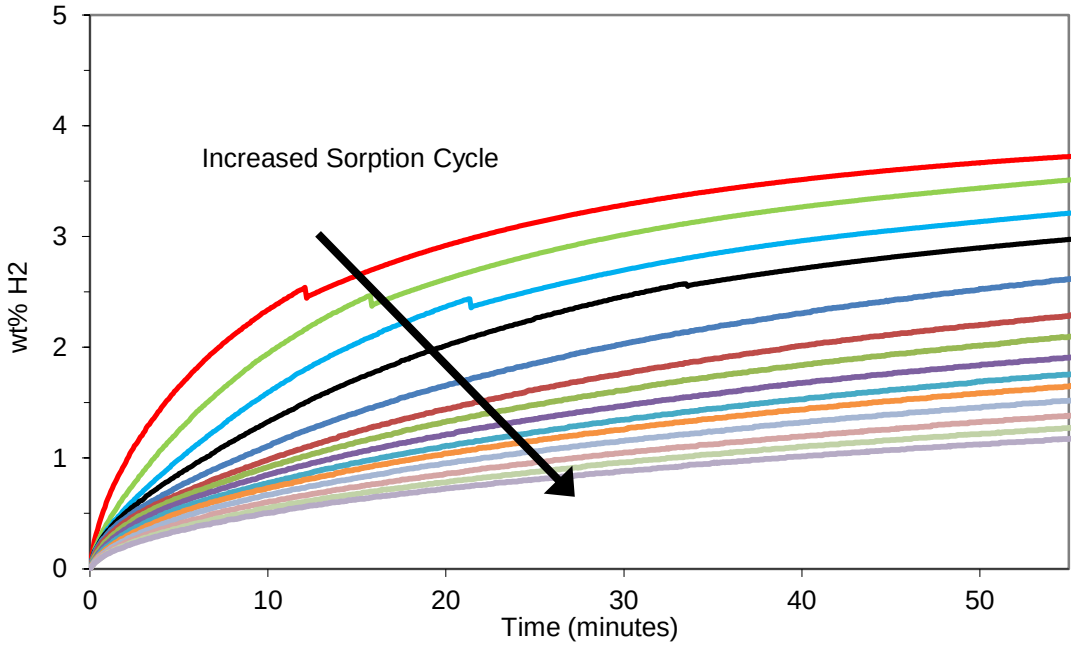

Figure 4-6 6 Hydrogen absorption measurements of a 1 µm-thick Mg-30 at %Al thin film catalysed by 7.5/7.5 nm Pd/Ta layers deposited on surface. Measurements are performed with a modified Sieverts apparatus at 250°C and 30 bar.

As seen in the sorption measurements in Figure 4-6 the Mg-30 at % Al sample readily absorbs hydrogen with similar character to the Mg sample, presented earlier. Again, at 250°C the Mg-30at%Al sample quickly absorbed hydrogen at 250°C with little or no immersion time required. There is no barrier for hydrogen absorption for the experimental conditions. At these temperatures it is anticipated that the Mg-Al sample

would take up hydrogen at a faster rate than the pure magnesium sample, but the measurements indicate that the absorption rates are comparable.

One remarkable difference in the absorption curves is the quick deterioration of the amount of hydrogen being absorbed with each cycle. Originally it was anticipated that the aluminum would precipitate out of the Mg-Al solid solution and become a catalysts for hydrogen absorption. Obviously another process occurred, preventing either absorption or desorption.

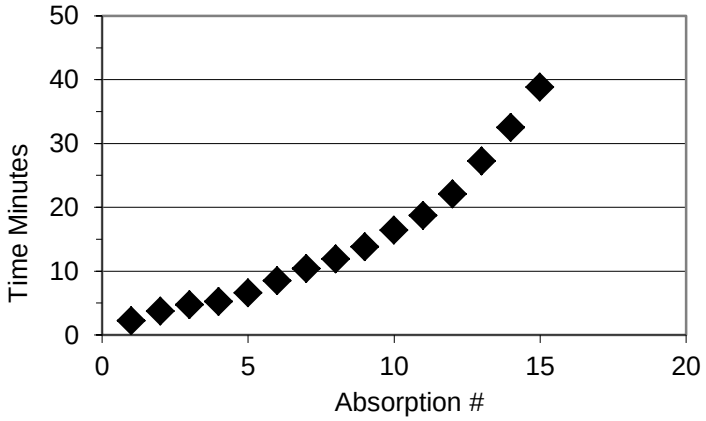

Figure 4-7 Hydrogen absorption time to 1 wt% as a function of cycle number of a 1µm-thick Mg-30 at %Al sample catalysed by Pd/Ta bilayer catalyst deposited on surface.

Plotting the time required to reach 1 wt% versus the absorption cycle shows that the Mg-30at% Al sample degrades with each cycle number. The time required for 1% weight change is chosen to allow a comparison of all the absorption cycles as several of the later cycles did not absorb much at all. At present there are no published results of the hydrogen absorption cycling behaviour of Mg-Al alloys that the author knows of; therefore a comparison cannot be made. More details about the degradation mechanisms are suggested in the investigation of the crystal phases (see Section 4.5)

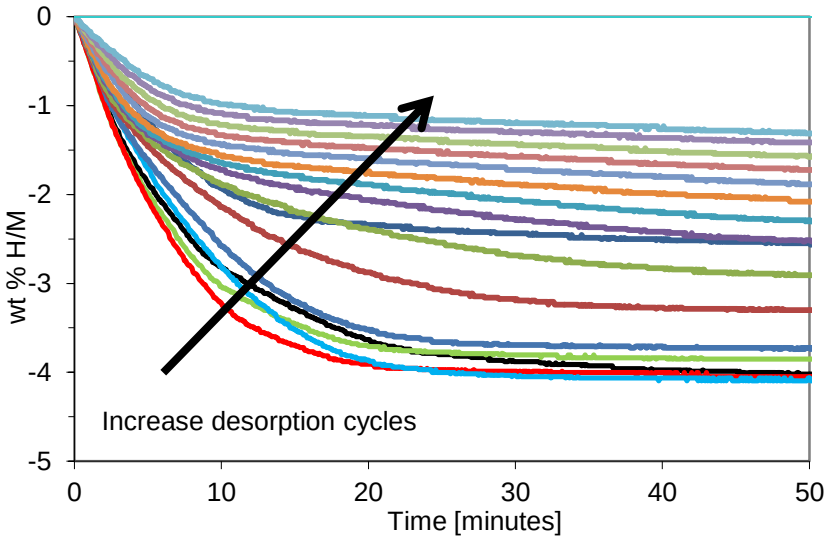

Figure 4-8 Hydrogen desoprtion measurements of a 1 µm-thick Mg-30 at %Al thin film catalysed by a 7.5/7.5 nm Pd/Ta catalysed layer deposited on surface. Measurements are performed with a modified Sieverts apparatus at 250°C and 30 bar. Desorption measurements are relative to the weight of the metal (Mg Al) and not the hydride.

Hydrogen desorption (hydrogen release) of the Pd/Ta catalysed Mg-30at% Al layers proceeds in a manner similar to the hydrogen absorption (see Figure 4-8) where the amount of hydrogen being absorbed steadily decreases. Also, there is a difference in the total amount of hydrogen being absorbed and desorbed for each cycle. For instance, at the first absorption cycle there is only a ~3.5 wt% H increase whereas the total amount of desorption is ~4%. This difference in absorption is due to the delay induced from lowering the reservoir pressure and resetting the instrument for desorption. The volumetric absorption system cannot be measured while preparing for desorption or absorption measurements.

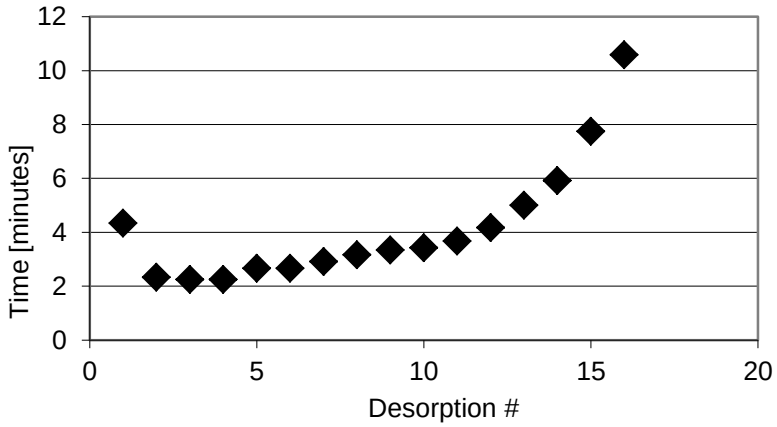

Figure 4-9 Hydrogen desorption time to 1 wt% as a function of cycle number for a 1µm-thick Mg-30 at %Al sample catalysed by a Pd/Ta bilayer catalyst deposited on surface

Plotting the time required to reach 1 wt% versus desorption cycle (see Figure 4-9) shows that the Mg-30 at % Al sample degrades with each cycle number. Again, a time of 1 wt% desorption is used to allow comparison of all desorption measurements. It is remarkable that the hydrogen desorption maintains a constant release rate up to an ~12 desorption cycle as opposed to the absorption plot (see Figure 4-7) where the amount of time required to reach 1 wt% steadily increases. Therefore, this result would suggest that the system is limited not by desorption but by absorption. Only after the amount of absorption decreases to nearly 1 wt% does the rate of desorption decrease. The observation of that hydrogen absorption is slower than desorption qualitatively suggests that the system is steadily forming a non-absorbing hydrogen alloy, an observation that should be confirmed by crystal analysis.

4.5.Mg-Al X-ray Diffraction

X-ray diffraction (XRD) measurements illustrate that the as-sputtered Mg-30at% Al alloy consists of HCP magnesium with aluminum as a substitute addition to magnesium. The appearance of only the (200) diffraction peak is attributed to a high degree of texture in

the sputtered magnesium films. For example, Wu et al [68] illustrated that only the (002) diffraction peak appears at 34.4° in the diffraction pattern of a highly textured Mg thin film. In the case examined here, the diffraction pattern is of magnesium with aluminum in solid solution. The addition of the aluminum causes a contraction of the (200) crystal planes, resulting in a shift to 35.8°. The shift in the diffraction peak is similar to the shift observed when Ti is introduced into Mg as a solid solution. For example, Vermeulen et al [69] measured a continual shift in the (200) diffraction peak as the amount of titanium in solid solution to Mg is increased. The diffraction peaks corresponding to palladium and tantalum are not clearly visible, most probably due to the small thickness of these layers.

Upon heating the sample to 250°C and pressurizing to 30 bar hydrogen, the sample undergoes a phase transformation into two separate phases -namely- α and γ magnesium hydride. This is in contradiction to several other studies of ball-milled magnesium-aluminum that noted that during hydrogenation the Mg_xAl_y alloy transforms from a solid solution into α-MgH_2 with little or no γ-MgH_2. The overall reaction scheme of: $Mg_xAl_y + xH_2 = xMgH_2 + yAl$ is still valid but does not allude to the formation of two MgH_2 crystal phases or any intermediate reaction steps.

The crystal phase β-MgH_2 may form during the hydrogenation process as this phase is only stable at relatively high hydrogen pressures and it decomposes into γ-MgH_2 when the pressure is released. The diffraction patterns illustrated in Figure 4-10 are taken ex-situ to the absorption measurements and are therefore taken in air at one atmosphere.

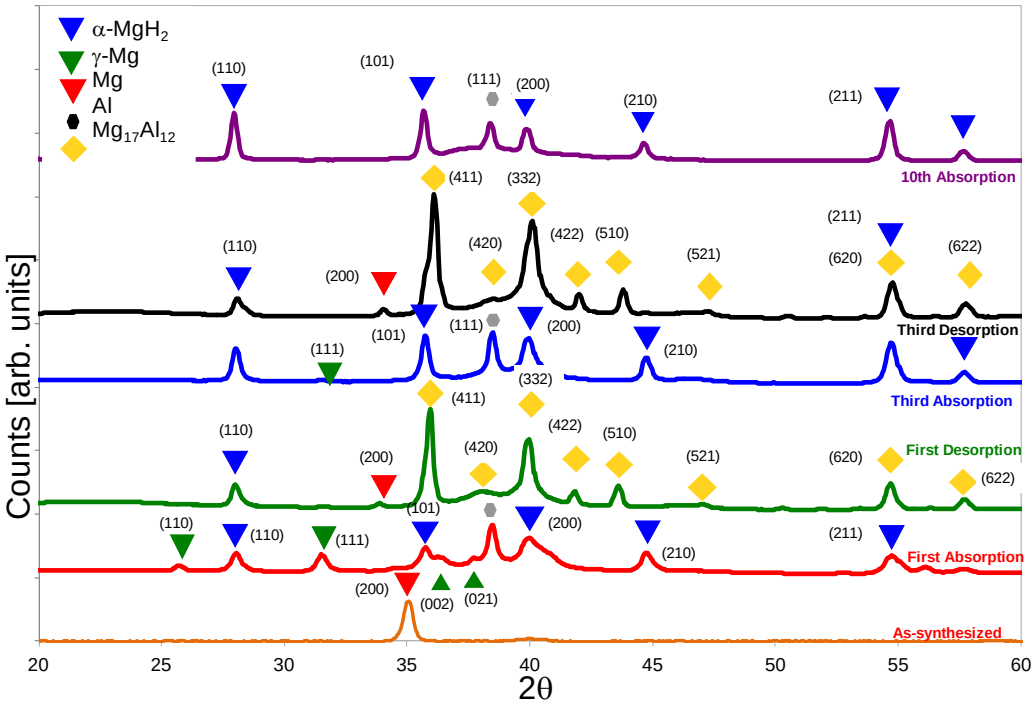

Figure 4-10 X-ray diffraction pattern of Mg- 30 at% Al at the first, third and 10th absorption, and the third desorption

Upon reducing the hydrogen pressure to ~0.01 bar (first desorption), the hydrogen is dissociated from the Mg-Al alloy and it results in the formation of magnesium with $Mg_{17}Al_{12}$ precipitates, as illustrated in Figure 4-10. X-ray diffraction measurements of the samples were taken once desorption rate fell below $1x10^{-3}$ wt %/min. The amount of MgH_2 is assumed to be minimal and is apparent in the X-ray spectra (see Figure 4-10). It is presumed that the low hydrogen desorption rate is due to the presence of the $Mg_{17}Al_{12}$ inter-metallic alloy as re-arrangement from this disordered phase to MgH_2 would be slow. Transformation of $Mg_{17}Al_{12}$ into MgH_2 is possible and proceeds in a two-step reaction at 350 C. In this process the $Mg_{17}Al_{12}$ transform into Al_3Mg_2 and subsequently decompose into a-MgH_2 with Al precipitates [35]. This overall reaction is relatively slow as compared to pure magnesium at 250°C and therefore may contribute to the observed slow kinetics.

Upon further cycling , the Mg- 30 at% Al alloy preferentially forms a more stable $Mg_{17}Al_{12}$ alloy. Since the formation and dissociation from $Mg_{17}Al_{12}$ to MgH_2 and Al is considerably slow, the sorption (absorption and desorption) kinetics should also be extremely slow. Therefore, the alloy sorption rates steadily decrease with increased sorption cycling.

4.5.1. Volumetric Absorption Conclusions

4.5.1.1. Pure Magnesium Film

Hydrogenation of magnesium (powders and thin-films) has been extensively studied and many reports exist within the literature. Huot *et al.* report hydrogenation of ball-milled magnesium at 300°C to 8.2 wt% [H/M] within 50 minutes at a hydrogen pressure of 10 bar [70]. The high temperature and pressure required are assumed to be due to a hydrogen diffusion barrier from the formation of surface β-MgH_2. The observed absorption and desorption curves published by Huot *et al*. are very similar to the curves illustrated in Figure 4-2 and Figure 4-4. (i.e. the basic shape and hydrogen absorption and desorption times are comparable).

Higuchi *et al* report hydrogenation between 2.9 wt% and 6.6wt% for several prepared Pd-capped magnesium films fabricated through RF sputtering. Dehydrogenation occurs at 200°C under a vacuum [71]. Singh et al reports 7.5 wt% hydrogenation of a Pd-capped 1µm magnesium thin film at 200°C and 10 bar [25]. Further cycling reveals that full hydrogenation after two cycles is impossible and is attributed to delamination of the palladium catalyst layer with the magnesium. In this study Singh only provides indirect evidence for delamination and cannot confirm this conclusion through TEM micrographs. Furthermore, Singh notes Pd-Mg alloying has been observed during hydrogenation

above 250°C. Delamination and alloying of the Pd layer seems to contradict each other but are possible given that two independent samples are used and the two experiments are carried out at different temperatures. Yoshimura reports hydrogenation of a magnesium thin film exposed to a 4% hydrogen gas mixture is possible within 5 seconds at room temperature [72]. Furthermore, Yoshimura achieves full hydrogenation within 40 minutes even after repeated recycling.

Stress is known to build within a sputtered thin film depending upon the sputtering conditions and thickness of the film [73]. Trinidade *et al* measure negligible stress within a sputtered 3 μm thin film from XRD measurements [74]. Jain *et al* reported similar first cycle hydrogenation of the magnesium thin films at a lower pressure to the experiments reported in this thesis [75]. An increase in the absorption temperature causes a decrease in the absorption time. Also, the state of stress can change the pressure required for hydrogenation and therefore can cause either an increase or decrease in absorption rates [76]. Furthermore, since the temperature of hydrogenation (250°C) is within the temperature expected for a stress relaxation process the above differences in sorption time, and character, may be attributed to differences in the internal stress created from sputtering. However, within the first few hydrogenation cycles, the stress within the thin-film sample may relax as there is no longer residual stress due to the sputter deposition. This assumption is similar to a finding by Gremaud that hydrogenation relaxes the internal stress of a Pd thin film [77].

The crystal phases of the hydrogenation of the magnesium samples measured here are expected to be similar to those reported by Huot et al who find that Υ-MgH_2 and β-MgH_2 are formed despite the use of ball-milled magnesium samples [78]. Another

investigation by Ye at al [79] illustrated that hydrogenation of Mg samples is possible at a low temperature but degradation by the formation of a Mg-Pd intermetallic at higher temperatures inhibits further hydrogenation. As far as this author is aware, repeated hydrogenation of a pure magnesium sample catalysed by a stable catalyst has not been published. Typically there are only reports on repeated hydrogenation of Mg-X alloys with a stabilized Pd catalyst [80, 81, 37].

4.5.1.2. Mg-Al Thin Film

The literature reports little about the hydrogenation character of ball-milled Mg-Al allows and only sparse studies performed on hydrogenation of sputtered Mg-Al samples. The first report of hydrogenation of MgAl was created by Douglass in 1975[36]. In that paper he concludes that hydrogenation of MgAl progresses by an initial nucleation of MgH_2. The reaction was limited by the rate of hydrogen diffusion across the metal/hydride interface. A study performed by Garcia illustrated that Mg-30at%Al was the optimal stoichiometry for this particular alloy in terms of absorption kinetics [82]. Andreasen [38] shows that the hydrogen uptake rate increased for Mg-Al samples compared to pure magnesium sample. There is no evidence of destabilization as Andreason assumes that Mg-H_2 forms during the hydrogenation process [38]. A study of Mg-Al thin films by Ferrer [83] reveals that the presence of aluminum aids in hydrogenation of the magnesium layers, but desorption rates remain comparable to those of a pure magnesium sample.

A study by Andreasen illustrates that hydrogenation of the Mg Al causes it to segregate into MgH_2 and Al while during dehydrogenation an intermetallic of MgAl forms [38]. This

is further confirmed by a study of MgAl thin films by Gremaud [37], wherein the MgAl transforms from a solid solution mixture of Mg Al to a segregated MgH_2 - Al mixture.

These observations are very similar to those noted in the previous section. Hydrogenation of the Mg-Al proceeded through magnesium transforming to magnesium hydride with aluminum precipitates. Upon dehydrogenation, the Mg-Al tends to form a stable $Mg_{17}Al_{12}$ intermetallic that degrades the hydrogenation recycling. As far as this author is aware there are no published data on the repeated hydrogenation of an MgAl alloy; therefore a direct comparison is not possible.

5. Neutron Reflectometry Study of Surface Catalysts

Since both magnesium and magnesium oxide are inactive toward hydrogen dissociation, the first step in the absorption process requires a surface hydrogen dissociation catalyst. Classically these catalysts consist of single-element or multi element homogeneous films typically palladium and transition metal oxides. These surface catalysts operate by decreasing the dissociation barrier and facilitate the reduction of stable sub-surface hydrogen traps. Homogenous films are typically easily deposited on surfaces without introducing defects, deleterious oxides, or alloys into the bulk material, which would typically result in reduced kinetics for the system.

In this section a detailed study of the changes in the character of a Pd catalyst incorporated onto Mg and Mg-Al alloys are presented. The Mg-Al alloy of Mg-30 at% Al and Mg-40 at% Al are chosen based upon previous studies as it was shown that these alloys show optimal kinetics. A pure magnesium sample is also studied and used to compare with the results from the literature.

5.1.Mg – Pd

In order to investigate the absorption mechanisms and the effectiveness of surface binary catalysts, NR is used to observe and compare the hydrogenation (hydrogen or deuterium) mechanisms of a catalysed Mg-30 at % Al thin film. The composition Mg-30 at % Al is chosen for the comparison it has the optimal sorption properties and would not limit the absorption and therefore significantly alter the surface catalyst comparison.

The NR measurements are performed *in-situ* at distinct stages in the absorption process. It is assumed that after the measurement time the system reaches a stage at which the system does not undergo any noticeable changes in the structure (e.g. an increase in hydrogen concentration, microstructure, etc). Thus, this is termed a quasi equilibrium condition. These quasi equilibrium measurements are taken from early deuteration of the catalyst layers up to the full saturation of the samples. The deuterium profiles obtained offer new insights into how the absorption proceeds and how the use of certain catalysts may lead to improved materials.

The analysis of the hydrogen sorption character of a surface catalyst commences by investigating through NR the deuterium sorption character of a Pd- catalysed Mg-30 at % Al thin film deposited on a Ta-coated silicon wafer, a structure illustrated in Figure 5-1. This examination of a well-known catalyst is used for a comparison with other catalysts.

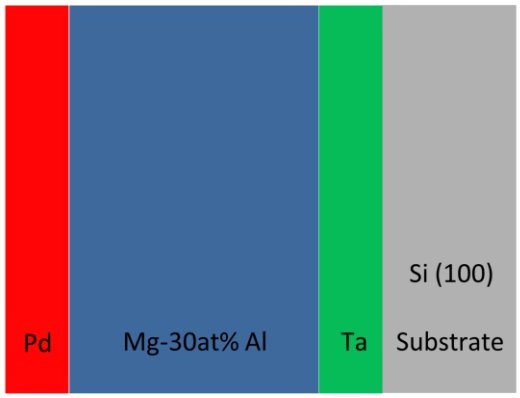

Figure 5-1 Illustration of the Pd catlayzed Mg thin film deposited on a Ta (10 nm)-coated (100) silicon wafer

The neutron reflectivity measurement of the Pd catalysed thin-film is illustrated in Figure 5-2. The measured (open circles) and calculated (solid line) reflectivity curves of the Ta/ Mg-30 at % Al / Pd film structure are shown as a function of the scattering vector q in Figure 5-2. The visible oscillations, referred to as Kiessig fringes, are associated with the characteristic thickness of the film.

The as-prepared sample measured in air (see Figure 5-2a) clearly indicate the as-synthesized structure as a Pd (10nm), Mg - 30 at % Al (50nm), and Ta (10nm) buffer layer on top of a Si (100) substrate. The SLD of each of these as-synthesized layers is well within 10% of the expected SLD from bulk measurements [51]. The sharp delimitation of each layer indicates minimal interfacial roughness and little or no mixing between each layer.

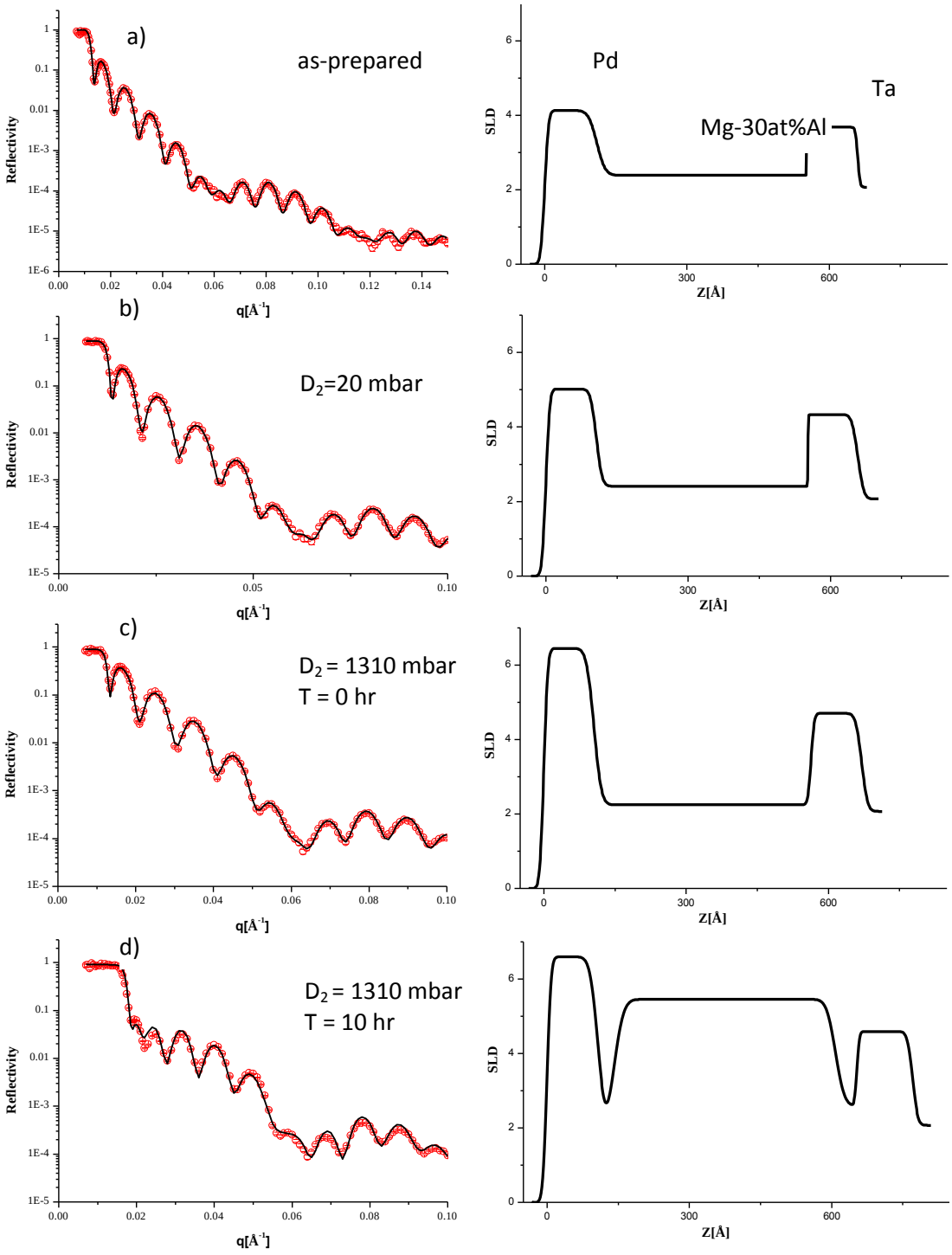
a)
as-prepared
Pd
Ta
Mg-30at%Al
b)
D2=20 mbar
c)
D2 = 1310 mbar
T = 0 hr
d)
D2 = 1310 mbar
T = 10 hr
Reflectivity
q[Å-1]
SLD
Z[Å]

Figure 5-2 Neutron reflectometry measurements of a Pd (10nm)-capped Mg-30 at %Al (50nm) thin film deposited on a Ta (10nm)-covered (100) Si substrate (see Figure 5-1). (a) As-sputtered state. (b) D_2 = 20 mbar. (c) D_2=1310 mbar t = 0 hr. (d) D_2 = 1310 mbar, t = 10 hr. Absorption experiments are performed in situ to neutron reflectometry measurements and performed at room temperature (20°C). The sample was held at 20mbar for ~30minutes before reflectometry measurements taken. The history of the pressure is indicated in Figure 5-3.

Subsequent to taking reflectometry measurements of the as-synthesized structure, deuterium is introduced into the sample cell, and reflectometry measurements are taken again. As a consequence of the large coherent scattering length of the deuterium, the SLD of the absorbing layer increases, as seen in Figure 5-2b. In particular, at a pressure of 20 mbar (see Figure 5-2b) there is an increase in the SLD of the bottom Ta and Pd layers but little, or no, change in the SLD of the Mg – 30 at% Al layer.

After a further deuterium pressure increase to 1.3 bar, the SLD of the Pd and Ta increases further to 6.5 x 10^{-6}Å^{-2} and 5 x 10^{-6}Å^{-2}, corresponding to a D/M of 46% and 20%, respectively (see Figure 5-2c). Also there are no noticeable changes in the SLD of the Mg – 30 at% Al layer. After immersion in a 1.3 bar deuterium for more than 10 hours (see Figure 5-2d), the SLD of the $Mg_{70}Al_{30}$ layer at 5 x 10^{-6}Å^{-2} and undergoes a ~25% expansion, corresponding to a D/M of 1.4. This observed hydrogen concentration is consistent with the formation of a MgD_2 and Al as an inert precipitate.

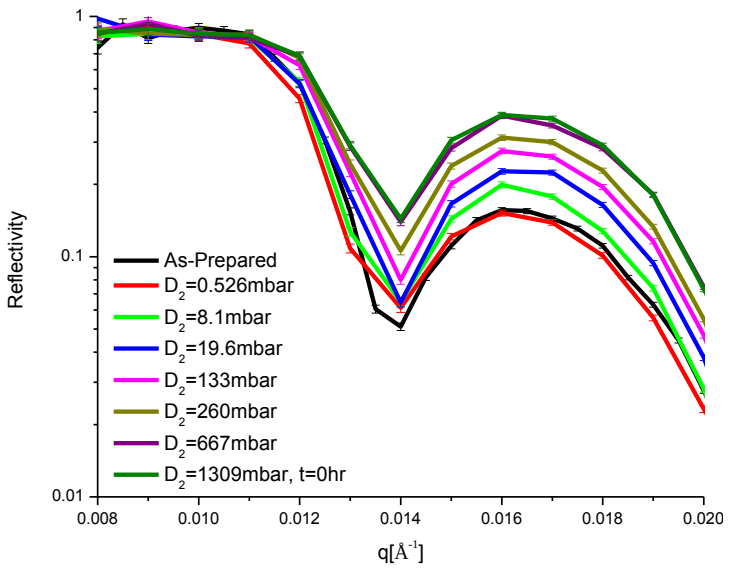

Figure 5-3 Neutron reflectometry critical-edge measurements of a Pd (10nm)-catalysed Mg-30 at %Al thin film deposited on a 10nm Ta-coated (100) Si wafer (see Figure 5-1) and performed under a deuterium atmosphere as indicated. Measurements are taken after reaching a quasi-steady state. The samples was held at each pressure for ~1.5 hours before increase the pressure again. i.e. 30 minutes to reach equilibrium and 1 hour to take the full reflectometry measurements.

The measurements presented in Figure 5-2 represent a state of quasi-equilibrium of the Pd/Mg30 at % Al system, resulting in limited information pertaining to the absorption process of the system. Consistent with Equation **3-7**, a large shift in the critical edge measurements corresponds to a large amount of deuterium absorption in the thin film. Conversely small shifts in the critical-edge measurements correspond to a small amount of deuterium absorption in the thin film. In Figure 5-3 the critical edge measurements taken at several deuterium pressures in the quasi-equilibrium state are plotted. The full NR measurements presented in Figure 5-2 show that the top and bottom catalysts layers absorb deuterium prior to absorption in the Mg-30 at % Al layer. As illustrated in Figure 5-3, the critical-edge measurements slowly shift to the right (higher angles) with increased deuterium pressure. Also the first Kiessig fringe periodicity does not change, suggesting little or no change in the characteristic thickness of the film. These two

observations (small critical-edge shift and little change in Kiessig oscillation frequency) suggest that sorption only occurs in the thin, catalytic layers; an observation supported through the analysis presented in Figure 5-2.

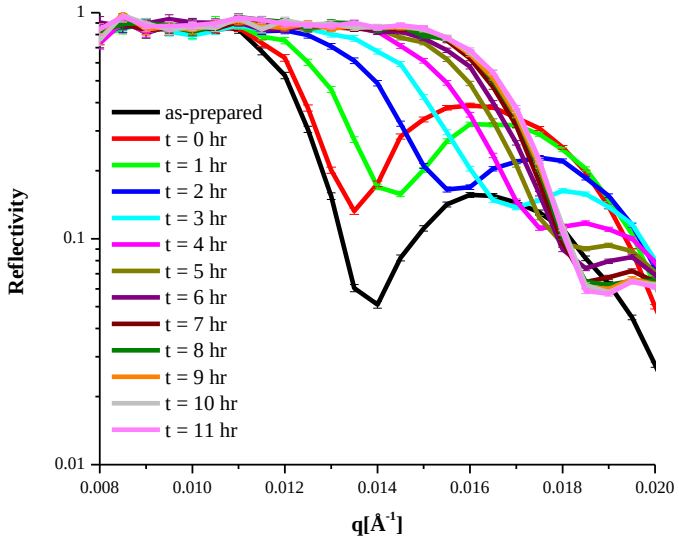

Figure 5-4 Neutron reflectivity critical-edge measurements (low q) of a Pd-catalysed Mg-30 at %Al thin film deposited on a Ta (10 nm)-coated (100) silicon wafer (see Figure 5-1). Measurements are taken at room temperature at 1309 mbar after a slow increase in the deuterium pressure as presented in Figure 5-2.

Only at 1.3 bar does the Mg-30 at % Al start to absorb a measureable amount of hydrogen, albeit, over a period of several hours. The deuterium concentration distribution in Figure 5-5 represents the equilibrium concentration after 1 hour and 10 hours of thin-film immersion in the 1.3 bar deuterium environment. Time-resolved hydrogen absorption measurements are achieved through neutron reflectivity critical-edge measurements. As illustrated in Figure 5-4 there is little shift in the critical-edge measurements from the as-sputtered sample to the sample immersed in 1.3 bar deuterium for a short period. After 1 hour immersion in the deuterium atmosphere, there is a significant shift in the critical edge, indicating a substantial uptake of

deuterium in the thin film. As expected the deuterium uptake is significant at first, though the uptake rate slowly tapers off, corresponding to a sigmoidal type of hydrogen absorption.

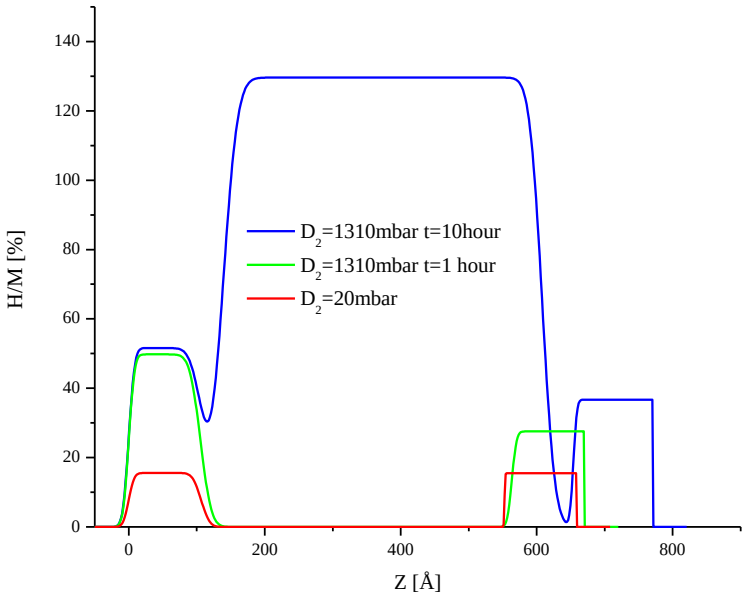

Figure 5-5 Hydrogen concentration profile of a Pd (10nm)-catalysed Mg-30 at %Al thin film deposited on a Ta (10nm)-coated (100) Si substrate. The thin film structure being investigated is illustrated in Figure 5-1.

Upon completion of the reflectivity curve measurements, the hydrogen concentration profile of the Pd catalysed structure as a function of the applied deuterium pressure (Figure 5-5) is determined from the SLD profile that was fitted to the measured data. These measurements are obtained using deuterium but it is estimated that there is little difference due to the use of hydrogen. As suggested by the changes in the SLD of the sample in 20mbar of deuterium, the hydrogen concentrations in the Pd and Ta catalysts are 15.6% and 15.5%, respectively. The concentration of hydrogen in the Pd is surprising given the solubility limit recorded by Pundt and Kirchheim as being 3% H/Pd and 1.5% H/Pd for nanocrystalline and polycrystalline Pd respectively [14]. In contrast, the solubility limit of H in Pd-H is measured at 44% H/Pd and 58% H/Pd for nanocrystalline

and polycrystalline Pd respectively. Therefore, the measured hydrogen concentration of the Pd layer at 6.7 mbar suggests a mixture of Pd and Pd-H and not purely a solid solution. Also, the final hydrogen concentration in the Pd layer mimics that of a polycrystalline Pd-H rather than nanocrystalline Pd-H. Finally, the deuterium concentration of 15.5% H/Ta in tantalum is consistent with polycrystalline Ta (bulk measurements) as previously reported [84].

After the deuterium pressure is increased to 1.3 bar, the deuterium concentration in the Pd and Ta layers increases to an H/M of 49.8% and 21.7% respectively. The high deuterium concentration is comparable to Pundt and Kirchheim's measurements of nanocrystalline Pd-H at 1.3 bar [14]. At this early stage there is still no substantial deuterium in the Mg-30 at % Al layer even though the equilibrium concentration is considerably higher.

After 10 hours of thin-film immersion in the 1.3 bar deuterium atmosphere, the Mg-30at% Al layer takes up a significant quantity of deuterium. The observed requirement of 1.3 bar pressure to hydrogenate the Mg-Al layer is surprising given the ease with which the catalysts layers are hydrogenated. Thermodynamically the Mg-Al layer should be more stable given that the enthalpy of formation of these hydrides is ΔH_{Mg}=-75kJ/mol [85], ΔH_{Pd}=-35kJ/mol [86], and ΔH_{Ta}=-70kJ/mol [84]. According to these equilibrium hydride formation enthalpies, the Mg-Al should tend to form a hydride prior to the catalysts, Pd and Ta. This leaves the supposition that the deuterium (hydrogen) absorption is hindered by a phase-transformation (Mg to Mg-H_2) barrier. These NR measurements are taken such that no noticeable changes in the reflectometry curve occur over the measurement period; therefore the hydrogen uptake in the Mg-Al layer may be

kinetically hindered. The source of the absorption barrier in these measurements cannot be determined and further experiments to address this point are presented later. In this section the aim is to illustrate the effects of the catalyst layer. The absorption process of the underlying Mg-Al layer is presented in Section 0.

5.2.Pd Catalysed Mg-x at % Al at Elevated Temperatures

In this section the effects of increased temperature on hydrogen sorption behaviour, catalyst stability, and the microstructure of a Pd catalysed Mg-x at % Al alloy are explored. It is important to increase the temperature due to the extremely low pressure at with magnesium absorbs and desorbs large amounts of hydrogen. According to the van't Hoff equation, at room temperature, this plateau pressure occurs at 10^{-6} atm – a pressure deemed too low for any practical system. Moreover, the hydrogen diffusion in magnesium is too slow to allow fast sorption kinetics. Therefore, the effects of increased temperature on hydrogen absorption in the magnesium alloy and catalyst are examined.

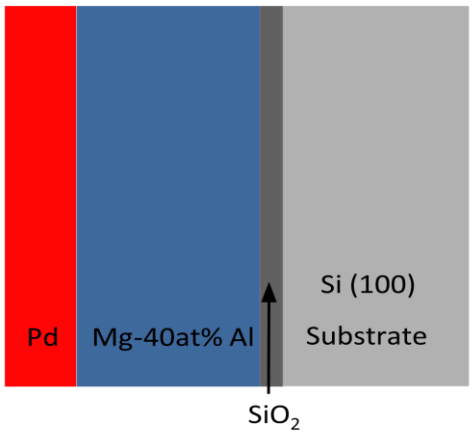

Figure 5-6 - Structure used to study the sorption behaviour of a Pd-catalysed Mg-40 at %Al thin film. The film consists of a Pd (10nm)-covered Mg-40 at %Al (50nm) native oxide (~1nm) silicon (100) wafer

The examination of the hydrogen absorption behaviour of a Pd catalyst at elevated temperature begins through ex-situ NR measurements of a Pd catalysed Mg-40 at % Al

thin film. This examination of a well-known catalyst (Pd) is being used as a baseline comparison for other catalysts developed for this study. As illustrated in Figure 5-6, the structure used to measure at elevated temperatures consists of a 10nm Pd-covered Mg-40 at % Al film deposited on a native oxide (1nm) silicon wafer. The Ta diffusional barrier is eliminated in this study to exclude its catalytic effects on hydrogen sorption.

The neutron reflectivity measurement of the Pd catalysed Mg-40 at % Al thin-film is illustrated in Figure 5-7. The measured (open circles) and calculated (solid line) reflectivity curves of the Ta/$Mg_{70}Al_{40}$/Pd film structure are shown as a function of the scattering vector q in Figure 5-2. The visible oscillations, referred to as Kiessig fringes, are associated with the total thickness of the film. In this study the desorption measurements are the focus as this is the area where degradation of the catalysts occurs.

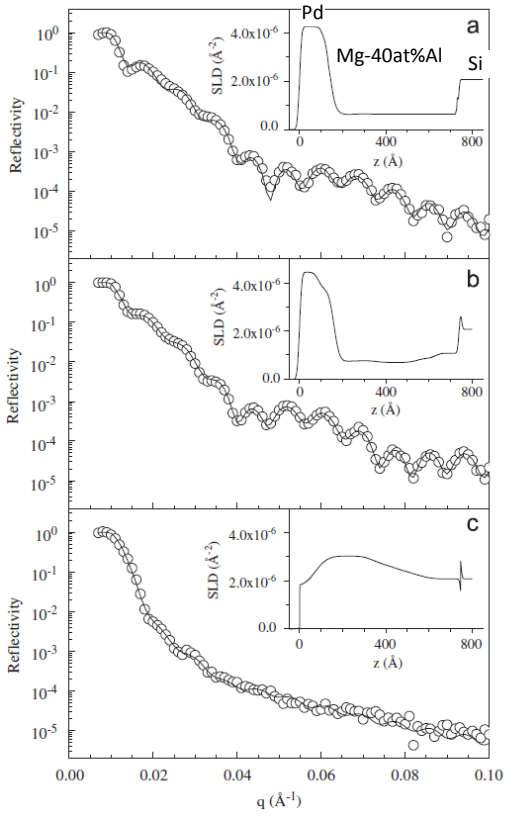

Figure 5-7 Neutron reflectometry measurements of a Pd-covered (10nm) Mg-40 at %Al thin film on a (100) Si substrate (see Figure 4 16). (a) Hydrogenated at 125°C and 30 bar and measured ex situ in an inert atmosphere at room temperature. (b) Measured at 200°C in an inert atmosphere. (c) Measured at room temperature in an inert atmosphere after annealing at 200°C for 24 hours. This figure is published in[87] and reproduced without alteration.

The fully hydrided Mg-40at% Al thin film is clearly indicated by a low SLD of the Mg layer compared to the as-deposited Mg- 40 at % Al layer (not shown). In this state the interfacial roughness and thickness of the Pd layer is nearly identical to that of the as-sputtered structure. This observation is not surprising given that the formation enthalpy is much lower for Mg-Pd than Mg-H_2, resulting in a lower Gibbs free energy, which favours the formation of Mg-H_2 over Mg-Pd intermetallics; however no conclusion about formation kinetics can be made.

The difference between the SLD of the as-sputtered structure and hydrogen-absorbed structure can be used to determine the hydrogen concentration within each layer. In

this study the hydrogen is absorbed prior to the neutron experiments and neutron reflectometry experiments performed in air at room temperature. Therefore, it is expected that the hydrogen within the palladium desorb but the more stable magnesium hydride remains stable during NR measurements. As illustrated in Figure 5-7 the SLD of the Pd in the absorbed state is nearly identical to the bulk Pd SLD at 4.0 $x10^{-6}$ $Å^{-2}$. The change in the SLD of the Mg-40 at % Al layer corresponds to a hydrogen concentration of 85 % H/M or a hydrogen gravimetric capacity of 3.1 wt%.

The as-prepared sample is similar to the previous sample measured in air (see Figure 5-2a) and clearly indicates the as-synthesized structure as a Pd (10nm), Mg-30 at % Al (50nm), and Ta (10nm) buffer layer on top of a Si (100) substrate. The SLD of each of these as-synthesized layers is well within 10% of the expected SLD from bulk measurements [51]. The sharp delimitation of each layer indicates minimal interfacial roughness and little or no mixing between each layer.

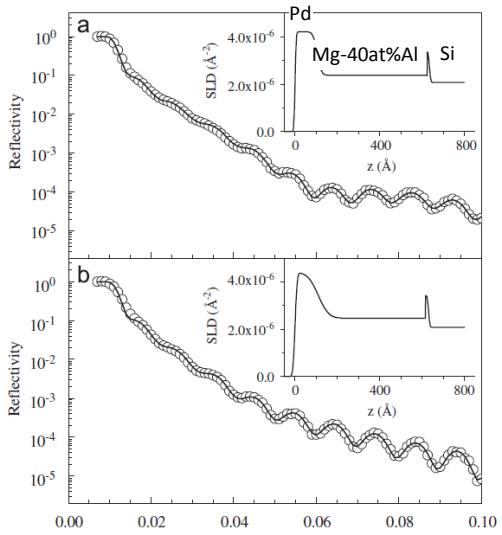

Figure 5-8 Neutron reflectometry measurements of a Pd-covered (10nm) Mg-40 at %Al thin film on a (100) Si substrate (see Figure 4 16). (a) As prepared film in an inert atmosphere. (b) Measured at room temperature in an inert atmosphere after being annealed at 200°C for 24 hours. Note the silicon substrate native oxide is not removed prior to deposition and can be easily seen in the scattering length density profile. This figure is published in [87] and reproduced without alteration here.

To study the influence of hydrogen absorption/desorption on interdiffusion an as-prepared Mg-40at%Al film is annealed at 200°C for 24 hours. The difference in the NR curves can be seen in Figure 5-8, where (a) represents the as-prepared state and (b) represents 24 hours annealing at 200°C. The main effect of annealing is an increase in the Pd/Mg-40 at% Al interface roughness from 1.5 to 3 nm. However, the Pd layer is easily distinguishable in contrast to a Mg-40at % Al film that has been charged with hydrogen and annealed at 200°C for 24 hours (see Figure 5-7c). The most probable reason for enhanced inter-diffusion in the films that have been charged with hydrogen is the well-known effect of hydrogen distorting the film structure and creating voids and pores within the magnesium layer; a property observed by Sunitha *et al* [88].

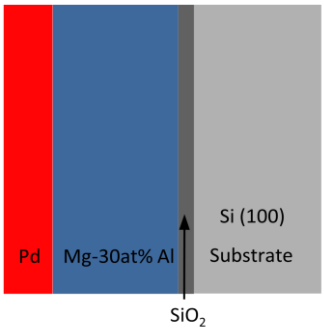

Figure 5-9 Structure used to illustrate the sorption behaviour of Pd-catalysed Mg-40 at %Al thin film

Neutron reflectometry scans of a Mg-30at % Al thin film (see Figure 5-9) annealed at 200°C for 1 hour, 3 hours, and 9 hours are shown in Figure 5-10. The data presented in Figure 5-10 can only be fitted with a seven layer slab model as a reduced layer model does not adequately fit the measured data. As can be deduced from Figure 5-10, the film is desorbed after 1 hour annealing at 200°C with the Pd layer still intact. After 3 hours at 200°C the SLD at the location of the Pd layer decreases from 4 to 3.5 $x10^{-6}Å^{-2}$ and at the same time the SLD of the Mg--Al in contact with the Pd layer decreases. This certainly demonstrates palladium interdiffusion into the Mg-Al layer. After 9 hours of annealing (see Figure 5-10c) the Pd layer cannot be discerned from the Mg-Al layer. Interestingly, the Pd distribution within the Mg layer is not homogenous and suggests a higher concentration of Pd in the centre of the film.

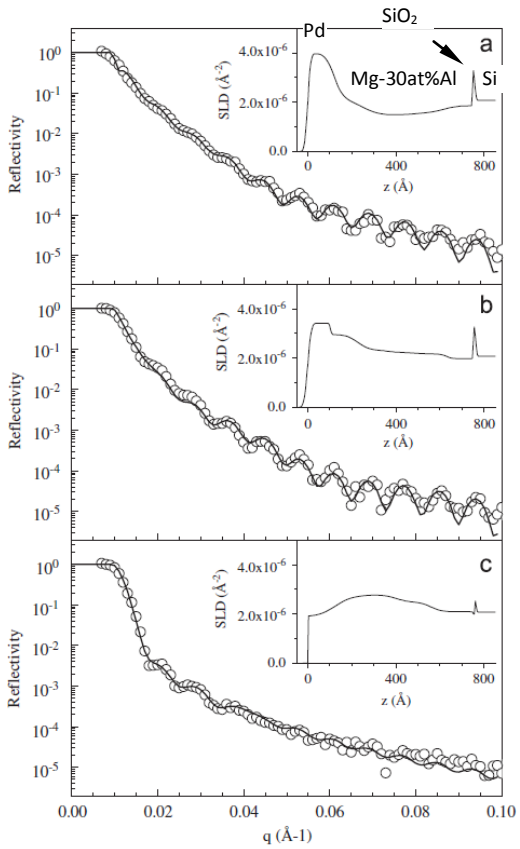

Figure 5-10 Neutron reflectometry measurements of Pd (10nm)-covered Mg-30 at %Al (50nm) thin film on a (100) oriented Si substrate. (a) After 1 hour annealing at 200°C. (b) After 3 hours at 200°C. (c) After 9 hours annealing at 200°C. Experiments are performed in air at room temperature ex situ to sorption experiments. This figure is published in [87] and reproduced here without alteration.

Sunitha at al. describe a detailed experiment of the interdiffusion of Pd in Mg with and without a high concentration of defects [88], which supports the conclusion stated above. Sunitha et al use Rutherford backscattering to measure the atomic distribution and therefore determine the interdiffusion rates. In the measurements they discern that at elevated temperature (> 200°C) diffusion occurs across the Pd-Mg interface. It is also surprising that they can measure Pd diffusion into the Mg and out diffusion of Mg through the Pd layer. This observation of mixing is consistent with the NR measurements in Figure 5-7 and Figure 5-10, where the Pd exists in the middle of the film rather than as an alloy close to the surface (an elevated SLD). Therefore, these

measurements support the conclusions of the mechanisms behind hydrogen-assisted interdiffusion of the Mg-Pd, as stated above.

5.3.Conclusions about a Simple Pd-Catalysed Mg-x Al System

The motivation for these experiments is to illustrate the kinetics and hydrogenation stages of a simple system at room temperature and elevated temperatures. In this investigation the measurement results obtained conclusively illustrate the hydrogen uptake mechanisms. These results have not been seen before when using an in-situ technique. As expected, the single Pd catalyst works as it does in previous studies, with hydrogenation at room temperature requiring relatively high hydrogen pressure with low uptake rates. Moreover, the Pd catalyst absorbs hydrogen prior to absorption in the main Mg alloy layer.

The present study provides insight into the hydrogen absorption mechanism of nanoscale films at room temperature; in particular, the hydrogenation of Pd catalysed Mg alloys. A non-absorbing region develops between the Mg and Pd catalysts, which is the result of stress created between the nonexpanding Pd layers and absorbing Mg layers and the considerable traction between the layers. Finally, the deuterium absorption in the Mg – 30 at % Al reaches 1.35 D/M or the equivalent of ~5.4 wt % H/M, a substantial value at room temperature. These findings clearly indicate that a degree of optimization can be achieved by controlling the nanoscale thin-film structure. This research can be used to generate a new set of hydrogen materials and processes that can be scaled up to commercial quantities.

At elevated temperatures, hydrogenation occurs more rapidly but at the expense of degradation of the Pd layer during de-hydrogenation. A study performed by Sunitha *et*

al. [88] illustrates that an interdiffusion of Mg/Pd occurs at a critical temperature for a given thickness of the Pd catalyst. The thicker the Pd layer, the higher the temperature or pressure required for the onset of hydrogen diffusion. Degradation of the Pd catalysts occurs through diffusion of Pd into Mg in conjunction with Mg out-diffusion through the Pd layer to the surface. The resulting Mg-rich surface can severely degrade the hydrogen sorption kinetics and may eventually eliminate the Pd catalytic effect. Du et al. [89] conclude that even a small amount of Pd on a Mg surface will increase the hydrogen sorption kinetics through a hydrogen spillover mechanism.

6. Binary Catalysts

Borgschulte et al. [90] describes palladium as the best hydrogen-dissociative catalyst, with several other catalysts only showing promise. The deleterious effect of Pd-Mg mixing drastically reduces the usefulness of Pd as a catalyst; therefore it has spurred the use of a bi-layer catalyst. Depending on the nature of the support layers, the hydrogen absorption may be enhanced or hindered. Previous studies of the thermodynamics of bi-layer catalysts illustrate the presence of strong metal support interactions (SMSI) [91]. In the case of hydrogen-storing films, the intermediate layer between the surface catalyst and the base material serves the critical role of reducing deleterious inter-diffusion while increasing the sorption rates. [92]

Rembhof et al. are first to utilize a metallic Nb intermediate layer between the catalytically active palladium cap and the hydrogen storing yttrium phase, though they do not provide a comprehensive understanding of the effects, if any, of the support layer. [93] Pasturel reports an early study of the effects of using bilayer catalysts [94]. In this study the kinetics of absorption are characterized through optical transmittance and reflectance of the thin film structure (Mg_2Ni/50nm and TM/10nm) at moderate pressure and room temperature. Through investigation of several transition metals (TMs) such as Ti, V, Cr, Mb, Fe, Co and Ni, a strong correlation between kinetics and enthalpies of the solution of H in the TM is observed. This investigation, albeit detailed, does not measure the hydrogen concentration distribution within the film but rather deduces it through correlation with theoretical predictions. The diffusion model generated is based on chemical potentials of the hydrogen in the metals and agrees qualitatively with the experimental results.

In this section the role of catalysts is explored by using NR measurements to obtain the hydrogen distribution within the film. The NR experiments are performed *in-situ* to the absorption measurements, potentially providing a detailed understanding of the sorption process without making assumptions about the hydrogenation process.

6.1.Mg-30 at % Al with a Pd/Ta Bi-layer Catalyst

The investigation of bi-layer catalysts begins with NR measurements of a Pd/Ta bilayer catalyst on a Mg-30 at % Al thin film deposited on a 10nm Ta-coated silicon wafer (see Figure 6-1).

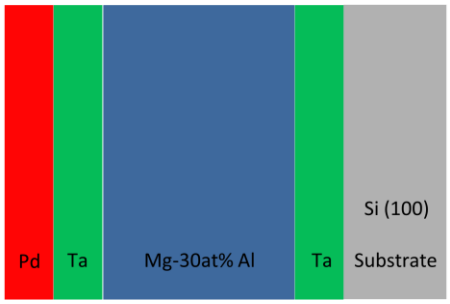

Figure 6-1 Pd/Ta (5nm/5nm)-catalysed Mg-30 at %Al thin film deposited on a Ta (10nm)-coated (100) silicon wafer. Note the native oxide is removed prior to Ta deposition by an in situ back sputtering method motivated by a reduction in complexity.

Figure 6-1 shows the thin film structure used to determine the hydrogen sorption behaviour of the Pd/Ta (5nm/5nm) bilayer catalyst. The main hydrogen storage medium is the Mg-30 at % Al as is the composition with the highest hydrogen sorption rates. The Ta layer, sandwiched between the Si substrate and the Mg layer, prevents Mg-Si intermetallic formation and acts as a good neutron contrast to the other layers, a requirement suggested in section 3.2.

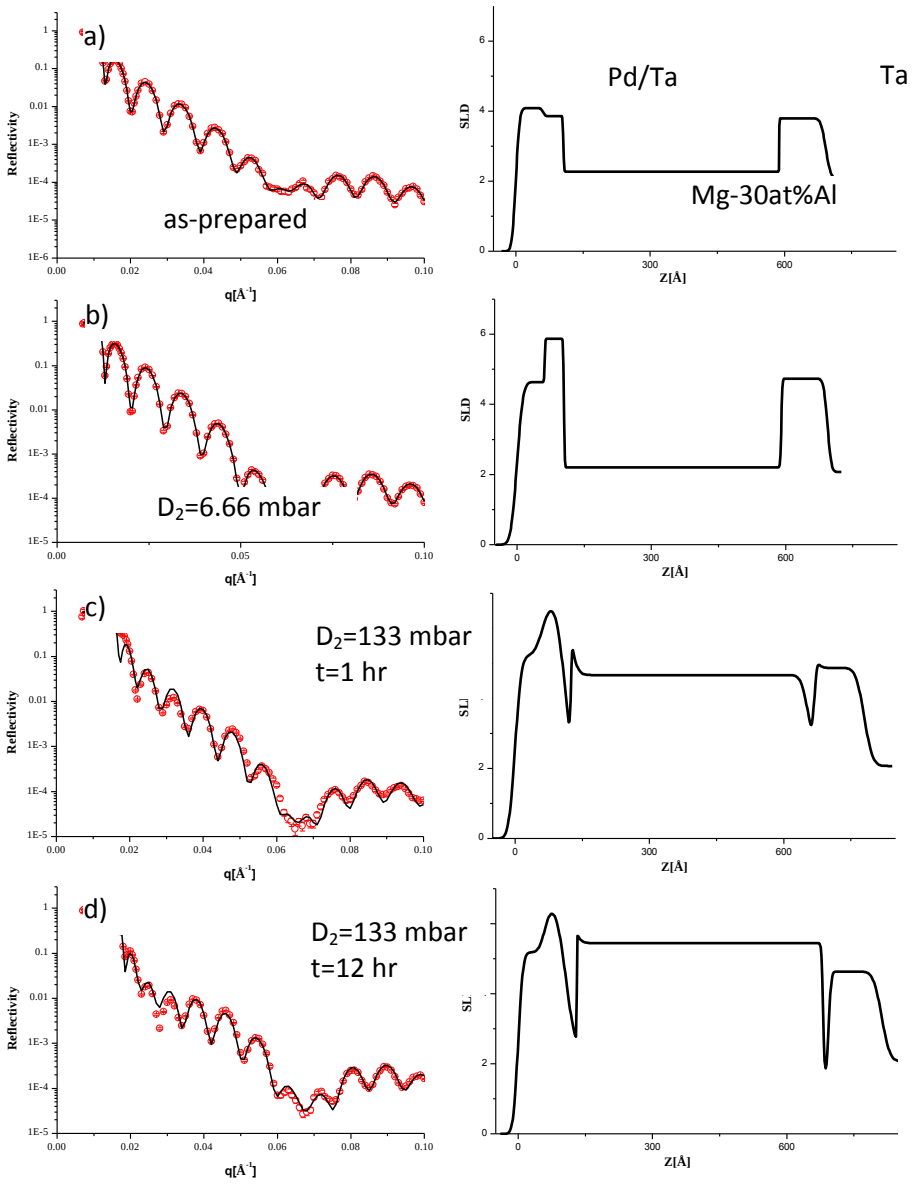

Figure 6-2 2 Neutron reflectometry measurements of Pd/Ta (5 nm/5nm)-catalysed Mg-30 at% Al thin film deposited on a Ta (10nm)-coated (100) Si substrate (see Figure 6-1) (a) As-sputtered state. (b) D_2 = 6.66 mbar. (c) D_2=133 mbar, t = 1 hr. (d) D_2=133 mbar, t = 12 hr. Absorption experiments are performed in situ to neutron reflectometry measurements and performed at room temperature (20°C). The sample was held at 6.66mbar for a total of 5 hours and 133mbar for 14 hours. The time indicated above is the time the sample was at the indicated pressure before the measurement was taken.

The NR measurements of the Pd/Ta catalysed Mg-30 at % Al (50 nm) thin film deposited on a 10nm Ta-coated silicon wafer are given in Figure 6-2. The reflectivity measurements are illustrated on the left with the corresponding real-space representation of the structure on the right. The SLD and layer thickness of the as-

deposited microstructure corresponds to expected values from synthesis and previous bulk measurements [51]. Following the measurement of the as-deposited film in vacuum, deuterium is slowly introduced into the sample cell within the NR apparatus. Throughout the pressure increase, critical-edge measurements are continuously taken to deduce if any hydrogen sorption has occurred. Once the critical edge stabilizes for ~1/2 hour, a full NR measurement is taken. At 6.66 mbar D_2, the SLD profile shows an increase in the top and bottom layers while the SLD of the Mg-30 at % Al remains unchanged. Therefore, appreciable absorption in the catalysts layers occurs but little or no deuterium is present in the Mg-30 at % Al layer.

Upon increasing the deuterium pressure to 133 mbar, appreciable changes in the reflectivity and SLD of the thin film are observed, corresponding to absorption in the Mg-30at% Al layer. In this instance a simple four layer model is insufficient for properly fitting the reflectivity curve, but a six layer model adequately correlates to the measurements. The two extra layers in the model correspond to small gaps that are ~10 to 20Å in width between the Mg and Ta catalytic layers. After another 11 hours at a deuterium pressure of 133 mbar, there is a slight increase in the SLD of the Mg-Al layer, corresponding to a D/M=1.3, or the equivalent of 5 wt.%. This value is approximately 20% higher than the 4.1 wt%, reported previously– likely the result of the in situ approach, which prevents partial desorption in air.

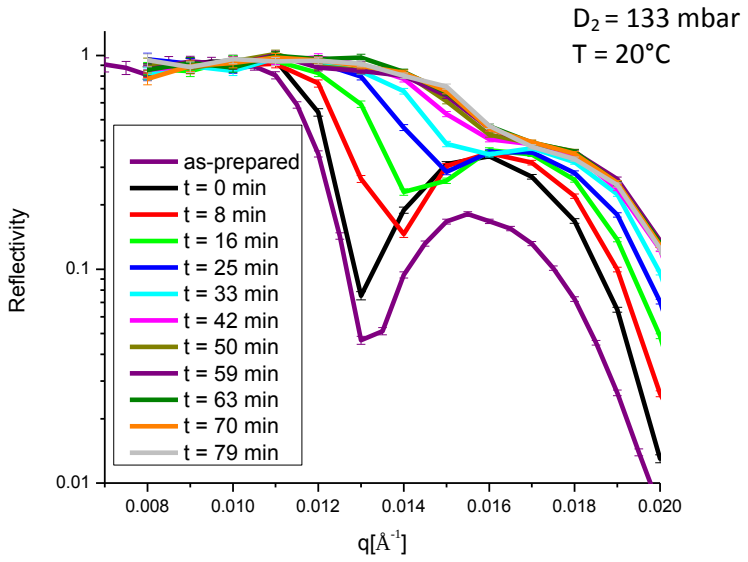

Figure 6-3 Neutron reflectometry critical-edge measurements of Pd/Ta (5nm/5nm)-catalysed Mg-30 at %Al thin film deposited on a 10nm Ta-coated (100) Si wafer (see Figure 6-1). Measurements are performed at room temperature in situ to deuterium absorption at a deuterium pressure of 133 mbar

The neutron reflectivity critical-edge measurements of the Pd/Ta catalysed thin film (Figure 6-1) are plotted in Figure 6-3. These critical edge measurements are important in that they can be quickly acquired and can provide a qualitative understanding of the absorption process. For instance, that at t_0 - that there is little or no absorption in the Mg-Al layer but there is appreciable deuterium absorption in the catalyst layers (Pd, Ta).

As illustrated in Figure 6-3 the critical-edge moves noticeably to the right with a larger shift upwards in the first Kiessig fringe oscillation after 8 minutes of immersion in deuterium. Later it is argued that the increased amplitude of the Kiessig oscillations is due to an increase in the contrast between the catalyst layers and bulk Mg-30 at % Al layer, i.e. a larger difference in the SLD of the catalyst layer than the Mg-Al layer. The evidence that supports this claim is the absence of a large shift in the critical edge, meaning only a small amount of deuterium is being absorbed-assuming each layer uniformly absorbs deuterium and there is only a small gradient within each layer. Since

there is little or no shift in the critical edge, the absorption of deuterium therefore occurrs only in the smaller layers (i.e. the Ta or Pd layers). These observations are similar to the observations regarding the Pd catalysed Mg-Al film in Figure 5-4 and the corresponding SLD of the film in Figure 5-2.

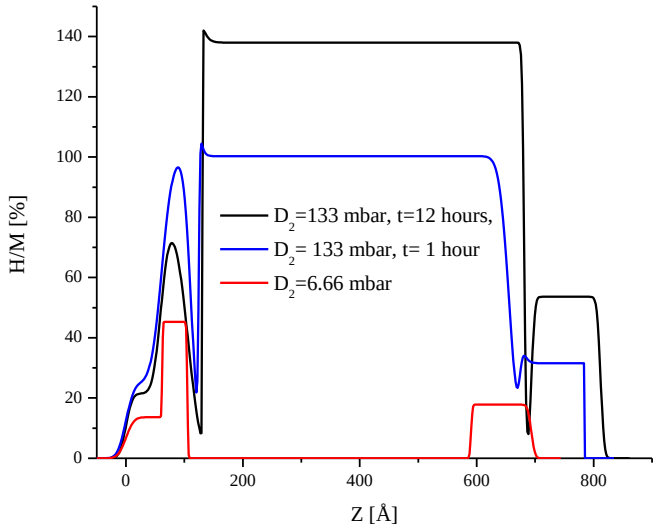

Figure 6-4 Hydrogen concentration profile of a Pd/Ta (5nm/5nm)-catalysed Mg-30 at %Al thin film deposited on a Ta (10nm)-coated (100) Si substrate (see Figure 6-1).

Upon completion of the neutron reflectivity measurements in Figure 6-2, and calculation of the SLD profiles, the hydrogen concentration profile through the surface normal of the film is calculated. As given by the SLD profile, the hydrogen is absorbed in the Pd/Ta catalysts layers prior to the main Mg-Al layer. This observation is in accordance with the neutron measurements of the pure Pd catalysed film (see Figure 5-5). Furthermore, given that Mg can thermodynamically transform into a metal hydride at

$H_2 \approx 0.09$ mbar at room temperature, it is expected that MgH_2 will form. Therefore, the unexpected low absorption at 6.66 mbar may be attributed to the nucleation barrier for Mg-MgH_2 formation.

On increasing the deuterium pressure to 133 mbar, the deuterium concentration in the Pd, Ta layers increases and appreciable deuterium absorption in the bulk Mg-Al layer occurs. Comparison of the Pd/Ta catalyst and the single Pd catalyst layer shows that the Mg-Al takes hydrogen up at a significantly reduced pressure. This observed pressure difference may be attributed to the higher level of activity of the binary catalysts compared to the single catalyst. The pure Pd catalyst is slow enough at reduced pressure to allow full measurements with the conclusion that no absorption has occurred. Therefore, it can be concluded that there enhanced kinetics at this moderate pressure (133 mbar) and at room temperature for the binary Pd-Ta catalysts compared to the pure Pd catalyst.

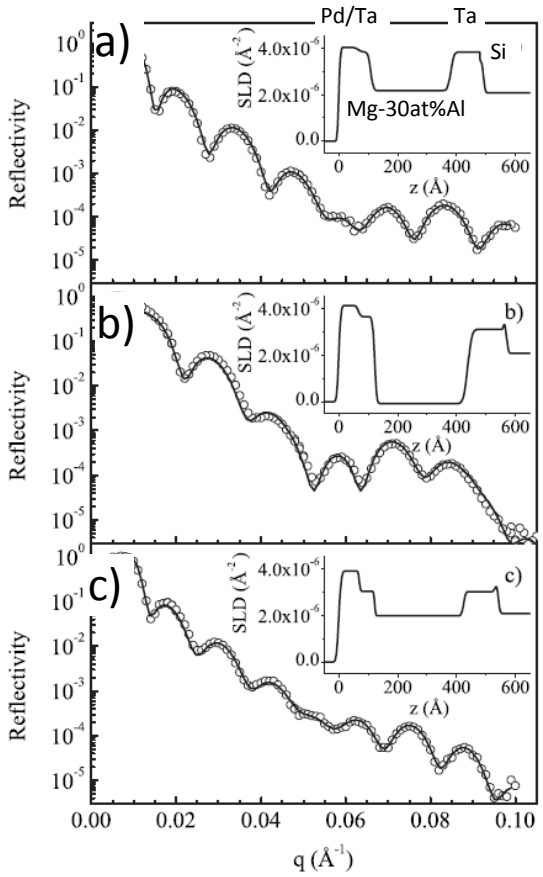

Figure 6-5 Neutron reflectometry measurements of Pd/Ta (5nm/5nm)-catalysed Mg-30 at %Al thin film deposited on a Ta (10nm)-coated (100) silicon wafer (see Figure 5 1a). (b) After hydrogen is absorbed by the thin film for 24 hours at 125°C and 40 bar hydrogen (measurements performed under an inert argon atmosphere at room temperature). (c) Desorption measurements are performed in situ in the sample cell equipped with a heater. The sample is kept at the described temperature for at least 1 hour before neutron reflectometry measurements commence

In addition to deuterium sorption experiments, sorption measurements involving hydrogen are performed to confirm the results. Figure 6-5 shows the neutron reflectivity measurements of the Pd/Ta catalysed Mg-30 at % Al thin film deposited on a 10nm Ta silicon wafer, a structure depicted in Figure 6-1. Measurements are taken before hydrogen absorption (see Figure 6-5a), after hydrogen absorption at 25°C in an inert atmosphere (see Figure 6-5b), and after full desorption at 100°C (see Figure 6-5c). Changes in the film structure are indicated by changes in the SLD profile depicted in the

insets of each reflectivity curve. In all cases the model used to describe the profile consists of a four-slab model, corresponding to each of the deposited layers.

The effect of hydrogen sorption on the thin film structure is easily seen through a comparison of the as-deposited SLD and the sorbed and unsorbed SLD profile. The negative scattering length of the hydrogen causes the SLD of the Mg-30 at % Al structure to drop from 2.2 $x10^{-6}$ $Å^{-2}$ for the as-deposited film to 7.3$x10^{-8}$ $Å^{-2}$ for the fully absorbed film, yielding a hydrogen concentration of 4.7wt% in the Mg-30 at % Al film. After a full anneal at 100°C for 1 hour, the SLD of the Mg-30at%Al thin film returns to 2.0 $x10^{-6}$ $Å^{-2}$, suggesting release of hydrogen. The SLD may not reach the as-sputtered SLD values due to the creation of cracks and voids that are much smaller than the coherency length of the neutrons and therefore results in lowering of the SLD for that layer. Or, the SLD may not reach the as-sputtered SLD value due to only a partial desorption at 100°C and 1 hour. Furthermore, the SLD of the Ta layer decreases during the desorption process leading to the conclusion that a small amount of hydrogen is being stored in that Ta layer. The sharp interfaces between the Ta and Mg-30at%Al suggest that the Ta is intact and therefore is stable over the applied temperatures.

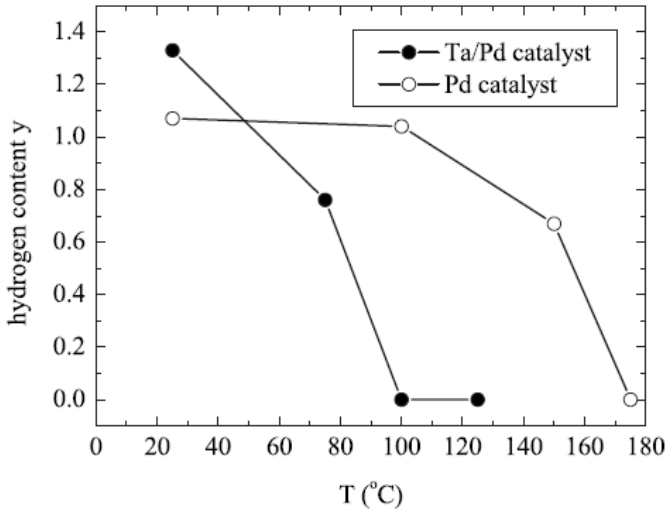

Figure 6-6 – A comparison of the equilibrium hydrogen concentration at several temperatures of Pd/Ta (5nm/5nm) and Pd (10nm)-catalysed Mg-30 at %Al thin film structure depicted in Figure 5-9 and Figure 6-1 respectively.

Comparison of hydrogen content of the Pd/Ta catalyst to that of the Pd catalyst (see Figure 6-6) at the temperatures investigated shows that the bi-layer catalyst reduces the temperature necessary to achieve full dehydrogenation from 170°C to 100°C as compared to the pure Pd catalyst. This result is extremely surprising as one would expect that the bi-layer catalyst would only increase the rate of absorption but should not affect the ability to take up hydrogen. This could be explained if it were assumed that the rate of hydrogen uptake in the Pd-catalysed sample was severely limited and the catalyst did not change the temperature at which hydrogen absorption occured(i.e. the rate would be slow enough that no appreciable hydrogen sorption would occur during the measurement period). This observation is consistent with the high-temperature measurements illustrated in Figure 4-6. A JMAK curve fails to fit these measurements; therefore a simple phase transformation process does not occur. Given that the surface catalysts play a large role in the hydrogen uptake measurements, one cannot exclude their contribution.

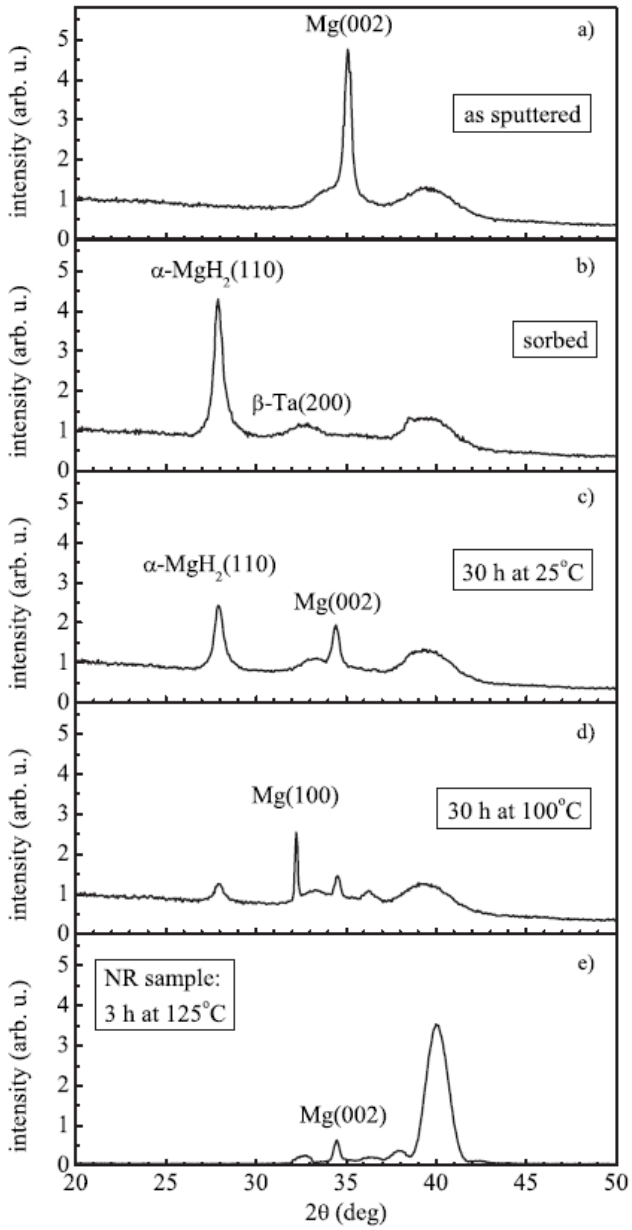

Figure 6-7 - X-ray diffraction measurements of Pd/Ta (5nm/5nm)-coated Mg-30 at %Al thin film deposited on a Ta (10nm)-coated (100) silicon wafer (see Figure 6-1).

Confirmation of the NR results is achieved by examining the crystal phases of the thin-film structure through XRD experiments. Figure 6-7 shows the XRD measurements of the Pd/Ta catalysed thin-film structure depicted in Figure 6-1, (a) as deposited, (b) measured immediately after hydrogen absorption, (c) as measured at room temperature after storage for 30 hours after absorption, and (d) as annealed at 100 °C in argon for 30

hours. For comparison, the XRD measurement of the sample immediately investigated after hydrogenation. The NR was also measured and displayed in Figure 6-7e.

The as-synthesized microstructure consists of a supersaturated Al solid solution in a Mg solute. The absence of several diffraction peaks suggests a preferred orientation of (100), oriented perpendicular to the surface of the sputtered thin-film. The diffraction peak of the Mg (002) at 2θ=35.1°, which marks a clear shift from the pure Mg peak of 34.4°. This diffraction peak shift is consistent with a contraction of the lattice parameters and Vegard's law for the behaviour of the solid solution. After sorption, the Mg (002) peak disappears and the α-Mg-H_2 (110) peak appears at 2θ=27.9°. This observation is consistent with the expected values and no shift due to Al in solution. These measurements do not illustrate any ternary hydride formation and no Mg peaks, indicating a full Mg to Mg-H_2 transformation. The XRD pattern illustrated in Figure 4-10 illustrate that formation of ternary hydrides, Al hydride, or the formation of any Pd-Mg or Pd-Ta intermetallics were not possible under the experimental conditions (pressure, temperature)

The diffraction pattern of the sorbed film stored at room temperature for 30 hours is shown in Figure 6-7c). The relative intensity of the α-Mg-H_2 decreases with the appearance of an magnesium peak. This clearly indicates that desorption has occurred at room temperature even though the system should be kinetically limited. Heating the film to 100°C in an inert atmosphere for 30 hours indicates the microstructure consists of Mg with only a small amount of α- Mg-H_2. No other diffraction peaks are observed and the formation of $Mg_{17}Al_{12}$ or other intermetallic cannot be confirmed. Further XRD

experiments, illustrated in Figure 4-10 , confirm the absence of other intermetallic compounds during desorption at room temperature or at 100°C.

The NR sample (see Figure 6-7e), when heated to 125°C for 3 hours does not show the presence of MgH_2. This suggests that either (a) full desorption has occurred or (b) partial absorption occurred and the diffraction peak from MgH_2 does not show through the background noise of the X-ray diffractometer. It is not surprising that full desorption of the sample occurs given the small size of the sample.

6.2.Mg-30 at% Al with a Pd/Ti Bi-layer Catalyst

The investigation of the effects of bi-layer catalysts continues through examination of a Pd/Ti catalyst, which has garnered a substantial amount of interest [33, 24]. Interest in using a Ti diffusion barrier has been generated by observed precipitation of Ti/(Ti-H_2) in a supersaturated Mg-Ti alloy, see for a few examples[95, 96, 97, 34, 98]. This observed incoherence between the Ti/(Ti-H_2) phases has led Baldi [24] to use the Pd/Ti catalyst as a method to alleviate the traction problem between the Mg and Pd catalyst and thus allow full hydrogenation of the Mg layer at a reduced pressure.

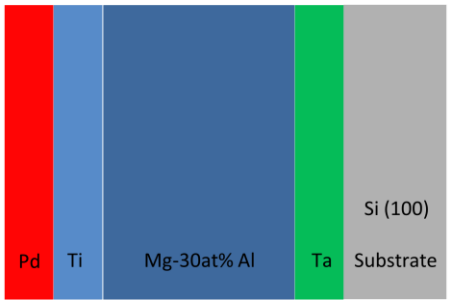

Figure 6-8 Pd/Ti (5nm/5nm)-catalysed Mg (50 nm) thin film deposited on a Ta (10nm)-coated (100) silicon substrate

The catalyst effect of a Pd/Ti (5nm/5nm) catalysed Mg-30at% Al alloy deposited on a Ta (10nm)-coated silicon wafer is investigated (see Figure 6-8). The catalyst thicknesses of

5nm/5nm are chosen to directly compare the Pd/Ta catalyst performance and not to independently optimize of the catalyst. Further research must be conducted to optimize the catalyst deposition parameters (e.g. thickness, deposition rate, etc).

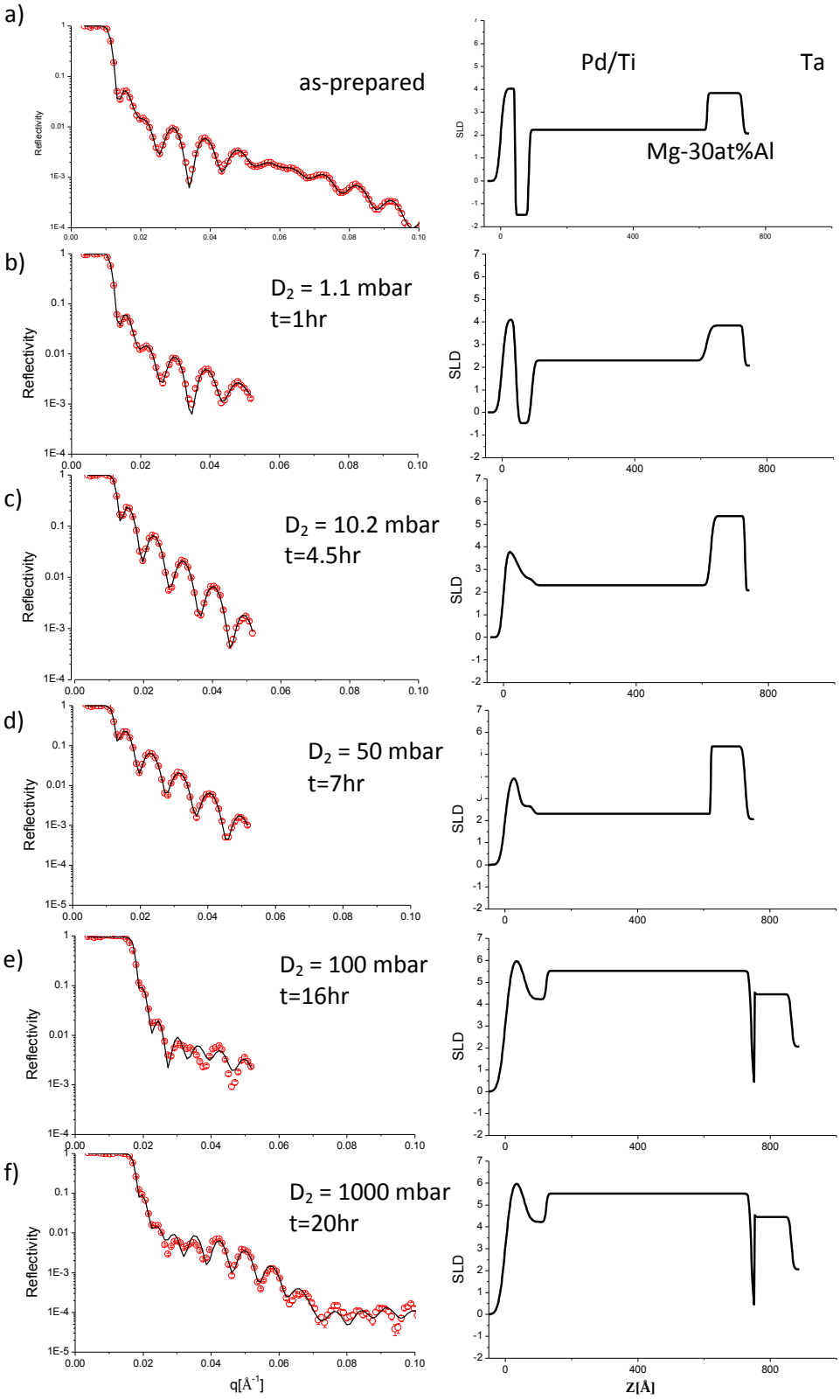

Figure 6-9 Neutron reflectometry measurements of Pd/Ti (5nm/5nm)-catalysed Mg-30 at %Al thin film deposited on a Ta (10nm)-coated (100) Si wafer. (a) As-sputtered state. (b) D_2 = 1.1 mbar for 0.5 hours (c) D_2 = 10.2 mbar for a total 3 hours. D2=2- mbar for a total of 0.75 hours (not shown) (d) D_2 = 50 mbar for a

total of ~1 hour. (e) D_2 = 100 mbar for a total 9 hours. (f) D_2 = 1000 mbar for a total of 4 hours. Absorption experiments are performed at 20°C and in situ to NR measurements. The time stated above is the time at which the scan was initiated.

The neutron reflectivity measurements of the Pd/TI catalysed Mg-30 at% Al thin film (50nm) deposited on a Ta (10nm)-coated silicon wafer are depicted in Figure 6-9. The reflectivity measurements are depicted on the left, and the corresponding real-space SLD representation of the structure is on the right. The SLD and layer thickness of the as-deposited microstructure are consistent with the expected SLD values and synthesis methods (see Figure 6-9a) [51]. Titianium has a large negative SLD and any deuterium being absorbed in that layer can be easily seen. Following the measurement of the as-deposited film in vacuo, deuterium is slowly introduced into the sample cell within the neutron beam. At every pressure increase NR measurements were taken until no noticeable changes have occurred. Once no noticeable changes occurred over a period of half an hour, a full NR measurement is taken. In the NR measurements illustrated in Figure 6-9(b-e), these NR measurements were only taken up to q=0.05 $Å^{-1}$, limiting the real space resolution. Great care has been taken to correlate the SLD to the reflectivity curves but small differences may occur. For instance a small interface devoid of hydrogen may exist between the Ta and Mg layers in panels (b-e) in Figure 6-9 but cannot be concluded. Even the interface noted in panel e was included for consistency to the longer scan of panel f.

Upon increasing the deuterium pressure to 1.1 mbar, the sample absorbs deuterium only in the top Pd/Ti catalyst bi-layer. In particular, the Ti layer absorbs a significant amount of deuterium as indicated by significant changes in the SLD. Furthermore, there is little, or no, deuterium in the Mg-Al, Pd, and Ta layers, consistent with previous bulk measurements. After an increase in pressure to 10.2 mbar, the deuterium concentration in the catalyst layers (Pd/Ti and Ta) significantly increases. Moreover the absence of

deuterium in the Mg-Al layer is attributed to the relatively large nucleation barrier for Mg-(Mg-H_2) formation and therefore a greater driving force (or pressure) is required for full absorption. Increasing the deuterium pressure to 50 mbar causes only a small increase in the SLD of the Mg-Al layer, corresponds to a small increase in deuterium absorption in the film (see Figure 6-9d). Only after increasing the deuterium pressure to 100 mbar does significant absorption occur. The deuterium absorption in the Mg-Al layer is significant, similar to the absorption measurements of the Pd/Ta catalysed film (see Figure 6-2). The SLD that seems to fit the reflectivity curve requires a region of lower SLD between the Mg-Al and the underlying Ta layer. This conclusion is consistent with a longer scans at a higher deuterium pressure of 1bar (see Figure 6-9f). According to previous measurements, the depressed SLD regions, hereafter referred to as gaps, are attributed to traction between the Mg and rigid catalysts layers. Qualitatively, Mg-Ti is immiscible, therefore there is little traction between the Mg and Ti layers. However, Mg-Ta can form intermetallic mixtures, albeit very slowly, suggesting significant traction between the Mg and Ta layers. Such reduction of the traction between the layers allows the thin Mg layer to expand and transform from Mg to Mg-H_2, effectively behaving as a free layer. If significant traction between the layers exists, the Mg is not free to expand, resulting in a large strain adjacent to the interface and arresting absorption. Previous studies have illustrated that due to elastic constraints, the equilibrium pressure of hydrogen absorption increases. – a result not conclusively shown here. Increasing the deuterium pressure to 1 bar, a gap a gap persists between Mg and Ta but no gap is observed in the Ti/Mg interface. Moreover, at 1 bar there is full hydrogenation of the Ti and Mg-Al layers, as suggested by the small change in the SLD over several hours.

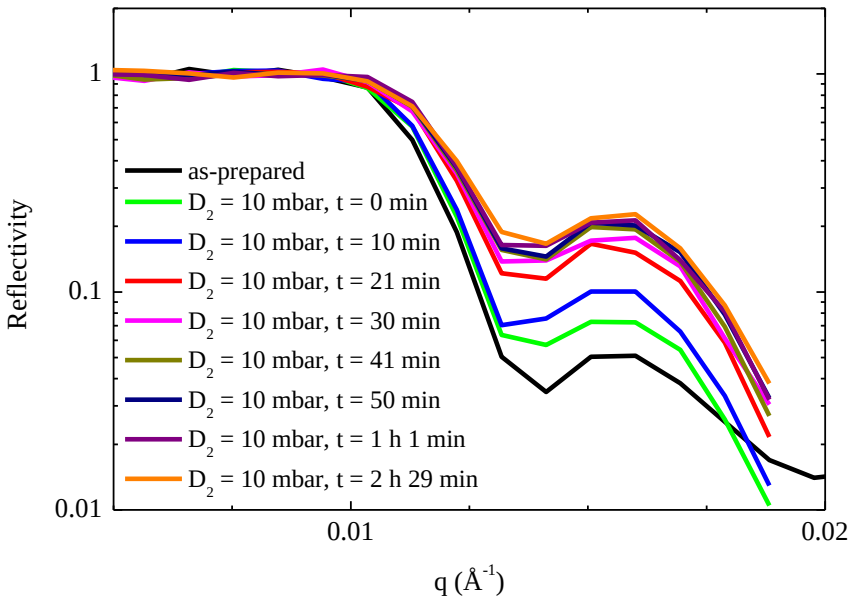

Figure 6-10 Neutron reflectometry critical-edge measurements of Pd/Ti (5nm/5nm)-catalysed Mg-30 at % Al thin film deposited on a 10nm Ta (100)-coated silicon wafer

Critical-edge measurements of the Pd/Ti catalysed Mg-30 at% Al thin film immersed in a 10 mbar deuterium environment are depicted in Figure 6-10. These critical-edge measurements are performed quickly and give a qualitative understanding of the absorption kinetics, as suggested by Equation **3-7**. At a deuterium pressure of 10 mbar, there is only a slight shift in the critical edge with a noticeable change in the Kiessig fringe oscillation. The change in the Kiessig fringe oscillations suggests a loss of contrast between adjacent layers, a property shown in the full NR measurement presented in Figure 6-9b. Full absorption in the catalyst layers (Pd, Ti and Ta) at moderate pressure requires 2.5 hours to complete. These slow kinetics are attributed to the slow diffusion through the Ti-H_2 FCC crystal phase that is expected to form at this temperature and pressure.

Slow diffusion through the Ti layer, as compared to the Ta layer, has been observed by Baldi *et al* [24], who used a pure Mg absorbing sample and not an Mg-Al. Further investigation of the differences between these two layers is given later in this chapter.

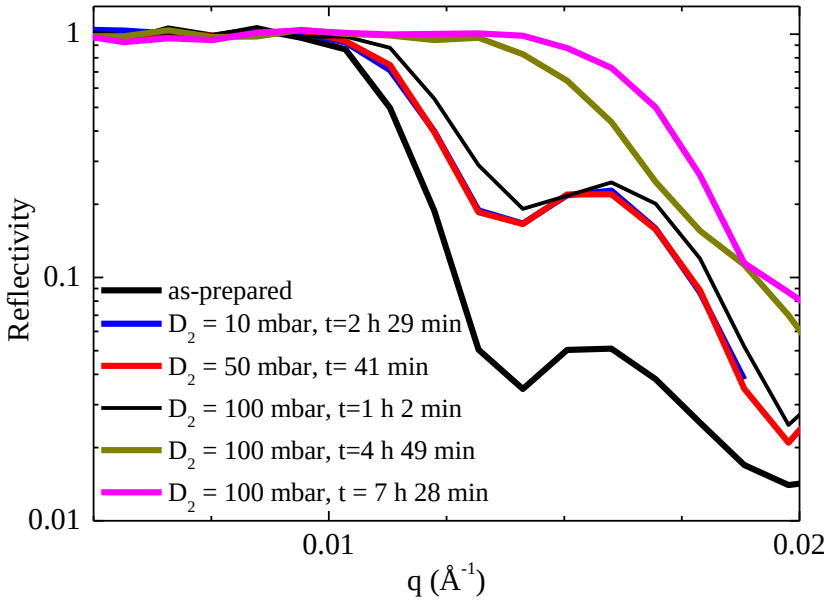

Figure 6-11 - Neutron reflectometry critical-edge measurements of Pd/Ti (5nm/5nm)-catalysed Mg-30 at %Al thin film deposited on a Ta (10nm)-coated (100) silicon wafer (see Figure 6-8). Measurements are performed in situ either in vacuo (as-prepared), at D_2 = 10 mbar, at D_2 = 50 mbar, and at D_2 = 100 mbar, all at room temperature. The sample was immersed in the deuterium at 10 mbar for 2 h and 29 minutes, then at 50 mbar for 41 minutes, and then at 100 mbar for 7 hours and 28 minutes.

Critical-edge measurements of the Pd/Ti catalysed Mg-30 at% Al thin film immersed in 50mbar and 100 mbar deuterium environments are depicted in Figure 6-11. These measurements are obtained quickly and provide a qualitative understanding of the absorption process. For comparison, the critical-edge measurements of the as-prepared film in vacuo and at a deuterium pressure of 10 mbar after 2 hours are included. As illustrated, there is only a slight increase in the critical edge once the deuterium pressure is increased to 10 mbar, 50 mbar, and 100 mbar, even though there is a

noticeable change in the amplitude of the Kiessig fringe oscillations, suggesting a change in the SLD of the catalyst layers. Only after immersion in the 100 mbar deuterium environment for 4 hours is there a significant change in the critical edge. This suggests that the absorption kinetics are rather sluggish at this relative low pressure and temperature. Even after a further 3 hours of immersion, for a total of 7 hours, there is little change in the critical edge, suggesting that the Mg-30 at% Al layer is fully hydrogenated and little absorption will occur with an increase in pressure – a supposition supported by the previous measurements illustrated in Figure 6-10.

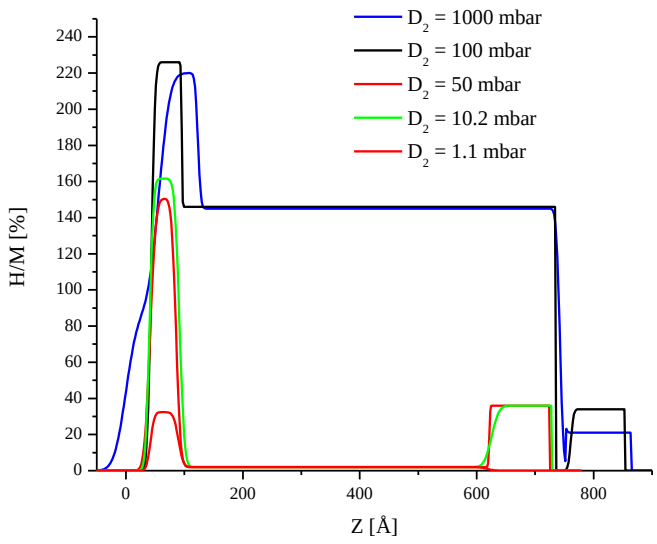

Figure 6-12 – Hydrogen concentration distribution of a Pd/Ti (5nm/5nm) catalysed Mg-30 at% Al thin film deposited on a Ta (10nm) coated (100) silicon wafer (see Figure 6-8).

The calculated hydrogen concentration profile from the SLD measurements of the Pd/Ti catalysed Mg-30 at% Al thin film (see Figure 6-9) is illustrated in Figure 6-12. As suggested by the SLD profile, the hydrogen is absorbed in the Pd/Ta catalysed layers prior to the main Mg-Al layer, an observation in accordance with the Pd/Ta catalysed Mg-Al thin film (see Figure 6-4).

After increasing the deuterium pressure to 1.1 mbar, there is noticeable deuterium absorption in the titanium layer and bottom tantalum layer. The high affinity of Ti toward absorbing deuterium explains the absorption at such a low pressure. Ti has an enthalpy of absorption of -164 kJ/mol [99]. After increasing the deuterium pressure to 10.2 mbar, the deuterium concentration in the Ti catalyst layers also increases from ~30at% to ~150at% - a value closer to the stoichiometric ratio for Ti-H_2 (200at% D_2).

6.3. Mg-30 at% Al with a Pd/Ni Bi-layer Catalyst

The investigation of the bilayer catalysts continues with an exploration of a catalyst that does not easily absorb deuterium at the pressures and temperatures under investigation. For this reson, nickel is used as an addition to the catalyst layers as Griessen et al suggest it is a good comparison candidate.

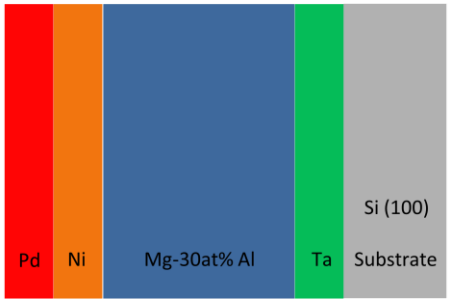

Figure 6-13 Illustration of the Pd/Ni catalyzed Mg-30at%Al thin film deposited on a Ta (10nm) coated (100) silicon wafer.

The non-absorbing catalyst layers are investigate using a Pd/Ni (5nm/5nm) catalysed Mg-30 at% Al alloy deposited on a Ta (10nm)-coated silicon wafer (see Figure 6-13). The catalyst thicknesses of 5nm/5nm are chosen to directly compare with the kinetics of other catalysts, such as the Pd/Ta bi-layer catalyst. As in the the other experiments, the optimization of the Pd/Ni catalyst deposition parameters is left to a further investigation.

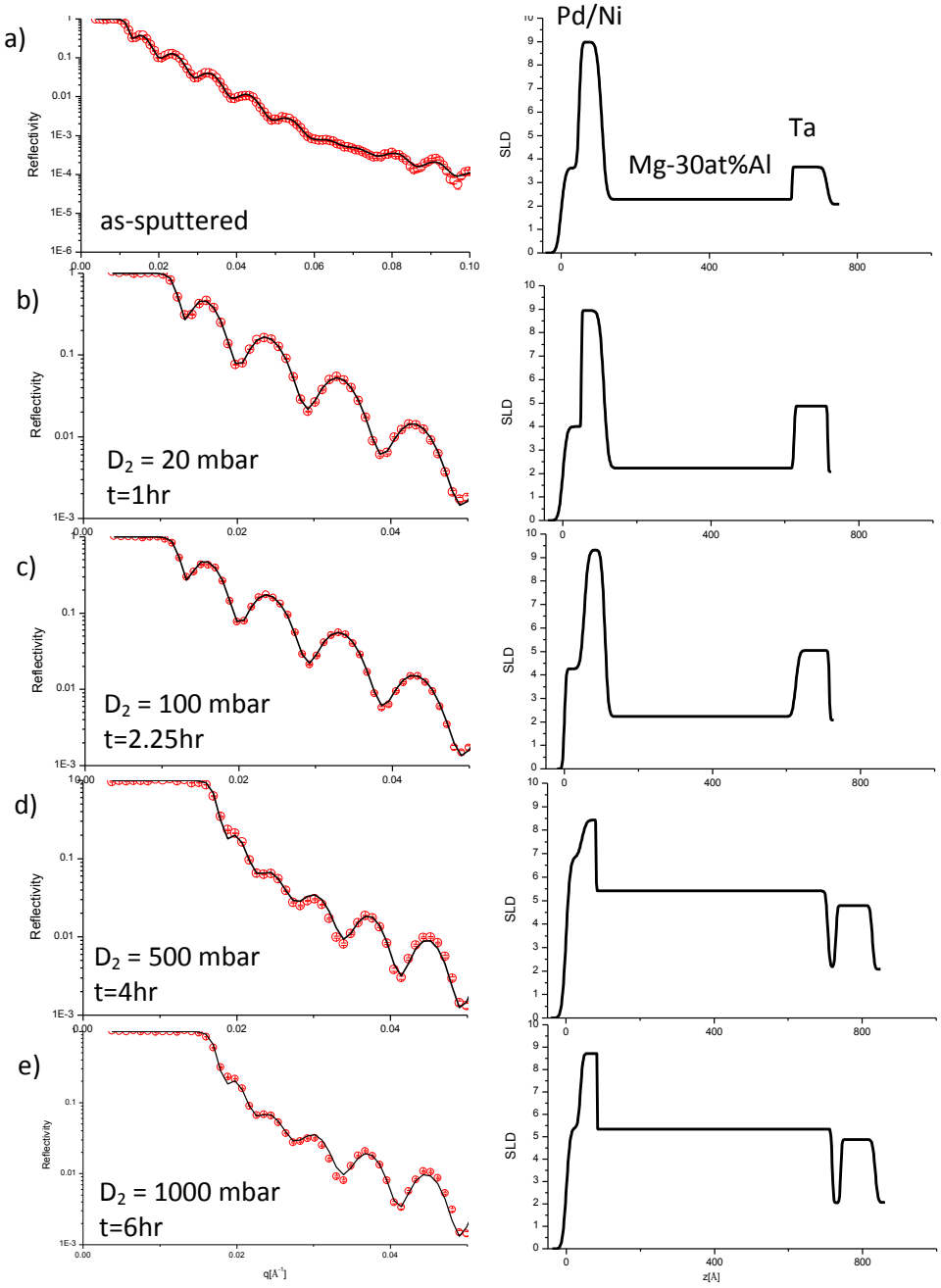

Figure 6-14 Neutron reflectometry measurements of Pd/Ni (5nm/5nm)-catalysed Mg-30 at % Al thin film coated on a Ta (10nm)-coated (100) silicon wafer (see Figure 6-13)) . (a) As-deposited state. (b) D_2 = 20 mbar. (c) D_2 = 100 mbar. (d) D_2 = 500 mbar. (e) D_2 = 1000 mbar. The time indicated is the time at the commencement of the scan. The sample remained at 20 mbar, 100 mbar, 500 mbar and 1000 mbar for 1 hour, ~30minutes, 30minutes, 1 hour respectively.

Neutron reflectivity measurements of the Pd/Ni catalysed Mg-30 at% Al thin-film structure (see Figure 6-13) are illustrated on the left side of Figure 6-14 and the corresponding real-space representation of the SLD is illustrated on the right of Figure

6-14. The SLD of the as-sputtered microstructure (Figure 6-14) is consistent with the expected result from the synthesis procedure and tabulated SLD's. The high SLD observed at 5-10 nm into the film of the as-sputtered microstructure is due to the nickel which has a large coherent scattering length. Following deuterium exposure (in situ) at 20 mbar, the sample absorbs deuterium mainly in the top Pd layer, as well as in the bottom Ta layer, with negligible amounts of deuterium in the main Mg-30 at% Al layer. This observation is consistent with previous measurements of the Pd/Ta catalyst. (see Figure 6-2). Even with a pressure increase to 100 mbar, there is negligible deuterium absorption in the Mg-Al layer, as illustrated in Figure 6-14. Only after increasing the deuterium pressure to 500 mbar, is there appreciable absorption in the Mg – 30 at% Al layer. The kinetics are relatively fast at 500 mbar as most of the deuterium is absorbed within ~1 hour (see Figure 6-15). The absorption process is accompanied by the appearance of gaps seemingly devoid of deuterium between the Mg – 30 at% Al and Ta layers, as noted in the previous samples. In this sample there are no definitive gaps between the Mg – 30 at% Al and Ni layer. The apparent absence of gaps may be due to the limited resolution of the measurements.

A further increase in the deuterium pressure to 1 bar did not result in any further changes in the SLD of any of the film's layers. In contrast to the previous Ta catalysts, the Ni layer did not absorb appreciable amounts of deuterium during any stage of the experiment as expected at these experimental pressure and temperature conditions.

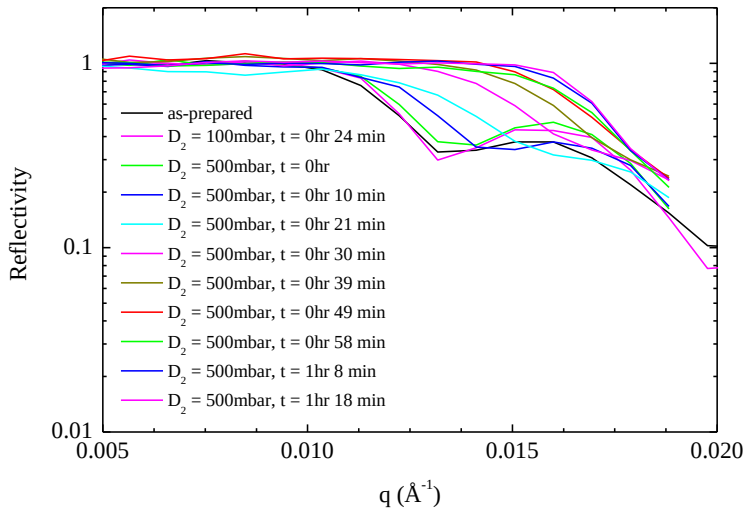

Figure 6-15 Neutron reflectometry critical-edge measurements of a Pd/Ni (5nm/5nm)-catalysed Mg-30 at % Al thin film deposited on a Ta (10nm)-coated (100) Si wafer (see Figure 6-13), measured at room temperature in situ to the deuterium atmosphere.

The critical edge measurements of the Pd/Ni catalysed Mg – 30 at% Al thin film are given in Figure 6-15. Critical-edge measurements are taken over a period of 1 hour to illustrate the kinetics at a deuterium pressure of 500 mbar. There is little absorption measured with this sample at deuterium pressures lower than 500 mbar. The 100 mbar critical edge measurement is plotted for comparison as there is little difference between the as-sputtered samples. In this sample, deuterium absorption at 500mbar occurred over a period of 1 hour. Nickel does not form a stable hydride under these experimental conditions; therefore a protective hydride layer cannot form, which does not inhibit hydrogen uptake. Deuterium requires a certain amount of energy to enter the nickel and subsequently diffuse into the underlying magnesium layer. The only advantage that nickel has over the previous bilayer is that it does not oxidize and therefore does not degrade.

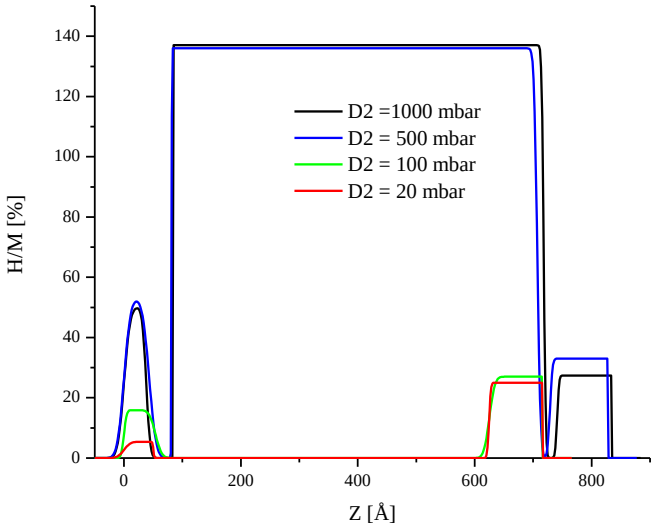

Figure 6-16 Hydrogen concentration distribution of Pd/Ni (5nm/5nm)-catalysed Mg-30 at % Al thin film deposited on a Ta (10nm)-coated (100) silicon wafer. The structure being examined is illustrated in Figure 6-13.

The calculated hydrogen profile of the Mg/Ni sample is plotted in Figure 6-16. The resultant profiles are not surprising given the qualitative understanding of the reflectometry and critical-edge measurements curves in Figure 6-16. Deuterium absorption in this case proceeds in a manner to absorption in the previous samples such that the top and bottom catalyst layers absorb the deuterium prior to the main Mg-Al layer.

6.4. Mg – 30 at% Al with a Ni/Ta Bi-layer Catalyst

To illustrate the influence of the Pd and Pd/x catalyst layers, a catalyst known to work at a much slower rate, the Ni catalyst is compared. The Ni catalyst is deposited on the Ta-coated Mg – 30 at% Al sample. Nickel, similar to palladium, can take up hydrogen without forming a deleterious surface oxide layer [100] from residual oxygen.

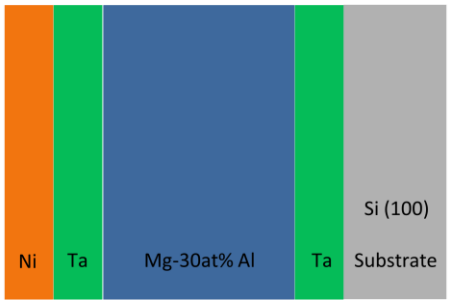

Figure 6-17 Ni/Ta (5nm/5nm)-catalysed Mg-30 at % Al thin film (50 nm) deposited on a Ta (10nm)-coated (100) silicon wafer

Figure 6-17illustrates the thin film structure used to determine the hydrogen sorption behaviour of the Ni/Ta (5nm/5nm) bilayer catalysts. In this structure, consistent with previous samples, the main hydrogen storage media is the Mg – 30 at% Al alloy. Again the Ta layer between the Si substrate and main Mg-Al layer is to maintain consistency and to prevent Mg-Si intermixing.

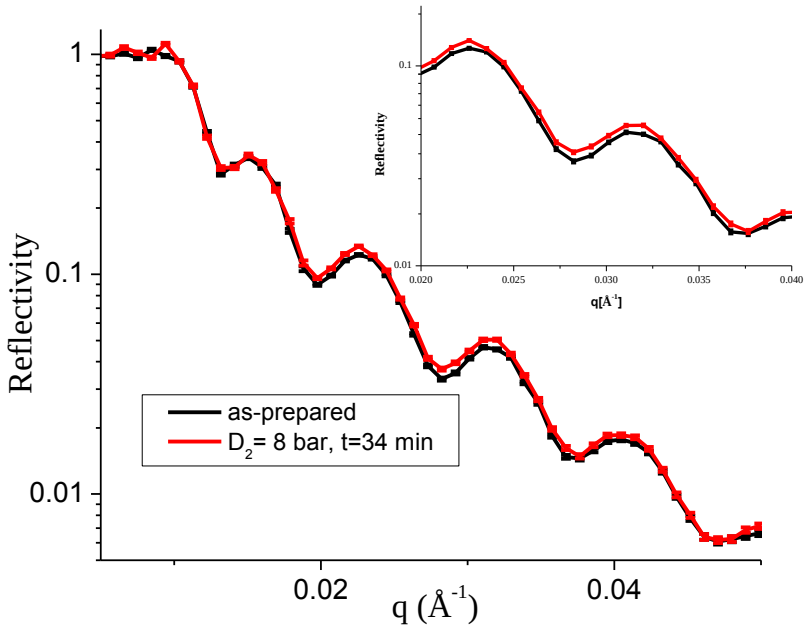

Figure 6-18 Neutron reflectometry measurements of Ni/Ta (5nm/5nm)-catalysed Mg-30 at % Al thin film deposited on Ta (10nm)-coated (100) silicon wafer

The measured reflectivity curves of the Ni/Ta catalysed Mg – 30 at% Al thin film in the as-prepared state and under an 8 bar deuterium environment is illustrated in Figure 6-18 with an enlarged section displayed in the inset. In this NR measurement, there is little absorption in the film as a whole primarily due to the constriction caused by the nickel. (i.e. hydrogen does not dissociate as easily on a nickel surface as compared to a palladium surface.) The change in amplitude of the Kiessig fringes suggests deuterium absorption occurs only in the catalyst layers and that little or no absorption occurs in the bulk Mg-Al layer.

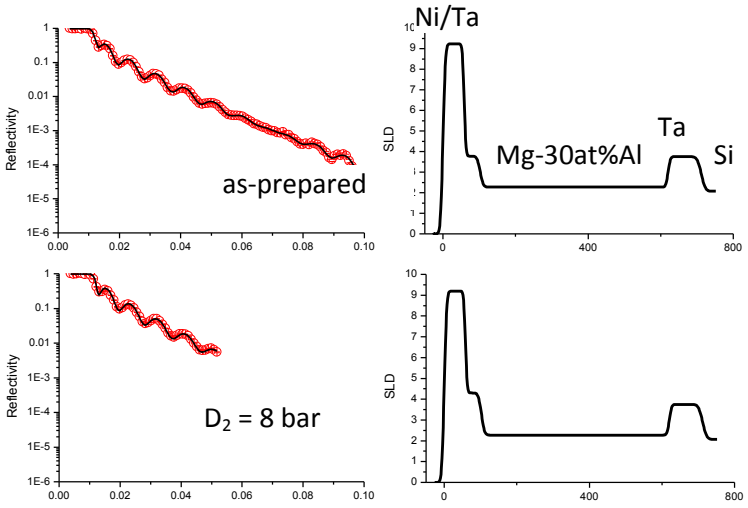

Figure 6-19 Neutron reflectometry measurements of Ni/Ta (5nm/5nm)-catalysed Mg-30 at % Al thin film deposited on a Ta (10nm)-covered (100) silicon substrate (a) in vacuum at room temperature and as-prepared and (b) immersed in an 8-bar deuterium environment at room temperature for 34 minutes. The structure being investigated is illustrated inFigure 6-17. The reflectivity curves presented here are the same as that presented in Figure 6-18 but with the fitted SLD curve to the measured data.

Further examination of the NR measurements of the Ni/Ta catalysed Mg- 30 at% Al alloy support the conclusions that deuterium absorption occurs in the catalyst layers. For instance, the SLD of the catalyst layers increases from the as-sputtered microstructure to the sample immersed in the 8 bar deuterium environment. This increase is attributed to a small amount of deuterium being absorbed into the top Ta layer.

Measurements of Ni as a catalyst layer support the evidence that Pd acts as a good dissociative hydrogen catalyst. A study by Cao [101] measured the hydrogen diffusion rate through pure nickel and concluded that diffusion is possible but much slower than diffusion through magnesium. Since this layer is quite thin (~5 nm) nickel should not hinder hydrogen diffusion to the extent noted above. In conclusion, nickel is not easily dissociate hydrogen and should not be used as a surface catalyst. This set of observations support the conclusion that palladium is responsible for hydrogen dissociation and hydrogen absorption into magnesium is not accomplished through other means.

6.5. Conclusions about Binary Surface Catalysts

The aim of the previous section was to illustrate the effects of the surface catalysts through a thorough analysis of various surface catalysts without altering the underlying bulk alloy (Mg-Al). Previous studies could not illustrate the hydrogen distribution throughout the sample using an in situ measurement technique similar to the measurement technique used here. The hydrogen absorption character of the Pd/Ta catalysed structure has been shown to be superior to the Pd catalysts because it increases the hydrogen sorption rates at room temperature. These experimental findings are in agreement with calculations of the binding energy among Pd alloys. [102] Furthermore, the findings clearly indicate that a promising technique to reduce desorption temperature is choosing the appropriate binary catalysts for the underlying layer in this case the Mg alloy.

With the pure palladium catalyst, as presented in the previous section, the deuterium uptake progresses rather slowly compared to using the Pd/Ta catalyst sample. Furthermore, the Pd/Ta exhibits hydrogen uptake at a 100mbar pressure within a 10-hour period- a result not previously observed in the literature as far as the author knows. Even the Mg sample catalysed with Pd/Ta shows excellent hydrogen uptake at a pressure of 100mbar. Differences exist between the hydrogenation mechanisms of the Mg-Al alloy and the pure Mg sample, but these differences do not account for the differences noted in the catalyst behaviour (see section 7.3 for further analysis). Moreover, the Pd/Ti catalysed Mg-Al sample shows partial absorption at 50 mbar with full absorption occurring at 100 mbar and an absorption time comparable to that of the Pd/Ta-catalysed sample. One commonality between the two systems is the heat of hydride formation of Ti and Ta. In contrast, the nickel stratified layer (part of the

catalyst), which does not form a stable hydride under the experimental conditions, requires an elevated pressure (500mbar) for full hydrogenation of the underlying Mg-Al layer. Moreover, hydrogenation at 500mbar for the Pd/Ni-catalysed sample occurs much more quickly than for the other samples. It is not surprising that the Ni/Ta-catalysed sample does not show any hydrogenation up to a pressure of 8 bar at room temperature, illustrating the relative inert catalyst effect of Ni. In conclusion, the hydrogen uptake of the Pd/Ti and Pd/Ta catalysts are optimal combinations to act as a dissociation catalyst for an Mg alloy sample.

7. Magnesium Absorption Process

In the previous section the catalyst absorption process of several bi-layer catalysts was thoroughly investigated while the underlying Mg-Al layer was ignored. Although the absorption process for magnesium is very well understood, the absorption process of an Mg-Al alloy is not. In this section the absorption process is studied through comparison of the absorption of an Mg thin film catalysed by a Pd/Ta bi-layer against a Mg-Al thin film also catalysed by a Pd/Ta bi-layer.

7.1.Pd/Ta Catalysed Mg – 30 at% Al sample

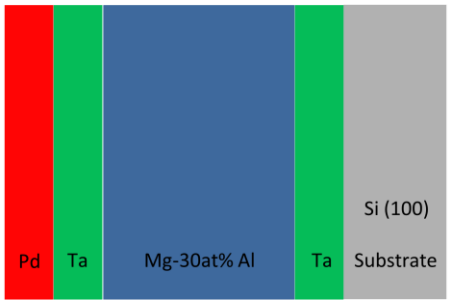

Figure 7-1 Pd/Ta-catalysed Mg-30 at % Al thin film deposited on a Ta (10nm)-coated silicon wafer used in the measurement of the absorption process of the Mg-30 at % Al alloy. This sample is similar to that presented in Figure 6-1 but the following experiments were performed on a different sample.

The investigation commences with an examination of the Pd/Ta (5nm/5nm) catalysed Mg – 30 at% Al thin film deposited on a Ta (10nm)-coated silicon wafer (see Figure 7-1). A thickness of 5nm is chosen in order to directly compare the catalyst layers used in the previous studies in this thesis. Further research is needed to optimize the deposition parameters (e.g. thickness, deposition rate, surface roughness, etc.).

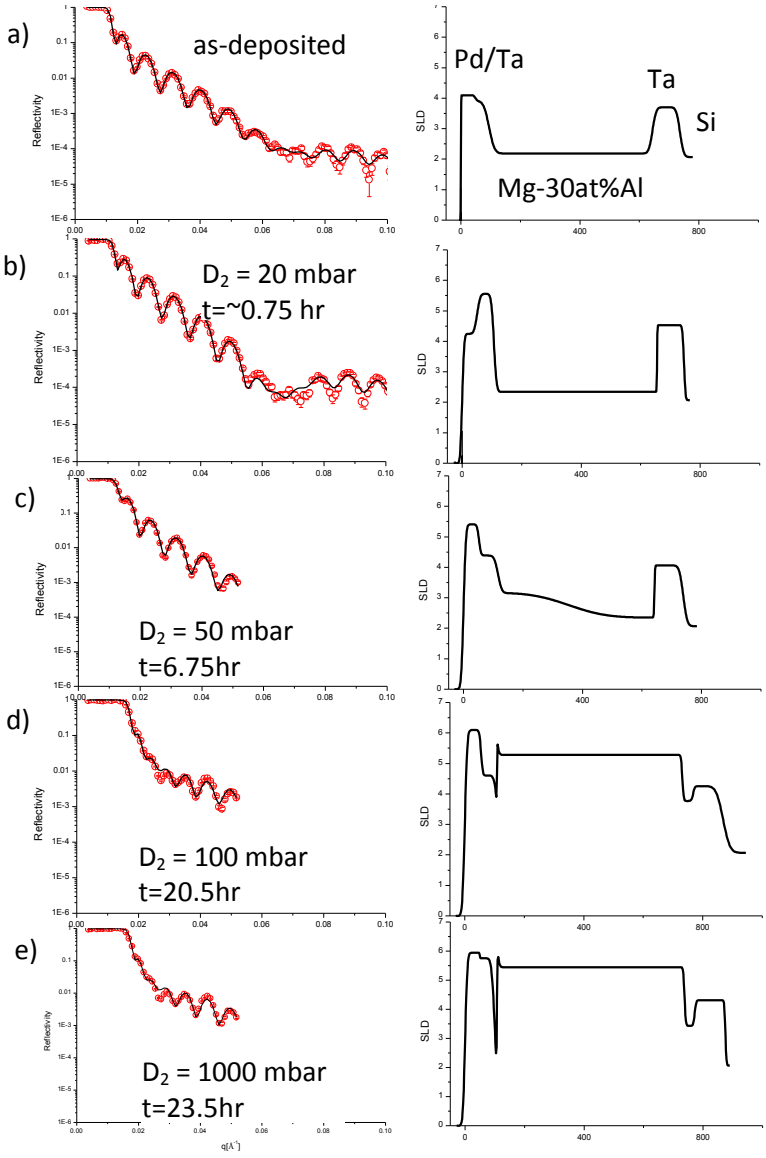

Figure 7-2 Neutron reflectometry measurements of Pd/Ta (5nm/5nm)-catalysed Mg - 30 at% Al thin film deposited on a Ta (10nm)-covered (100) Si substrate. (a) As-sputtered state. (b) D_2 = 20 mbar. (c) D_2 = 50 mbar. (d) D_2 = 100 mbar. (e) D_2 = 1000 mbar. Absorption experiments are performed in situ to neutron reflectometry measurements and performed at room temperature (20°C). Times indicated above are the times at which the measurement was taken. Therefore, the sample was at 20 mbar, 50 mbar, 100 mbar, and 1000 mbar for 4.75 hours, 2 hours, 19.75 hours, 3.5 hours respectively.

The neutron reflectivity measurements of the Pd/Ta catalysed Mg – 30 at% Al (50 nm) thin film deposited on a 10nm Ta-coated silicon wafer are plotted in Figure 7-2. The reflectivity measurements are illustrated on the left with the corresponding real-space representation of the structure on the right. The SLD and layer thickness of the as-deposited microstructure correspond to the expected values from synthesis and

previous bulk measurements [51]. After measuring the neutron reflectivity of the as-deposited film, deuterium is slowly introduced into the sample cell within the NR apparatus. Throughout the pressure increase, critical-edge measurements are continuously taken to deduce if any hydrogen sorption has occurred. Once the critical edge stabilizes for ~1/2 hour, a full NR measurement is taken. At 20 mbar D_2, the SLD profile shows an increase in the top and bottom layers while the SLD of the Mg-30at%Al remains unchanged. This observation suggests deuterium absorption occurs in the catalysts layers but little or no deuterium is absorbed in the Mg – 30 at% Al layer.

After an increase in the deuterium pressure to 50 mbar, there is an increase in the SLD of the catalysts layers. Furthermore, there is a noticeable increase in the SLD of the Mg layer at the Pd/Ta catalyst interface, indicating deuterium absorption in the Mg layer. However, the absorption proceeds at a very slow rate. Therefore, it is assumed that full absorption in the Mg – 30 at% Al layer may occur if absorption continues at this low pressure.

Upon increasing the deuterium pressure to 100 mbar, appreciable changes occur in the reflectivity and SLD of the thin film and correspond to absorption in the Mg – 30 at% Al layer. In this instance a simple four layer model is insufficient to properly fit the reflectivity curve, and a six layer model is used instead. The two extra layers in the model correspond to small gaps that are ~10 to 20Å in width between the magnesium layers and the tantalum catalytic layers- an observation consistent with measurements in the study of the other catalyst layers discussed (see Figure 5-2). The measurements presented here are in a quasi equilibrium state in which appreciable changes do not occur over the measurement time.

Only after increasing the deuterium pressure to 1 bar does full absorption occur. Also there are no subsequent changes in the NR reflectivity curve and thus the SLD curve. Even at 1 bar deuterium pressure, there are small gaps ~10 Å in width between the Mg – 30 at% Al layer and the Ta catalytic and barrier layers.

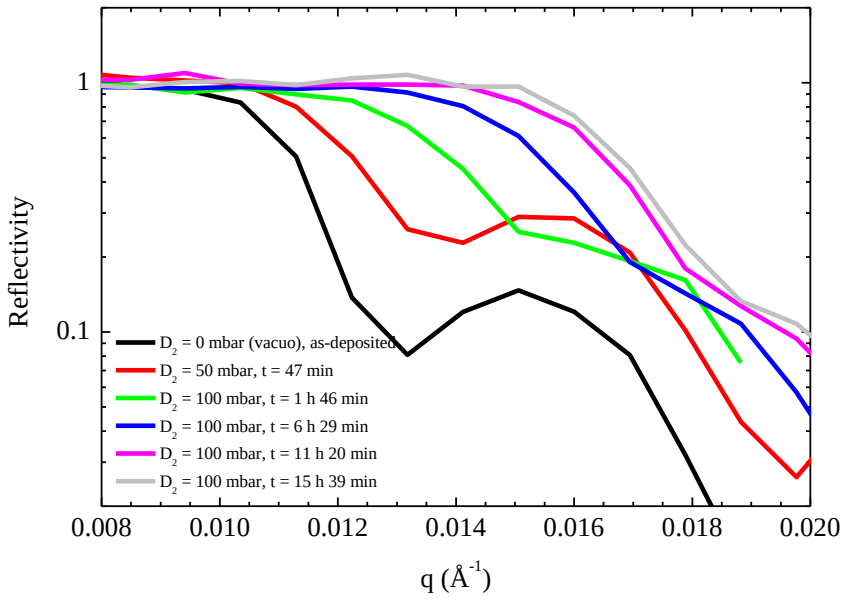

Figure 7-3 Neutron reflectometry critical-edge measurements of Pd/Ta-catalysed Mg thin film at a deuterium pressure of 100 mbar

In-situ critical-edge measurements are used to construct a qualitative in situ understanding of the absorption process. Immediately after the introduction of deuterium at 50 mbar, absorption in the sample commences and requires a long immersion time of ~45 minutes to become quasi stable. At this point, the critical-edge measurements suggest the top and bottom catalyst layers have absorbed deuterium given that they closely resemble the previous samples changes in reflectometry given in Figure 7-2. After increasing the deuterium pressure to 100mbar, the main Mg-Al layer starts to absorb deuterium, but complete absorption requires a significant amount of time- ~15 hours. In this case the deuterium absorption occurs steadily over the entire

duration as opposed to the Pd-Ni catalysed sample for which hydrogenation occurred suddenly and quickly.

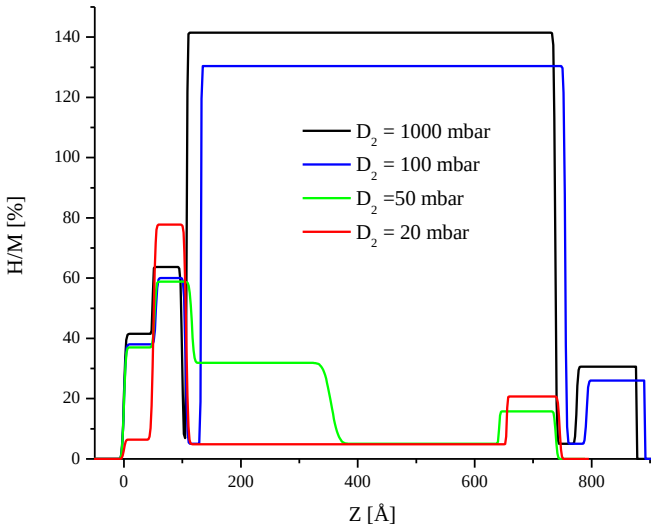

Figure 7-4 Hydrogen concentration distribution of Pd/Ta (5nm/5nm)-catalysed Mg-Al thin film deposited on a Ta (10nm)-coated (100) silicon wafer

Least square fitting of a model to an extended reflectivity scan of the sample supports the conclusions drawn from the qualitative measurements. Hydrogenation (deuterium absorption) commences at a modest pressure of 20 mbar with absorption in the top Pd/Ta layer and bottom Ta interfacial layers. Full hydrogenation of these catalyst layers is incomplete most probably due to the stress and strain imposed on the layers from a volume increase. An increase in the amount of strain on each layer would impose an absorption barrier, leading to impairment to further sorption. In order to overcome this strain barrier, either the temperature or pressure must be increased. In this instance, the temperature is constant and the pressure slowly increases.

At 50 mbar, the hydrogen concentration in the Mg-Al layer increases. Deuterium absorption starts at the top Ta/Mg interface and progresses downwards towards the

wafer. It is conjectured that the increase in hydrogen pressure is only required to increase the diffusion rate through the sample and allow hydrogen uptake to take place over the period of measurement.

It should be noted that the final deuterium concentration in the Mg-Al and bottom Ta layer is similar to tha of the Pd/Ni catalysed sample. These final deuterium concentrations should represent the equilibrium deuterium concentration in the respective layers; therefore further increasing the deuterium concentration requires a significant increase in either the deuterium pressure or temperature.

7.2.Pd/Ta Catalysed Mg Thin Film

In order to contrast the behaviour of the Pd/Ta Mg-Al alloy, and illustrate the role of the catalyst and the underlying bulk Mg-Al alloy, the deuterium absorption kinetics of a pure Mg sample catalysed by Pd/Ta are measured, as depicted in Figure 7-Pd/Ta-catalysed Mg thin film deposited on a Ta (10nm)-coated (100) silicon wafer used for neutron reflectometry measurements of a pure Mg sample. The choice of layer thickness is based is based upon the thickness of the previous measurements to allow a direct comparison of the experimental results. Optimization of the sputtering conditions and layer thickness was not performed and is left for another investigation.

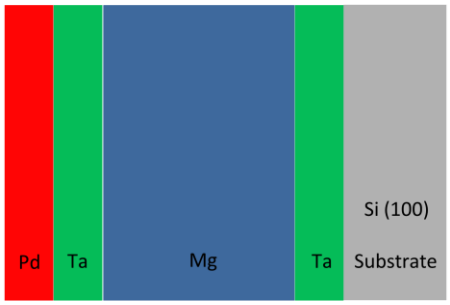

Figure 7-Pd/Ta-catalysed Mg thin film deposited on a Ta (10nm)-coated (100) silicon wafer used for neutron reflectometry measurements of a pure Mg sample

In this series of experiments, the conditions are reproduced from the hydrogenation experiments on Mg-Al samples (section 7.1). The dimension of the sample, sample preparation conditions, and handling conditions were replicated as much as possible to allow separation of effects from the Pd/Ta catalyst layer and the underlying Mg layer.

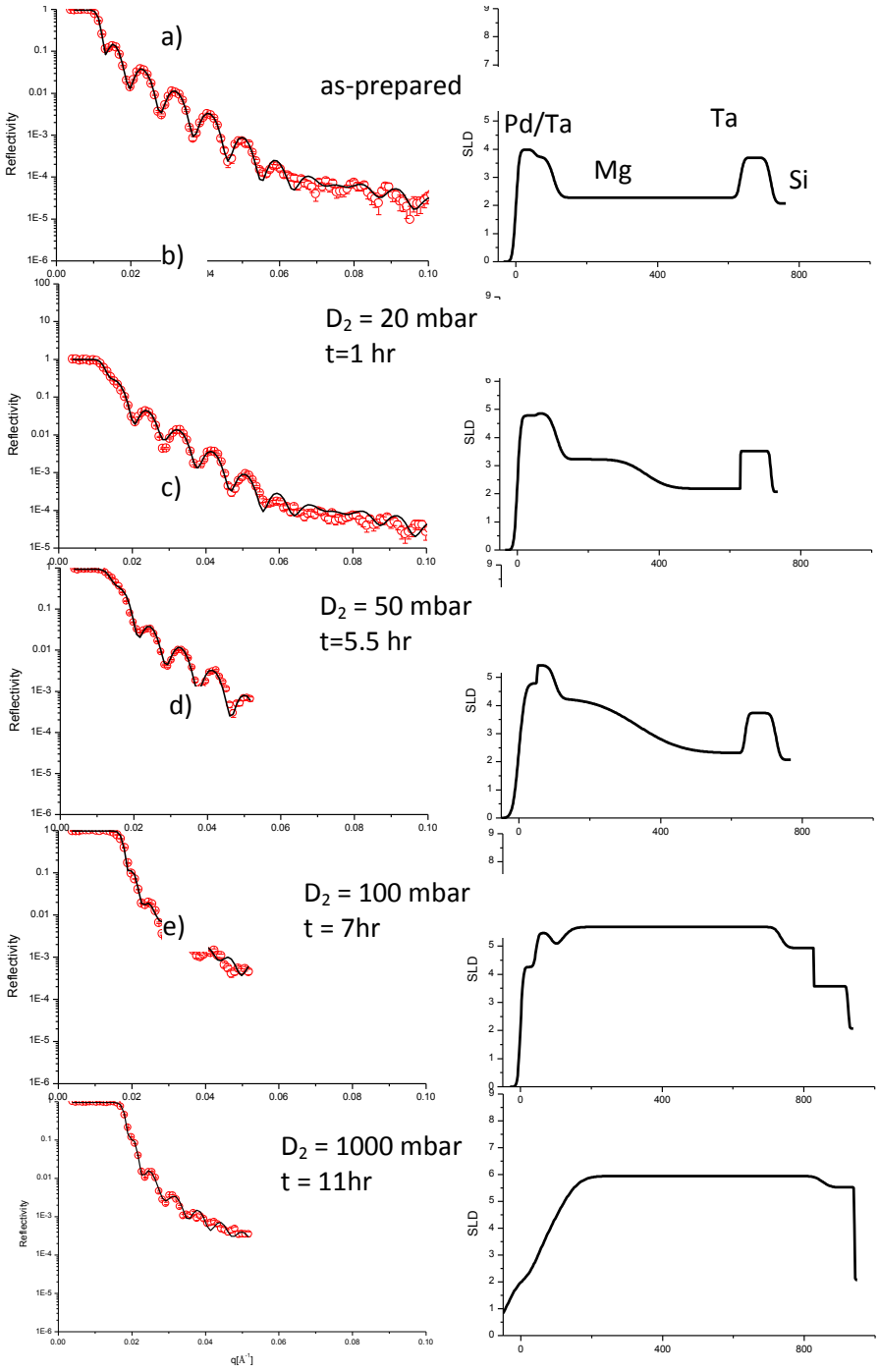

Figure 7-5 Neutron reflectometry measurements of Pd/Ta (5nm/5nm)-catalysed Mg thin film deposited on a Ta (10nm)-covered (100) silicon substrate at room temperature. (a) As-prepared. (b) 20 mbar, (c) 50 mbar. (d) 100 mbar. (e) 1000 mbar. The loss of the catalysts' contrast in (e) is due to the surface roughness resulting from deuterium absorption in the Mg layer and not due to the experimental procedure or other noise sources. The times indicated above are the times at which the measurement was taken. Therefore, the sample was at 20 mbar, 50 mbar, 100 mbar and 1000 mbar for 4 hours, 2 hours, 1.5 hours, and 4 hours respectively.

The neutron reflectivity measurements of the Pd/Ta catalysed Mg thin film are illustrated on the left side of Figure 7-5, and with the real-space representation of SLD is illustrated on the right side of Figure 7-5. The as-sputtered microstructure is illustrated in Figure 7-5a. The microstructure is similar to that expected from tabulated SLD and the expected thicknesses from the synthesis methods. It is interesting to note that a larger surface roughness between the Mg and Ta layer as compared to a Mg-Al samples. This surface roughness is not surprising given the characteristic roughness of a pure Mg thin-film [103]. This surface roughness may limit the accuracy of the SLD extracted from the neutron reflectivity curves as this contributes to diffuse scattering.

At a deuterium pressure of 20 mbar (see Figure 7-5b), there is deuterium absorption in the catalyst layer and absorption in the main Mg layer at outer Ta/Mg interface. The observation of deuterium absorption at this interface is similar to a core-shell type of deuterium absorption- an absorption process in which the outer material absorbs the deuterium with the absorption proceeding inward, away from the surface.

Further increasing the deuterium pressure to 50 mbar causes a further increase in deuterium absorption in the catalyst layers and the main Mg layer Figure 7-5c. These are indeed in situ measurements, and it is assumed that they illustrate a quasi-stable structure and therefore are representative of the actual SLD. In other words, they are not an artefact of absorption occurring while measurements are taken.

Only after increasing the deuterium pressure to 100 mbar does total absorption occur in the Mg layer (see Figure 7-5d). There are no gaps between the catalyst layers and the magnesium layer. This may be due to the absence of contrast between the main Mg layer and the catalysts or the large surface roughness imposed by the Mg-absorbing

deuterium. After a further increase in the deuterium pressure to 1 bar, there is no change in the SLD, suggesting that full deuterium absorption occurs at 100 mbar. Again the loss of the contrast in the surface catalyst layer is a by-product of the large surface roughness, leading to a large amount of noise in the experimental data.

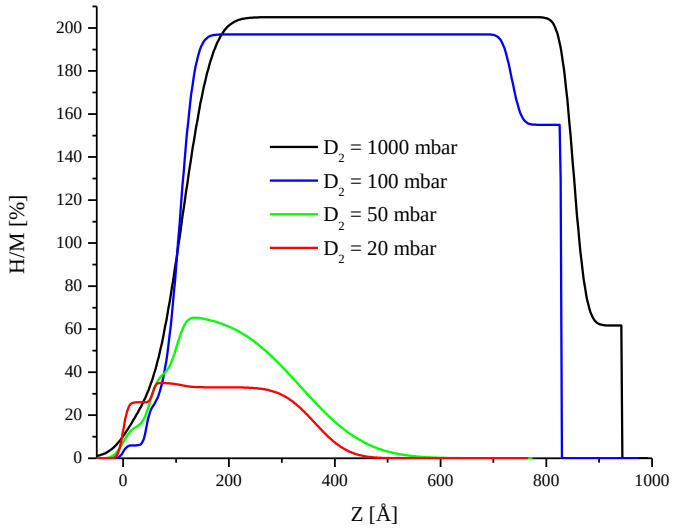

Figure 7-6 Hydrogen concentration profile of Pd/Ta (5nm/5nm)-catalysed Mg thin film deposited on a Ta (10nm)-covered (100) silicon substrate

7.3.Discussion

The observations in the previous section illustrate the early stages of deuterium absorption in solid-state hydrogen sorption. This observation is indicative of a spillover mechanism in which the hydrogen dissociates into the Pd or Pd-Ta layer and subsequently diffuses into the main Mg layers. This observation also suggests diffusion in the nanometric surface catalyst layers but does not significantly affect the absorption process as compared to diffusion through the bulk Mg layers. In other words, the surface layer thickness (and thus diffusion impediment) is insignificant as compared to the bulk Mg or Mg-Al layers.

Furthermore, the observation of late Mg hydride formation is surprising given that Mg-H_2 is much more stable than the Pd or Ta hydrides. This suggests that hydride formation in Mg is limited by a transformation barrier brought on by requiring a large size mismatch between Mg and MgH_2. This phenomenon is supported by experimental data showing that the Mg-Al and Mg layers expand by ~23% whereas the Pd and Ta layers modestly expand by ~2% and ~6%, respectively.

In Figure 7-4 a large deuterium concentration gradient in the Mg and Mg-Al films occurs during the absorption process. At a low temperature and pressure, deuterium diffusion through MgD_2 rather slow and contributes to decreasing the rate of absorption. Therefore, this suggests that the Mg has not reached equilibrium and, given enough time, will absorb more deuterium.

There is a gap between the Mg-Al and catalyst layers whereas the Mg sample does not show any evidence of such a gap. This observation may be the result of one of two phenomena: (a) The interfacial roughness of the Mg sample reduces the resolution so as to wash out evidence of the gap, or, (b) The region between the Mg-Al layer and Ta layers is not devoid of hydrogen but rather is a build-up of aluminum brought about by precipitation of Al from Mg solute due to the formation of MgH_2. The former observation seems more plausible given that the precipitation process at room temperature would occur rather slowly; much slower than the time given in this examination. Furthermore, the precipitation of the aluminum at a tantalum interface should result in an increase in the interfacial roughness, an observation not supported by these measurements.

8. Neutron Reflectometry Multilayer

The thermodynamic and kinetic properties of Mg hydrides require improvements to be applicable to viable solid state hydrogen storage devices. The material (Mg) possesses the sufficient gravimetric and volumetric capacity required for several applications, but slow kinetics and extremely low desorption pressure pose a significant problem. One approach is to change the thermodynamics of the system (i.e. destabilize the system), which may lead to increased kinetics. This approach assumes that if a material is destabilized, the diffusion of hydrogen through the material also increases. Increased diffusion through the material means the driving force (decrease pressure) required to liberate the hydrogen from the material is lowered. In other words, the pressure does not have to decrease in order to introduce a driving force to liberate the hydrogen from the material.

The approach in this study is fundamentally different. The aim of this study is to introduce alloy additions that act as high-diffusion pathways that effectively increase the effective hydrogen diffusion within the material without altering the hydrogen storage capacity In a previous study we were able to show that these alloy additions increase the hydrogen storage kinetics without altering the thermodynamics. The hydrogen kinetic pathway theory was suggested but not directly measured.

In this section an investigation of the deuterium absorption process of a catalyst imbedded within the Mg layer is carried out through neutron reflectivity measurements of several multilayer structures. These multilayer structures are analogous to the secondary precipitates within the Mg matrix proposed by Kalisvaart [104] and Baldi [33].

These multilayer structures are well defined and can be used to easily determine the absorption process.

8.1.FeTi-Mg Multilayer

The study of the multilayers begins with an analysis of an Fe-Ti catalysed Mg structure. The alloy Fe-Ti has exhibits exceptional hydrogen sorption characteristics owing to the materials' its high diffusion rates. Also, Fe-Ti is less stable than Mg and at 100°C does not form stable hydrides at 1bar. (~100C), see for instance [105, 106, 107, 108, 109, 110]. On its own, FeTi alloy, does not store appreciable amounts of hydrogen and therefore has a low gravimetric storage density of ~2.2wt% [H/FeTi]. On the other hand, hydrogen can easily diffuse through the FeTi alloy matrix, making it a potentially good hydrogen catalyst material for Mg. As suggested above, has an excellent hydrogen gravimetric capacity (8.4 wt% [H/Mg]) but at the expense of having slow kinetics at practical temperatures and pressures. Therefore marrying the benefits of the fast hydrogen diffusion of the FeTi phase with the high hydrogen storage capacity of Mg may result in an alloy with superior kinetics and good overall gravimetric capacity.

The Fe-Ti catalysed Mg alloy used to study hydrogen absorption consists of an FeTi/Mg multilayer deposited on a Ta (10nm)-coated silicon (100) wafer. The underlying Ta layer prevents Mg-Si interactions and produces an NR contrast mechanism. The main multilayers consist of a repeated (three layer repeated) Mg (20nm) and FeTi alloy (5 nm), as illustrated in Figure 8-Multilayer structure used to measure the influence of FeTi catalyst on hydrogen absorption characteristics of nanoscale Mg thin film. The bottom Ta layer is to prevent formation of Mg-Si intermetallic mixtures and act as a reflectometry measurement contrast agent. Furthermore, Pd/Ta (5nm/5nm) is

deposited on the surface to facilitate hydrogen dissociation and prevent oxidation of the FeTi and Mg.

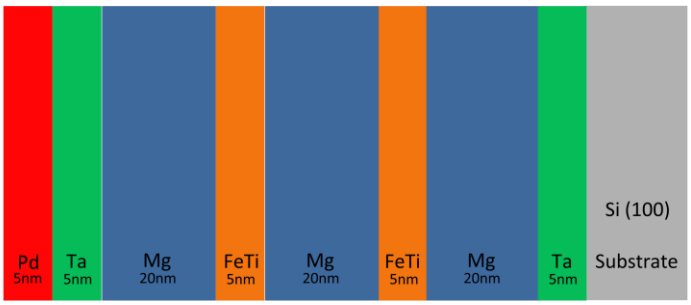

Figure 8-Multilayer structure used to measure the influence of FeTi catalyst on hydrogen absorption characteristics of nanoscale Mg thin film. The bottom Ta layer is to prevent formation of Mg-Si intermetallic mixtures and act as a reflectometry measurement contrast agent.

The structure is used to closely represent the wt% composition of a functional alloy material previously reported in the literature [111]. Furthermore, it is estimated that the precipitates presented by Kalisvaart at al are on the scale of the thickness of the FeTi catalyst layers fabricated here [104]. Furthermore the interface between the Mg and FeTi catalysts is an important factor to consider and with this geometry the interface is well controlled. By contrast, in the case of FeTi precipitates, the Mg/FeTi interface is not well controlled. Moreover, this structure resembles the multilayer structure presented by Baldi[33] for studying the Mg/Ti interface during hydrogenation.

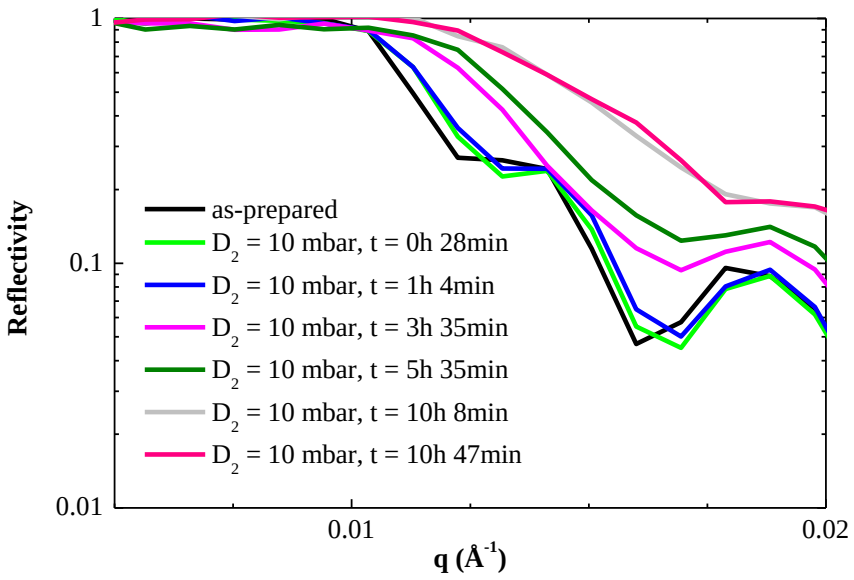

Figure 8-1 Neutron reflectivity critical edge measurements of FeTi catalysed Mg thin film structure, (see Figure 8-Multilayer structure used to measure the influence of FeTi catalyst on hydrogen absorption characteristics of nanoscale Mg thin film. The bottom Ta layer is to prevent formation of Mg-Si intermetallic mixtures and act as a reflectometry measurement contrast agent).

Neutron reflectivity critical-edge measurements of the Mg/FeTi multilayer are presented in Figure 8-1 and provide a qualitative understanding of the deuterium absorption kinetics. Similar to hydrogenation of the Pd/Ta catalysed Mg – 30 at% Al, absorption occur slowly at 10 mbar as illustrated by slow movements of the critical edge and a relatively small change in the Kiessig oscillations. Small changes in the position of the maxima and minima of the Kiessig oscillations suggest little or no film expansion and therefore further suggest hydrogenation is limited to the surface catalyst layers. Whereas the larger changes in the position of the maxima and minima of the Kiessig oscillations are associated with significant film expansion and therefore hydrogenation in a large Mg layer. Only after immersion in the deuterium environment for a prolonged period do the oscillations disappear. These qualitative observations illustrate that the catalyst layers absorb the deuterium prior to absorption in the Mg layers. Obviously

further investigation is required to support this tentative conclusion, and the results presented in the next section.

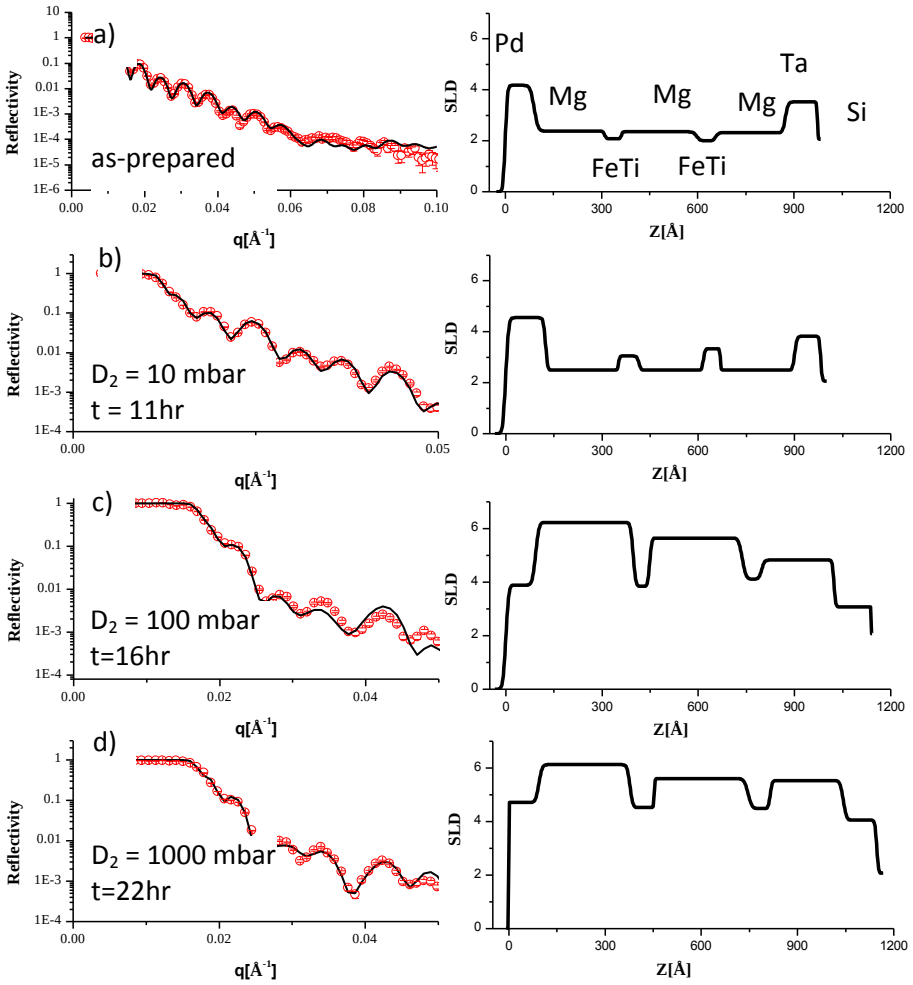

Figure 8-2 Neutron reflectivity measurements of a thin film multilayer consisting of an alternating stack of Mg and FeTi (see Figure 8-Multilayer structure used to measure the influence of FeTi catalyst on hydrogen absorption characteristics of nanoscale Mg thin film. The bottom Ta layer is to prevent formation of Mg-Si intermetallic mixtures and act as a reflectometry measurement contrast agent). The time indicated is the time at which the measurements were taken. Since each measurement required only 1 hour, the sample was at 10 mbar, 100 mbar and 1000 mbar for 11 hours, 15 hours, and 5 hours, respectively before the measurements were taken.

Neutron reflectivity measurements of the Mg/FeTi alloy multilayer structure (see Figure 8-Multilayer structure used to measure the influence of FeTi catalyst on hydrogen absorption characteristics of nanoscale Mg thin film. The bottom Ta layer is to prevent formation of Mg-Si intermetallic mixtures and act as a reflectometry measurement

contrast agent) are plotted on the left side of Figure 8-2, and the resultant spatial dependence of SLD is presented on the right side of Figure 8-2. The visible oscillations, referred to as Kiessig fringes, are associated with the characteristic thickness and SLD contrast between each layers of the film. Consistent with previous experimental procedures, NR measurements are taken of the as-prepared film in vacuo prior to immersion in a deuterium environment. As illustrated in Figure 8-2a, the reflectometry measurements clearly indicate the structure as distinct layers of Pd (10nm), followed by a repeated structure of Mg (20nm) and FeTi (5nm), followed by Mg (20nm) and a 10 nmTa layer deposited on a silicon substrate. The sharp delimitation of each layer suggests very little interfacial roughness and little mixing or alloying between each adjacent layer.

As a consequence of the large scattering length of deuterium, the SLD of the absorbing layers increase as deuterium is absorbed. In particular, at a pressure of 10 mbar, the diffusion catalyst FeTi layers absorb a noticeable quantity of deuterium as indicated by an increase in SLD. At modest pressure, there is little absorption in the Mg, Pd, and Ta layers, as indicated by little change in the SLD of the respective layers. These measurements are assumed to be in a state of quasi-equilibrium in which the kinetics evolves sufficiently slowly so that no noticeable absorption occurs over the acquisition period. After further increasing the deuterium pressure to 100mbar, there is a significant change in the SLD of the Mg layers, corresponding to deuterium absorption. However, the SLD of the Mg layers is not uniform and an apparent deuterium gradient exists within the layers.

After increasing the deuterium pressure to 1 bar, there is only a small change in the SLD of the deep Mg layer from the 100mbar measurement suggesting almost complete deuterium absorption in the Mg alloy and a phase transformation to an α-Mg-H_2 structure. Furthermore the observed Mg layer expansion is consistent with an Mg to α-Mg-H_2 phase transformation.

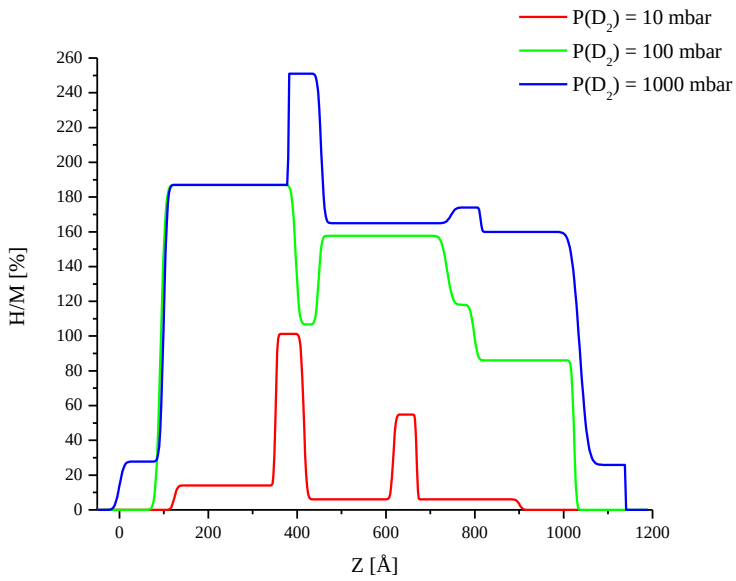

Figure 8-3 – Calculated hydrogen concentration profile of the Mg/FeTi multilayer structure at a deuterium pressure of 10, 100, and 1000 mbar. These profiles are compiled from the neutron reflectivity measurements of the multilayer structure illustrated in Figure 8-1.

Upon completion of the neutron reflectivity measurements, the hydrogen concentration profiles are calculated for deuterium pressures of 10, 100, and 1 bar from the SLD profiles (see Figure 8-2 and Figure 8-3). As suggested by the changes in the SLD profiles and the critical-edge measurements, the catalyst layers (FeTi) absorb considerable amounts of hydrogen prior to absorption in the thicker Mg layers. Consistent with other studies, the resistance of Mg-absorbing hydrogen is attributed to the required large

volume expansion that Mg undergoes to accommodate the hydrogen within its lattice. This expansion is in contrast to an Fe-Ti alloy which does not require a large volume expansion for appreciable hydrogen absorption.

As illustrated in Figure 8-3, the Fe-Ti alloy absorbs deuterium at 10 mbar to a concentration of 100% and 60% for the upper and lower catalysts layers respectively. It is not surprising that there is a concentration gradient between the catalyst layers as the limited diffusion and concentration within the Mg layers hinders the deuterium from diffusing into the bottom catalyst layers. Only after increasing the deuterium pressure to 100 mbar, is there appreciable absorption in the Mg layers. Once again there is an appreciable gradient in the hydrogen concentration between the Mg layers which is attributed to slow diffusion through the Mg and Mg-H_2 layers consistent with a core-shell model of hydrogen absorption [112]. One remarkable attribution of absorption at this modest pressure is the almost total absorption within the Mg layers. It might be expected that the limited diffusion through the material would impede complete absorption at these modest pressures at room temperature. After increasing the pressure to 1 bar, the deuterium concentration within the structure does not increase appreciably. This suggests that the hydrogen concentration profile is the result of from thermodynamic equilibrium in the system and not slow kinetics. Further investigation is required to confirm this speculation.

8.2.Mg-Al-Ti Multilayer

The hydrogen sorption influence of catalytic additions is further investigated by examining the hydrogen sorption properties of an Al-Ti catalysed Mg matrix. The alloy Al-Ti has been shown to exhibit a high affinity for hydrogen diffusion at modest

temperatures, but a full characterization of this material has not been performed [113]. Many articles have suggested that the Al_3Ti alloy exhibits excellent thermodynamics for hydrogenation at modest temperatures and pressures at the expense of slow hydrogenation kinetics [113, 114, 115, 116]. Equilibrium between the H_2 gas and metal surface is usually achieved, but limited kinetics prevent hydrogenation of the bulk material. The slow kinetics experienced with hydrogenation of the Al-Ti material also significantly limit the experiments performed; therefore the literature on the hydrogenation of Al-Ti is severely limited.

Early studies of the hydrogen sorption properties of the Al-Ti-Hx alloy suggest that there is little hydrogen absorption (~26 ppm) [113]. By contrast Ti_3Al has ~4.7 wt% [H/(Ti-Al)] absorption achieved at 127°C. Investigation into the hydrogen sorption character of Ti-Al alloy shows that considerable absorption occurs within the Ti_3-Al alloy with a decrease in uptake and increase in the aluminum concentration. Hashi [114] concludes that hydrogen-induced amorphisation occurs in the Al-Ti system for all mixtures with different stoichiometry than the Ti_3-Al alloy. The amorphisation is attributed to the difference in point defects, long-range order (or lack thereof) and hydrogen occupation sites. Furthermore Hashi demonstrates that the amorphous material is much more stable than the crystalline Ti_3Al material and therefore contributes to an increase in the hydrogen desorption temperature. Another investigation of the hydrogenation of a Ti rich Ti-Al alloy shows that some amount of amorphous phase forms but the temperature of hydrogen desorption from the main phase and the amorphous phase cannot be identified [117].

Much attention has been given to the gravimetric capacity of the Al-Ti alloy, but the kinetics of the system have not been studied in detail. It is anticipated that the low hydrogen concentration of the Al-Ti alloy at modest temperatures may indicate high diffusion rates and contribute to enhanced kinetics for an Mg alloy matrix, a result measured by Kalisvaart for an Al-Ti catalysed Mg thin film [104].

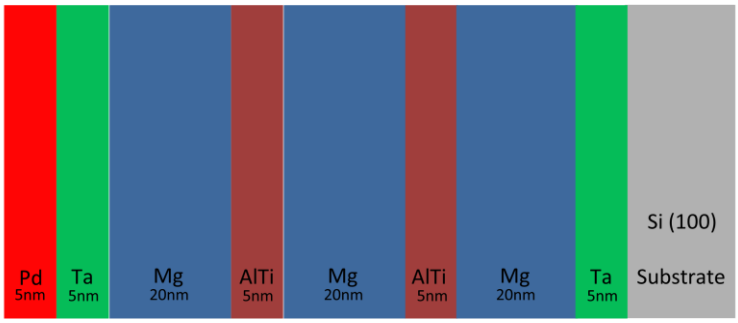

Figure 8-4 Multilayer structure used to measure the influence of an Al-Ti catalyst on the hydrogen absorption characteristic of a nanoscale Mg thin film. The bottom Ta layer is to prevent the formation of Mg-Si intermetallic mixture and also acts as a neutron reflectometry measurement contrast agent.

In this investigation the hydrogen sorption character of the Al-Ti catalysed Mg alloy is measured through an investigation of the deuterium absorption of an Al-Ti/Mg multilayer film deposited on a Ta (10nm) coated silicon (100) wafer. The underlying Ta layer is used to prevent alloy-Si interactions and facilitate a NR contrast. The multilayers consist of three repeated layers of an Mg (20nm) and Al-Ti alloy (5nm) making up a Mg/(Al-Ti) multilayer (see Figure 8-4). Again Pd (10nm) is deposited on the surface to facilitate hydrogen dissociation at room temperature and prevent oxidation of the underlying Mg and Al-Ti layers that may result in a debilitating hydrogen diffusion barrier.

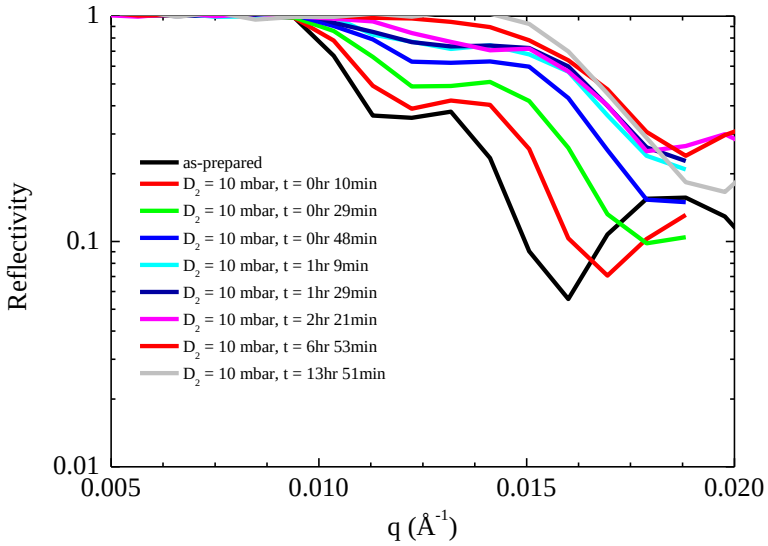

Figure 8-5 Neutron reflectometry critical-edge measurements of the Al-Ti catalysed Mg thin film structure as illustrated in Figure 8-4

Neutron reflectometry measurements of the Mg/(Al-Ti) multilayer are presented in Figure 8-5 and provide a qualitative understanding of the deuterium absorption kinetic process. Consistent with the previous measurements of the Mg/(Fe-Ti) multilayer, the absorption occurs slowly at a deuterium pressure of 10mbar. The absorption process, according to the critical-edge measurements of Figure 8-5 appears to proceed by absorption in the thin catalysts layers for a period of up to 1 hour followed by absorption in the thicker Mg layers. These qualitative observations are illustrated more explicitly through the thorough measurements in the next section.

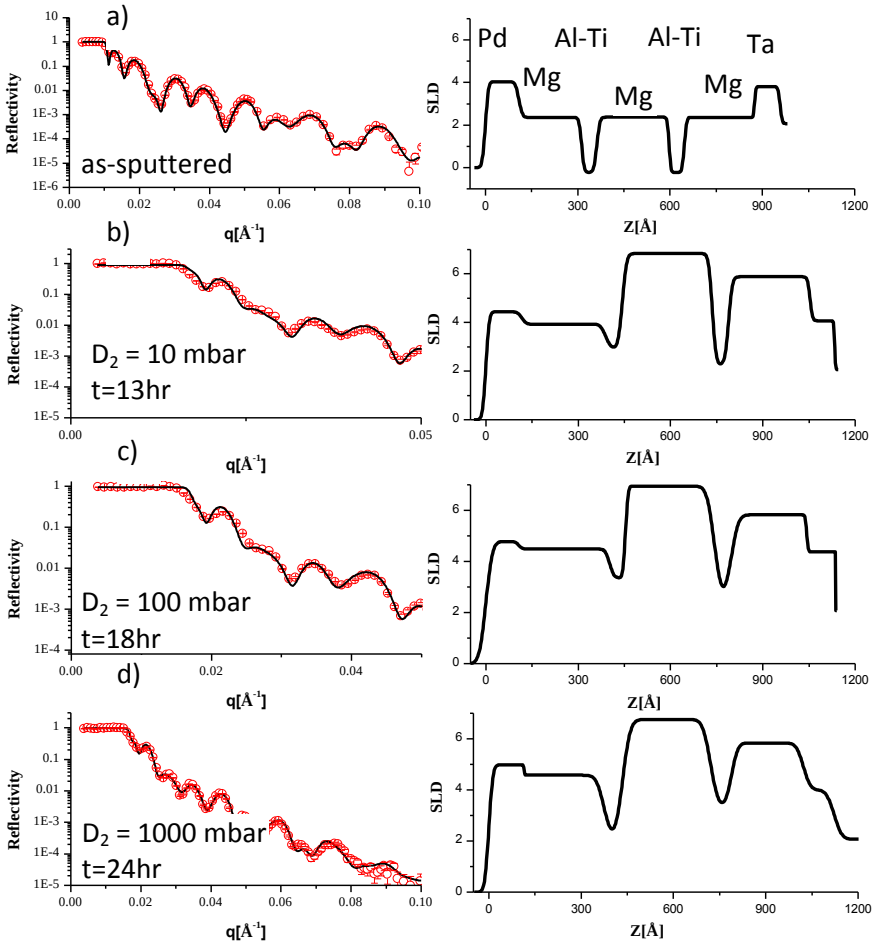

Figure 8-6 Neutron reflectivity measurements of a thin film multilayer consisting of an alternating stack of Mg and Al-Ti (Figure 8-4 Reflectometry measurements are represented on the left with the real-space representation of the scattering length on the right. Measurements are taken in situ in a deuterium environment at (a) vacuum, (b) 10 mbar, (c) 100 mbar, and (d) 1,000 mbar. Each scan required ~1 hour to complete. Therefore, the sample was at 10mbar, 100mbar, and 1000 mbar for 13 hours, 4 hours, and 5 hours respectively before the measurements were taken.

Neutron reflectometry measurements of the Mg/Al-Ti alloy multilayer structure (represented in Figure 8-4) are illustrated on the left side of Figure 8-6, and the real space representation on the right side of Figure 8-6. Again, the visible oscillations, referred to as Kiessig fringes, are associated with the characteristic thickness and SLD contrast between each layers of the film. Consistent with previous experimental procedures, NR measurements are taken of the as-prepared film in a vacuum prior to immersion in a deuterium environment. As illustrated in Figure 8-6, the reflectometry

measurements clearly indicated the structure as distinct layers of Pd (10nm), followed by a repeated structure of Mg (20nm) and Al-Ti (5nm) Mg (20nm) and a 10 nm Ta layer deposited on a silicon substrate. The sharp delimitation of each layer suggests very little interfacial roughness and little mixing or alloying between adjacent layers.

Due to the large scattering length of deuterium, the SLD of the absorbing layers increases. In particular, at a pressure of 10 mbar and at equilibrium, deuterium seems to absorb into all of the layers. The SLD of the middle Mg layer is substantially higher than that of the other two layers, suggesting the deuterium concentration is much higher than in the other layers. The bottom and top layers are either elastically constrained by the Ta and Pd layers, respectively, resulting in a higher equilibrium hydrogen pressure, or impeded kinetically. Increasing the deuterium pressure to 100 mbar and 1 bar does not substantially change the SLD of each of the layers; therefore it is assumed that close to complete absorption can be accomplished at 10 mbar.

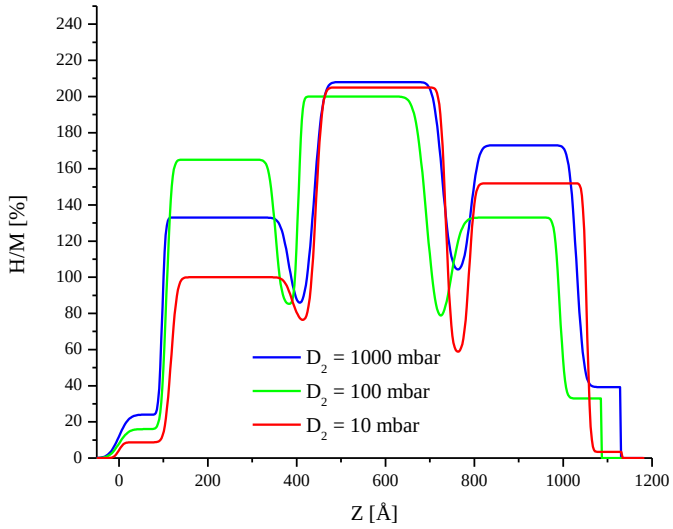

Figure 8-7 Hydrogen concentration profile at deuterium pressures of 10, 100, and 1,000 mbar of the Al-Ti-catalysed Mg thin film structure illustrated in Figure 8-4

Upon completion of the NR measurements (see Figure 8-6), the hydrogen concentration is calculated and plotted in Figure 8-7. As suggested by the changes in the SLD, the Al-Ti catalysed Mg multilayer takes up a considerable amount of hydrogen at 10 mbar. The hydrogen concentration of each of the Mg layers is not uniform and the layer sandwiched between the two Al-Ti catalysts has the largest amount of hydrogen. The diminished hydrogen concentration within the top and bottom Mg layers may be explained by a clamping effect from the Ta and Pd layers. This increased stress may result in a destabilizing effect and thereby may increase the equilibrium pressure or decrease the kinetic rates to such a value that absorption effectively does not take place. Increasing the pressure to 1 bar results in an increase in the hydrogen concentration of the bottom Mg layer but this concentration does not reach the same concentration of the middle layer. The hydrogen concentration in the Al-Ti catalyst-sandwiched Mg layer does not change with a change in the deuterium pressure. One expects the hydrogen

concentration to increase with increased pressure even though a phase transformation has not taken place (i.e. Mg to α-Mg-H_2).

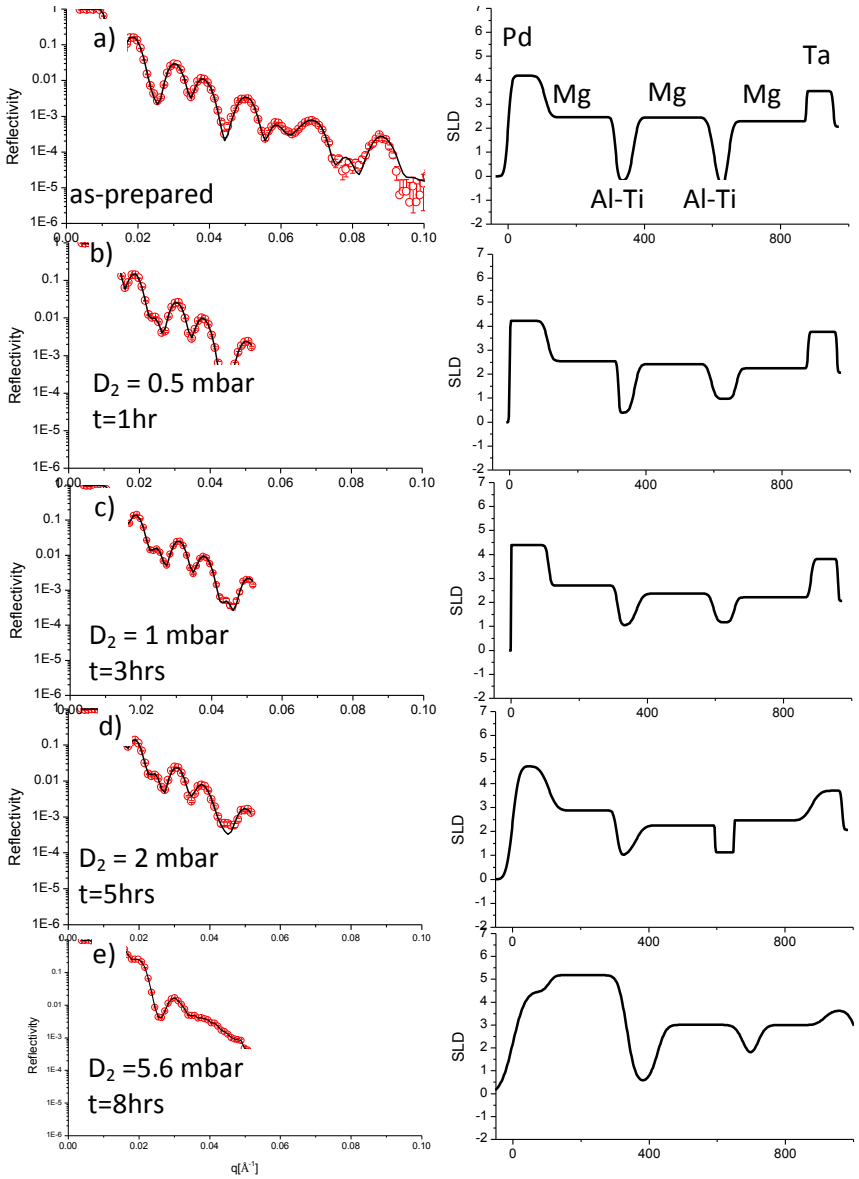

Figure 8-8 Neutron reflectivity measurements of a thin film multilayer consisting of an alternating stack of Mg and Al-Ti (see Figure 8-4). Reflectometry measurements are represented on the left with the real-space representation of the scattering length on the right. Measurements are taken in situ in a deuterium environment at (a) vacuum, (b) 0.5 mbar, (c) 1 mbar, (d) 2 mbar, and (e) 5.6 mbar. These measurements are used to complement the measurements taken previously at higher pressures. The time above is the time at which the measurements were taken. Since each measurement takes ~1 hour, the sample was at 0.5 mbar, 1 mbar, 2 mbar, and 5.6 mbar for 1 hour, 1 hour, 1 hour, and 2 hours respectively before the measurements were taken.

Neutron reflectometry measurements of the Mg/(Al-Ti) alloy multilayer structure (see Figure 8-4) taken at lower pressures than in the earlier measurements are presented in Figure 8-8. Again, consistent with previous measurements, the as-sputtered material is measured in vacuum prior to NR measurements in a deuterium atmosphere. The SLD

presented in Figure 8-8a represents a structure of Pd (10nm) followed by a repeated structure of Mg (20nm) and Al-Ti (5nm), Mg (20nm) and a 10nm Ta layer deposited on a silicon substrate. The sharp delimitation of adjacent layers suggests little interfacial roughness and little mixing or alloying.

Upon completion of the neutron reflectometry measurements of the as-sputtered material, the deuterium pressure was increased to 0.5 mbar and held for several hours prior to acquiring the measurement. As a result of the increase in deuterium pressure and long exposure time, the SLD of the Al-Ti layer increases, suggesting deuterium absorption within the Al-Ti layers. At this point there is insufficient concentration in the other layers (Pd, Mg, and Ta) to produce a noticeable change in the SLD. After the deuterium pressure is further increased to 1 mbar, the SLD of the Al-Ti also increases, corresponding to an increase in the deuterium concentration. Furthermore, there is a noticeable increase in the SLD of the Pd layer, suggesting the presence of deuterium. Only after increasing the deuterium pressure to 2 mbar is there no further increase in the SLD of the Al-Ti layers; however there is an increase in the SLD of the top Pd catalyst layer. At 2 mbar there is an increase in the SLD of the top Mg layer. Typically a much larger hydrogen pressure is required to observe hydrogenation of Mg at room temperature.

After increasing the deuterium pressure to 5.6 mbar, (see Figure 8-8c), there is an increase in the SLD of the top Mg layer, corresponding to an increase in deuterium concentration. At such a low deuterium pressure the presence of the top Mg-H_2 layer drastically reduces the diffusion rate and effectively arrests the hydrogenation of the other layers. The interfacial roughness between the Mg and Ti-Al layers significantly

increases and is attributed that of the Mg-to-Mg-H_2 phase change (i.e. swelling and buckling from an approximate 30% volume expansion due to the phase change).

8.3.Multilayer Conclusions

The sorption character of several multilayer structures is analysed to illustrate the hydrogen sorption process through complex multilayer structures. Previous studies have not used the power of NR to interrogate the hydrogen sorption profile through a hydrogen-loaded sample in great detail. The use of the multilayer structure with NR gives a novel look into the kinetics of hydrogen loading and unloading.

Generally speaking, the hydrogen loading of the multilayer structures passes through several stages prior to full hydrogenation. In the first stage, the catalytic layer absorbs hydrogen prior to the bulk magnesium alloy a result that is very surprising given the limited reporting of this effect. Moreover, there is little or no hydrogen within the Mg phase until the hydrogen reaches a critical pressure. It is anticipated that an increase in temperature will reduce the required hydrogen pressure as it is anticipated that the system is kinetically instead of thermodynamically, limited.

The second stage is complete hydrogen absorption in the main Mg layer. Complete absorption does not occur until a considerable amount of time has passed at a modest pressure and at room temperature- an unrealistic amount of time for a practical storage medium.

9. Conclusions and Future Work

The aim of this research to increase the hydrogen sorption rates of Mg alloys is accomplished through addition of the surface and bulk catalytic layers. The binary surface catalyst Pd/Ta is the most promising surface catalyst for Mg-based alloys. This catalyst decreases the required absorption temperature and remains intact through sorption cycling. In fact, the surface catalyst reduces the required sorption pressure by 10-fold at room temperature a feat not noted in the literature. Also, the choice of secondary catalytic layers greatly increases the diffusion through the structure with the Al-Ti alloy showing the most promise.

In conclusion, this study illustrates in detail the steps to store hydrogen within magnesium alloys through neutron reflectometry measurements. The catalyst layers absorb hydrogen before the main Mg layer which may be attributed to the large phase transformation barrier for Mg to alpha Mg hydride formation. Furthermore non-absorbing regions devoid of hydrogen form between the Mg alloys and the Ta or Pd catalysts. These regions are most probably the result of interfacial stress that increases the enthalpy of absorption thus preventing sorption under the moderate experimental conditions. This finding clearly indicates that a degree of optimization can increase the total sorption capacity if the proper catalyst (e.g. a Pd/Ti binary catalyst) is chosen to reduce the size of void regions. Further investigation is required to determine the effect of varying the thickness of the Mg layers on the catalysts or vice versa.

9.1.Future Work

The aim of this research is to show that addition of catalysts on the surface or within the bulk of an Mg alloy can increase the hydrogen sorption rates. This increase in sorption

rates is very important to any application of a storage medium because the limiting factor for several applications is the rate of sorption (absorption and desorption). Typically the system temperature is increased to offset the slow kinetics, but some applications- including hydrogen-tunable optical mirrors- cannot withstand higher temperatures.

9.1.1. Optical Mirrors

One application that is being widely examined is the role of the optical switching behaviour of storage material; switching between a black state and a reflective state [33, 118, 119]. This optical switching behaviour is very intriguing for hydrogen sensing or smart covers for solar collectors. This thesis does not examine the optical character of the materials but it is expected that a change in the optical character takes place between the hydrogen loaded and unloaded structures [118]. Further research should examine the optical character of these materials during hydrogen cycling.

Baldi [33] suggests the ability to "tune" the thermodynamics of the Mg alloy by adjusting its thickness below ~10 nm within the multilayer structure. This tuning, along with the knowledge that Mg-H_2 undergoes a large optical character change with hydrogen loading, allows for a tunable optical structure. Baldi also suggests that degradation of the Mg-TI structure occurs as the sandwiched Ti forms a very stable hydride; therefore full recycling is not possible. In this thesis the loading of the hydrogen appears recyclable and the film does not appear to degrade.

In this study the reflectometry measurements suggests the catalytic layers do not disconnect with the Mg layers and the interface remains intact. As shown in Figure 8-2, the interfacial roughness between the Al-Ti and the Mg does not increase; therefore the

interface between the Mg and Al-TI does not degrade. One might expect degradation if, for example, the Al-Ti forms either a stable hydride or disconnects with the Mg layers (disconnect requires the formation of voids and cracks in the interface). Moreover, the intermediate catalyst layers (Fe-Ti or Al-Ti) do not undergo a large expansion during hydrogen sorption; therefore a large interfacial stress does not exist,; further evidence that would limit degradation. Further study of the overall optical characteristics of the structure (e.g. the optical characteristics versus multilayer thickness, hydrogen uptake, etc.) is required.

For the application of hydrogen smart mirrors, the change in state of the hydrogen material, from a black state to a mirror state, can be utilized. The material will either absorb the light or reflect it. In one application, the hydrogen storage material can be used as a thermal regulator for a solar panel. A solar panel can seriously degrade due to an increase in the panel temperature.[120] Currently the designer must employ a series of temperature sensors and protection circuitry must be employed to mitigate against over temperature situations, leading to an increase in the system complexity and a possible failure pathway. Moreover, the protective circuitry cannot monitor the detailed temperature distribution across the panel and therefore must compensate only the whole panel as a single unit. The use of a solar mirror could automatically mitigate over temperature regions on the solar panel and therefore optimize the use of the panel.

9.1.2. Hydrogen Storage Material

Solid-state hydrogen storage is fundamentally limited by the rate of sorption although the thermodynamics and kinetics of the storage medium are inexorably linked. Mg and Mg alloys have still drawn attention as alternative hydrogen storage media given their

relatively high theoretical capacity (8.2wt% H/M) [121]. In this thesis the kinetics are decoupled from the thermodynamics by time and space resoled measurements of the hydrogen profile within the catalysed magnesium structure. These measurements give a novel view of the role of the catalytic layers and therefore offer new insight into alloy design.

Knowledge from this thesis can be used in conjunction with an Mg alloy with enhanced thermodynamics to allow the development of an efficient hydrogen storage alloy [122]. The thermodynamics may be altered by further alloy additions, nanostructuring, or other novel techniques. Development requires an examination of the fabrication methods as the development of these methods is generally not trivial (i.e. degradation from impurities introduced during fabrication may hinder alloy performance).

10. Bibliography

[1] K. Mette, A. Bergmann, J. Tessonnier, M. Havecker, L. Yao, T. Ressler, R. Schlogl, P. Strasser and M. Behrens, " Nanostructured Manganese Oxide Supported on Carbon Nanotubes for Electrocatalytic Water Splitting," *ChemCatChem ,* vol. 4, no. 6, pp. 851-862, 2012.

[2] J. Bolton, "Solar Photoproduction of Hydrogen: A Review," *Solar Energy,* vol. 57, no. 1, pp. 37-50, 1996.

[3] T. Minowa and T. Ogi, "Hydrogen production from cellulose using a reduced nickel catalyst," *Catalysis Today,* vol. 45, pp. 411-416, 1998.

[4] Z.-W. Liu, K.-W. Jun, H.-S. Roh and S.-E. Park, "Hydrogen production for fuel cells through methane reforming at low temperatures," *Journal of Power Sources,* vol. 111, pp. 283-287, 2002.

[5] K. Maeda, K. Teramura, T. Takata, N. Saito, Y. Inoue and K. Domen, "Photocatalyst releasing hydrogen from water - Enhancing catalytic performance holds promise for hydrogen production by water splitting in sunlight.," *Nature,* vol. 440, no. 7082, pp. 295-295, March 2006.

[6] Y. H. Jung and Y. H. Jeong, "Development of the once-through hybrid sulfur

process for nuclear hydrogen production," *International Journal of Hydrogen Energy,* vol. 35, no. 22, pp. 12255-12267, November 2010.

[7] Wikipedia, "Hydrogen Economy," [Online]. Available: http://en.wikipedia.org/wiki/Hydrogen_economy#Concentrating_solar_thermal. [Accessed 12 December 2010].

[8] Solid H, "Metal Hydrides," [Online]. Available: http://www.hydrogencomponents.com/hydride.html. [Accessed 12 12 2010].

[9] R. Ewald, "Requirements for advanced mobile storage systems," *International Journal of Hydrogen Energy,* vol. 23, no. 9, pp. 803-814, 1998.

[10] Knovel, CRC Handbook of Chemistry and Physics, 91st ed., E. Edition, Ed., Binghamton, N.Y. : Boca Raton, Fla. : CRC ; London : Taylor & Francis, 2010-2011.

[11] L. Zhou and Y. Zhou, "Determination of compressibility factor and fugacity coefficient of hydrogen in studies of adsorptive storage," *International Journal of Hydrogen Energy,* vol. 26, no. 6, pp. 597-601, 2001.

[12] A. Centrone, L. Brambilla and G. Zerbi, "Adsorption of H2 on carbon-based materials: a Raman spectroscopy study," *Physical Review B,* vol. 71, no. 24, p. 245406 , 2005.

[13] V. Berube, G. Radtke, M. Dresselhaus and G. Chen, "Size effects on the hydrogen storage properties of nanostructured metal hydrides: A review," *INTERNATIONAL JOURNAL OF ENERGY RESEARCH,* vol. 31, pp. 637-663, 2007.

[14] A. Pundt and R. Kirchheim, "Hydrogen In Metals: Microstructural Aspects," *Annual Review of Materials Research,* vol. 36, pp. 555-608, 24 April 2006.

[15] M. Lagos, G. Martinez and I. Schuller, "Kinetics of hydrogen absorption in transition metals and subsurface bonding," *Physical Review B,* vol. 29, no. 10, pp. 5979-5981, 1984.

[16] F. Katsuyuki, "Surface Hydrogen and Subsurface Hydrogen: Their Roles in Bulk Absorption and Surface Reaction," *Journal of the Vacuum Society of Japan,* vol. 53, no. 4, pp. 271-279, 2010.

[17] H. Conrad, G. Ertl and E. E. Latta, "Adsorption of hydrogen on palladium single crystal surfaces," *Surface Science,* vol. 41, pp. 435-446, 1974.

[18] K. H. Rieder, M. Baumberger and W. Stocker, "Selective transition of chemisorbed hydrogen to subsurface sites on Pd(110)," *Physical Review Letters,* vol. 51, pp. 1799-1802, 1983.

[19] E. Salomons, R. Griessen, D. G. de Groot and A. Magerl, " Surface Tension and Subsurface Sites of Metallic Nanocrystals Determined from H-Absorption," *Europhysics Letters,* vol. 5, p. 449.

[20] W. Ludwig, A. Savara, R. Madix, S. Schauermann and H.-J. Freund, "Subsurface Hydrogen Diffusion into Pd Nanoparticles: Role of Low-Coordinated Surface Sites and Facilitation by Carbon," *Journal of Physical Chemistry C,* vol. 116, pp. 3539-3544, 2012.

[21] S. J. Peighambardoust, S. Rowshanzamir and M. Amjadi, "Review of the proton exchange membranes for fuel cell applications," *Internationa Journal of Hydrogen Energy,* vol. 35, no. 17, pp. 9349-9384, 2010.

[22] B. Sakintuna, F. Lamari-Darkrim and M. Hirscher, "Metal hydride materials for solid hydrogen storage: A review," *International Journal of Hydrogen Energy,* vol. 32, pp. 1121-1140, 2007.

[23] J. Huot, G. Liang, S. Boily, A. Van Neste and R. Schulz, "Structural study and hydrogen sorption kinetics of ball-milled magnesium hydride," *Journal of Alloys and Compounds,* Vols. 293-295, pp. 495-500, 1999.

[24] A. Baldi, V. Palmisano, M. Gonzalez-Silveira, Y. Pivak, M. Slaman, H. Schreuders, B. Dam and R. Griessen, "Quasifree Mg-H thin films," *Applied Physics Letters,* vol. 95, no. 7, p. 071903, 2009.

[25] S. Singh, S. W. Eijit, M. Zandbergen, W. Legerstee and V. Svetchnikov, "Nanoscale structure and the hydrogenation of Pd-capped magnesium thin films prepared by plasma sputter and pulsed laser deposition," *Journal of Alloys and Compounds,* vol. 441, no. 1-2, pp. 344-351, 2007.

[26] A. Zaluska, L. Zaluski and J. Strom-Olsen, " Nanocrystalline magnesium for hydrogen storage," *Journal of Alloys and Compounds,* vol. 288, no. 1-2, pp. 217-225, 1999.

[27] J. F. Herbst, "On extending Miedema's model to predict hydrogen content in binary and ternary hydrides," *Journal of Alloys and Compounds,* vol. 337, pp. 99-

107, 2002.

[28] E. Johansson, C. Chacon, C. ZLotea, Y. Andersson and B. Hjorvarsson, "Hydrogen uptake and optical properties of sputtered Mg-Ni thin films," *Journal of Physics: Condensed Matter,* vol. 16, pp. 7649-7662, 2004.

[29] F. C. Gennari and M. R. Esquivel, "Structural characterization and hydrogen sorption properties of nancrystalline Mg2Ni," *Journal of Alloys and Compounds,* vol. 459, pp. 425-432, 2008.

[30] L. Z. Ouyang, S. Y. Dong and M. Zhu, "Effect of interfacial free energy on hydriding reaction of Mg-Ni thin films," *Applied Physics Letters,* vol. 90, p. 021917, 2007.

[31] H. Z. Yan, F. Q. Kong, W. Xiong, B. Q. Li, J. Li and M. Zhu, "The influence of ball milling process on formation and electrochemical properties of amorphous MgNi hydrogen storage alloys," *Materials Science and Engineering,* Vols. 435-436, pp. 711-716, 2006.

[32] C. Read, G. Thomas, G. Ordaz and S. Satyapal, "U.S. Department of Energy's System Targets for On-Board Vehicular Hydrogen Storage," *Material Matters,* vol. 2, no. 2, pp. 3-5, 2007.

[33] A. Baldi, G. K. Palsson, M. Gonzalez-Silveira, H. Schreuders, H. Slaman, J. H. Rector, G. Krishnan, B. J. Kooi, G. S. Walker, W. Fay, R. J. Wijngaarden, B. Dam and R. Griessen, "Mg/Ti multilayers: Structural and hydrogen absorption properties," *Physical Review B,* vol. 81, no. 22, p. 224203, 2010.

[34] G. Cakmak, Z. Karoly, I. Mohai, T. Ozturk and J. Szepvolgyi, "The processing of Mg-Ti for hydrogen storage; mechanical milling and plasma synthesis," *International Journal of Hydrogen Energ,* vol. 35, no. 19, pp. 10412-10418, 2010.

[35] J. C. Crivello, T. Nobuki, S. Kato, M. Abe and T. Kuji, "Hydrogen absorption properties of the -Mg17Al12 phase and its Al-rich domain," *Journal of Alloys and Compounds,* Vols. 446-447, pp. 157-161, 2007.

[36] D. L. Douglas, "The Formation and Dissociation of Magnesium alloy Hydrides and Their Use For Fuel Storage in the Hydrogen Car," *Metallurgical Transactions A,* vol. 6A, pp. 2179-2189, 1975.

[37] R. Gremaud, A. Borgschulte, C. Chacon, J. L. van Mechelen, H. Schreuders, A. Zuttel, B. Hjorvarsson, B. Dam and R. Griessen, "Structural and optical properties of of MgxAl1−xHy gradient thin films :a combinatorial approach," *Applied Physics A: Materials Science and Processing,* vol. 84, pp. 77-85, 2006.

[38] A. Andreasen, "Hydrogenation properties of Mg–Al alloys," *International Journal of Hydrogen Energy,* vol. 33, pp. 7489-7497, 2008.

[39] K. Komiya, N. Morisaku, Y. Shinzato, K. Ikeda, S. Orimo, Y. Ohki, K. Tatsumi, H. Yukawa and M. Morinaha, "Synthesis and dehydrogenation of M(AlH4)2 (M = Mg, Ca)," *Journal of Alloys and Compounds,* Vols. 446-447, pp. 237-241, 2007.

[40] M. Hanke, M. Dubslaff, M. Schmidbauer, T. Boeck, S. Schoder, M. Burghammer, C. Riekel, J. Patommel and G. Schroer, "Scanning x-ray diffraction with 200 nm

spatial resolution," *Applied Physics Letters,* vol. 92, no. 19, p. 193109, 2008.

[41] M. Dubslaff, M. Hanke, J. Patommel, R. Hoppe, C. Schroer, S. Schoder and M. Burghammer, "Scanning X-ray nanodiffraction: from the experimental approach towards spatially resolved scattering simulations," *Nanoscale Research Letters,* vol. 7, no. 1, pp. 553-561, 2012.

[42] Y. W. Lee, B. M. Clemes and K. J. Gross, "Novel Sieverts' type volumetric measurements of hydrogen storage properties for very small sample quantities," *Journal of Alloys and Compounds,* vol. 452, pp. 410-413, 2008.

[43] E. Zaremba and W. Kohn, "Theory of helium adsorption on simple and noble-metal surfaces," *Physical Review B,* vol. 15, no. 4, pp. 1769-1781, 1977.

[44] I. D. Lee, O. I. Smith and A. R. Karagozian, " Hydrogen and helium leak rates from micromachined orifices," *AIAA Journal,* vol. 41, no. 3, pp. 457-464, 2003.

[45] A. Qajar, M. Peer, R. Rajagopalan and H. C. Foley, " High pressure hydrogen adsorption apparatus: Design and error analysis," *International Journal of Hydrogen Energy,* vol. 37, no. 11, pp. 9123-9136, 2012.

[46] C. Zhang, X. S. Lu and A. Z. Gu, " How to accurately determine the uptake of hydrogen in carbonaceous materials," *International Journal of Hydrogen Energy,* vol. 29, no. 12, pp. 1271-1276, 2004.

[47] S. Emery, K. Rider, B. Little, A. Schrand and C. Lindsay, "Magnesium cluster film synthesis by helium nanodroplets," *The Journal of Chemical Physics,* vol. 139, p.

054307, 2013.

[48] L. Zhou and Y. Zhou, "Determination of compressibility factor and fugacity coefficient of hydrogen in studies of adsorptive storage," *International Journal of Hydrogen Energy,* vol. 26, pp. 597-601, 2001.

[49] R. Perry and D. Green, Perry's Chemical Engineers' Handbook (7th Edition), McGraw-Hill., 1997.

[50] T. P. Blach and E. M. Gray, "Sieverts apparatus and methodology for accurate determination of hydrogen uptake by light-atom hosts," *Journal of Alloys and Compounds,* Vols. 446-447, pp. 692-697, 2007.

[51] V. Sears, "Neutron scattering lengths and cross sections," vol. 3, pp. 26-37, 1992.

[52] T. Steiner, "The Hydrogen Bond in the Solid State," *Angewandte Chemie International Edition,* vol. 41, no. 1, pp. 48-76, 2002.

[53] X.-L. Zhou and S.-H. Chen, "Theoretical foundation of X-ray and neutron reflectometry," *Physics Reports,* vol. 257, pp. 223-348, 1995.

[54] J. Lekner, Theory of reflection: of electromagnetic and particle waves, Massachussets: Kluwer Academic Publishers, 1987.

[55] L. Nevot and P. Croce, "Caracterisation des surfaces par reflexion rasante de rayons," *Revue de physique appliquee,* vol. 15, pp. 761-769, 1980.

[56] G. L. Powell and J. R. Kirkpatrick, " SURFACE CONDUCTANCE AND THE DIFFUSION

OF H AND D IN PD," *Physical Review B,* vol. 43, no. 9, pp. 6968-6976, 1991.

[57] B. Bhati and D. Sholl, "Quantitative assessment of hydrogen diffusion by activated hopping and quantum tunneling in ordered intermetallics," *Physical Review B,* vol. 72, p. 224302, 2005.

[58] R. Lasser, "Solubility of protium, deuterium, and tritium in the or phase of palladium," *Physical Review B,* vol. 29, no. 8, pp. 4765-4768, 1984.

[59] C. Rehm, H. Fritzsche, H. Maletta and F. Klose, "Hydrogen concentration and its relation to interplanar spacing and layer thickness of 1000-angstrom Nb(110) films during in situ hydrogen charging experiments," *Physical Review B,* vol. 59, no. 4, pp. 3142-3152, 1999.

[60] H. Rauch, H. Wolwitsch, H. Kaiser, R. Clothier and S. A. Werner, "Measurement and characterization of the three-dimensional coherence function in neutron interferometry," *Physical Review A,* vol. 53, no. 2, pp. 902-908, February 1996.

[61] H.-Y. Tien, M. Tanniru, C.-Y. Wu and F. Ebrahimi, "Effect of hydride nucleation rate on the hydrogen capacity of Mg," *International Journal of Hydrogen Energy,* vol. 34, no. 15, 2009.

[62] M. Pozzo and D. Alfe, "Hydrogen dissociation and diffusion on transition metal (= Ti, Zr, V, Fe, Ru, Co, Rh, Ni, Pd, Cu, Ag)-doped Mg(0001) surfaces," *International Journal of Hydrogen Energy,* vol. 34, no. 4, pp. 1922-1930, 2009.

[63] M. Ismail, Y. Zhao, X. B. Yu and S. X. Dou, "Improved hydrogen storage

performance of MgH2–NaAlH4 composite by addition of TiF3," *International Journal of Hydrogen Energy,* vol. 37, no. 10, p. 8395–8401, 2012.

[64] M. Avrami, "Kinetics of Phase Change. I General Theory," *Journal of Chemical Physics,* vol. 7, no. 12, pp. 1103-1112, 1939.

[65] M. Avrami, "Kinetics of Phase Change. II Transformation-Time Relations for Random Distribution of Nuclei," *Journal of Chemical Physics,* vol. 8, no. 2, pp. 212-224, 1940.

[66] M. Avrami, "Granulation, Phase Change and Microstructure Kinetics of Phase Change. III," *Journal of Chemical Physics,* vol. 9, pp. 177-184, 1941.

[67] A. Borgschulte, R. Gremaud and R. Griessen, "Interplay of diffusion and dissociation mechanisms during hydrogen absorption in metals," *Physical Review B.,* vol. 78, no. 9, p. 094106, 2008.

[68] G. Wu, W. Dai, L. Song and A. Wang, "Surface Microstructurization of a Sputtered Magnesium Thin Film via a Solution-Immersion Route," *Materials Letters,* vol. 64, no. 3, pp. 475-478, 2010.

[69] P. Vermeulen, R. Niessen and P. Notten, "Hydrogen storage in metastable MgyTi(1 − y) thin films," *Electrochemistry Communications,* vol. 8, no. 1, pp. 27-32, 2006.

[70] J. Huot, M. Tremplay and R. Schulz, "Synthesis of nanocrystalline hydrogen storage materials," *Journal of Alloys and Compounds,* Vols. 356-357, pp. 603-607, 2003.

[71] K. Higuchi, H. Kajioka, H. Fujii, S. Orimo and Y. Kikuchi, " In situ study of hydriding-dehydriding properties in some Pd/Mg thin films with different degree of Mg crystallization," *JOURNAL OF ALLOYS AND COMPOUNDS,* vol. 293, pp. 484-489, 1999.

[72] K. Yoshimura, Y. Yamada and M. Okada, " Hydrogenation of Pd capped Mg thin films at room temperature," *Surface Science,* vol. 566, pp. 751-754, 2004.

[73] H. Windischmann, "Intrinsic stess in Sputtered Thin Films," *Journal of Vacuum Science and Technology A,* vol. 9, no. 4, pp. 2431-2437, 1991.

[74] B. Trindade, C. Coelho, G. Tome and F. Froes, "Production of Ti-Mg-Si Thin Films by Magnetron Sputtering and their phase transformations with Temperature," *Key Engineering Materials,* Vols. 230-232, pp. 64-67, 2002.

[75] I. Jain, C. Lal and A. Jain, "Hydrogen storage in Mg: A most promising material," *International Journal of Hydrogen Energy,* vol. 35, pp. 5133-5134, 2010.

[76] P. Tessier, R. Schulz and J. Strom-Olsen, "Elastic stress in composite FeTi hydrogen storage materials," *Journal of Materials Research,* vol. 13, no. 6, pp. 1538-1547, 1998.

[77] R. Gremaud, M. Gonzalez-Silveira, Y. Pivak, S. de Man, M. Slaman, H. Schreuders, B. Dam and R. Griessen, "Hydrogenography of PdHx thin films: Influence of H-induced stress relaxation processes," *Acta Materialia,* vol. 57, no. 4, pp. 1209-1219 , 2009.

[78] J. Huot, G. Liang, S. Boily, A. Van Neste and R. Schulz, "Structural study and hydrogen sorption kinetics of ball-milled magnesium hydride," *Journal of Alloys and Compounds,* Vols. 293-295, pp. 495-500, 1999.

[79] S. Ye, S. Chan, L. Ouyang and M. Zhu, "Hydrogen storage and structure variation in Mg/Pd multi-layer film," *Journal of alloys and Compounds,* vol. 54, no. 2, pp. 493-497, 2010.

[80] P. Vermeulen, R. Niessen and P. Notten, "Hydrogen storage in metastable MgyTi(1-y) thin films," *ELECTROCHEMISTRY COMMUNICATIONS,* vol. 8, no. 1, pp. 27-32, 2006.

[81] P. Vermeulen, P. Graat, H. Wondergem and P. Notten, "Crystal structures of MgyTi100-y thin film alloys in the as-deposited and hydrogenated state," *International Journal of Hydrogen Energy,* vol. 33, no. 20, pp. 5646-5650, 2008.

[82] G. Garcia, R. Domenech-Ferrer, F. Pi, J. Santiso and J. Rodriguez-Viejo, "Combinatorial Synthesis and Hydrogenation of Mg/Al Libraries Prepared by Electron Beam Physical Vapor Deposition," *J. Comb. Chem.,* vol. 9, pp. 230-236, 2007.

[83] R. Domenech-Ferrer, M. G. Sridharan, G. Garcia, J. Rodriguez-Viejo and F. Pi, "Hydrogenation properties of pure magnesium and magnesium–aluminium thin films," *Journal of Power Sources,* vol. 169, pp. 117-122, 2007.

[84] A. San-Martin and F. Manchester, "The H-Ta (Hydrogen-Tantalum) System,"

Journal of Phase Equilibria, vol. 22, no. 3, pp. 332-343, 1991.

[85] B. Bogdanovic, K. Bohmhammel, B. Christ, A. Reister, K. Schlichte, R. Vehlen and U. Wolf, "Thermodynamic investigation of the Magnesium-Hydrogen system," *Journal of Alloys and Compounds,* vol. 282, no. 1-2, pp. 84-92, 1999.

[86] Y. Pivak, R. Gremaud, K. Gross, M. Gonzalez-Silveira, A. Walton, D. Book, H. Schreuders, B. Dam and R. Griessen, "Effect of the substrate on the thermodynamic properties of PdHx films studied by hydrogenography," *Scripta Materialia,* vol. 60, pp. 348-351, 2009.

[87] H. Fritzsche, M. Saoudi, J. Haagsma, C. Ophus, C. Harrower and D. Mitlin, "Structural changes of thin MgAl films during hydrogen desorption," *Nuclear Instruments and Methods in Physics Research A,* vol. 600, no. 1, pp. 301-304, 2009.

[88] Y. Sunthia, G. Reddy, S. Kumar and V. Raju, "Studies on interdiffusion in Pd/Mg/Si films: Towards improved cyclic stability in hydrogen storage," *Applied Surface Science,* vol. 256, pp. 1553-1559, 2009.

[89] A. J. Du, S. C. Smith, X. D. Yao and G. Q. Lu, "Hydrogen Spillover Mechanism on a Pd-Doped Mg Surface as Revealed by ab initio Density Functional Calculation," *Journal of the American Chemical Society,* vol. 129, no. 33, pp. 10201-10204, 2007.

[90] A. Borgschulte, W. Lohstroh, R. Westerwaal, H. Schreuders, J. Rector, B. Dam and R. Griessen, "Combinatorial method for the development of a catalyst promoting hydrogen uptake," *JOURNAL OF ALLOYS AND COMPOUNDS,* vol. 404, pp. 699-705,

2005.

[91] J. Greely and M. Mavrikakis, "Alloy catalysts designed from first principles," *Nature Materials,* vol. 3, p. 810, 2004.

[92] J. Slack, J. Locke, S. Song, J. Ona and T. Richardson, "Metal hydride switchable mirrors: Factors influencing dynamic range and stability," *Solar Energy Materials and Solar Cells,* vol. 90, p. 485, 2006.

[93] A. Remhof, K. Song, Theis-Brohl and H. Zabel, "Reversible loading of epitaxial Y(00.1) films with hydrogen," *Physical Review B,* vol. 56, no. 6, pp. R2897-R2899, 1997.

[94] M. Pasturel, R. J. Wijngaarden, W. Lohstroh, H. Schreuders, M. Slaman, B. Dam and R. Griessen, "Influence of the chemical potential on the hydrogen sorption kinetics of Mg2Ni/TM/Pd (TM = transition metal) trilayers," *Chemistry of Materials,* vol. 19, pp. 624-633, 2007.

[95] S. X. Tao, P. Notten, R. A. van Santen and A. P. Jansen, "DFT studies of hydrogen storage properties of Mg0.75Ti0.25," *Journal of alloys and Compounds,* vol. 509, no. 2, pp. 210-216, 2011.

[96] J. A. Zhang, Y. N. Huang, C. Mao, C. G. Long, Y. M. Shao, J. Q. Fu and P. Peng, "Dehydrogenation Properties and Micromechanisms of MgH2 Hydrogen Storage Systems with Ti, V or Nb Doping," *Acta Chimica Sinica,* vol. 68, no. 20, pp. 2077-2085, 28 Oct 2010.

[97] I. J. Jensen, S. Diplas and O. M. Lowik, "Density functional calculations of Ti nanoclusters in the metastable Mg-Ti system," *Physical Review B,* vol. 82, no. 17, p. 174121, 2010.

[98] S. X. Tao, P. H. Notten, R. A. van Santen and A. P. Jansen, "Fluorite transition metal hydride induced destabilization of the MgH2 system in MgH2/TMH2 multilayers (TM=Sc, Ti, V, Cr, Y, Zr, Nb, La, Hf)," *Physical Review B,* vol. 82, no. 12, p. 125448, 2010.

[99] A. San-Martin and F. D. Manchester, "The H-Ti (Hydrogen-Titanium) System," *Bulletin of Alloy Phase Diagrams,* vol. 8, no. 1, pp. 30-42, 1987.

[100] H. Matsui and N. Takano, "Crack growth process in Ni-Single crystal with hydrogen cathodic charging," *International Journal of Fracture,* vol. 157, no. 1-2, pp. 45-53, 2009.

[101] Y. Cao, J. Szpunar and W. Shmayda, "Effects of textures on hydrogen diffusion in nickel," in *TEXTURES OF MATERIALS, PTS 1 AND 2*, TRANS TECH PUBLICATIONS LTD, BRANDRAIN 6, CH-8707 ZURICH-UETIKON, SWITZERLAND, 2002, pp. 1139-1144.

[102] J. Greeley and M. Mavrikakis, "Alloy catalysts designed from first principles," *Nature Materials,* vol. 3, pp. 810-815, 2004.

[103] M. Saraiva and D. Depla, "Texture and microstructure in co-sputtered Mg-M-O (M5Mg, Al, Cr, Ti, Zr, and Y) films," *Journal of Applied Physics,* vol. 111, no. 10, p.

104903, 2012.

[104] W. P. Kalisvaart, C. T. Harrower, J. Haagsma, B. Zahiri, E. Luber, C. Ophus, E. Poirier, H. Fritzsche and D. Mitlin, "Hydrogen storage in binary and ternary Mg-based alloys: A comprehensive experimental study," *International Journal of Hydrogen Energy,* vol. 35, no. 5, pp. 2091-2103, 2010.

[105] R. Checchetto, N. Bazzanella, A. Miotello and G. Principi, "D euterium thermal desorption from FeTi thin films," *Journal of Alloys and Compounds,* Vols. 356-357, pp. 521-525, 2003.

[106] A. Izanlou and M. K. Aydinol, "An ab initio study of dissociative adsorption of H2 on FeTi surfaces," *International Journal of Hydrogen Energy,* vol. 35, pp. 1681-1692, 2010.

[107] E. Lebsanft, D. Richter and J. Topler, "Inverstigation of the hydrogen diffusion in FeTiHx by means of quasielastic neutron scattering.," *Journal of Physics F: Metal Physics.,* vol. 9, no. 6, pp. 1057-1064, 1979.

[108] T. Chen, Z. L. Wu, B. S. Cao, J. Gao and M. K. Lei, "Solid state reaction of Fe/Ti nanometer-scale mutlilayers.," *Surface and Coatings Technology,* vol. 201, pp. 5059-5062, 2007.

[109] L. Dumitrescu, M. Hillert and N. Saunders, "Comparison of Fe-Ti Assessments," *Journal of Phase Equilibria,* vol. 19, no. 5, pp. 441-448, 1998.

[110] L. Zaluski, A. Zaluska, P. Tessier, J. Strom-Olsen and R. Schulz, "Effects of relaxation

on hydrogen absorption in Fe-Ti produced by ball-milling," *Journal of alloys and Compounds,* vol. 227, pp. 53-57, 1995.

[111] B. Amirkhiz, B. Zahiri, P. Kalisvaart and D. Mitlin, "Synergy of elemental Fe and Ti promoting low temperature hydrogen sorption cycling of magnesium," *International Journal of Hydrogen Energy,* vol. 36, no. 11, pp. 6711-6722.

[112] M. Konarova, J. N. Beltramini and M. Lu, "Synthesis and hydrogen storage properties of magnesium nanoparticles with core/shell structure," in *ADVANCES IN MATERIALS DEVELOPMENT: A FESTSCHRIFT HONOURING PROFESSOR SUBRATA RAY*, vol. 736, 2013, pp. 120-126.

[113] V. Kuznetsov, "Al-H-Ti (Aluminium - Hydrogen - Titanium)," in *Light Metal Systems. Part 3 Selected Systems from Al-Fe-V to Al-Ni-Zr*, vol. 11A3, Springer Berlin Heidelberg, 2005, pp. 1-9.

[114] K. Hashi, K. Ishikawa and K. Aoki, "Hydrogen Absorption and Desorption in Ti-Al Alloys," *Metals and Materials International,* vol. 7, no. 2, pp. 175-179, 2001.

[115] J. Morales-Hernandez, J. Velazquez-Salazar, L. Garcia-Gonzalez, F. J. Espinoza-Beltran, J. D. Barceinas-Sanchez and J. Munoz-Saldana, "Structure and thermal stability of ball milled Ti–Al–H powders," *Journal of Alloys and Compounds,* vol. 388, pp. 266-273, 2005.

[116] N. V. Kazantseva, A. G. Popov, N. V. Mushnikov, A. V. Skripov, A. V. Soloninin, B. Aleksashin, V. I. Novozhenov, V. A. Sazonova and A. G. Kharisova, "Thermally Unstable Hydrides of Titanium Aluminum Ti3Al," *The Physics of Metals and*

Metallography, vol. 111, no. 4, pp. 353-360, 2011.

[117] J. Morales-Hernandez, J. Valazquez-Salazar, L. Garcıa-Gonzalez, F. J. Espinoza-Beltran, J. D. Barceinas-Sanchez and J. Munoz-Saldana, "Structure and thermal stability of ball milled Ti-Al-H powders," *Journal of Alloys and Compounds,* vol. 388, pp. 266-273, 2005.

[118] W. Lohstroh, R. J. Westerwaal, J. L. van Mechelen, C. Chacon, E. Johansson, B. Dam and R. Griessen, "Structural and optical properties of Mg2NiHx switchable mirrors upon hydrogen loading," *Physical Review B.,* no. 70, p. 165411, 2004.

[119] T. J. Richardson, J. L. Slack, R. D. Armitage, R. Kostecki and M. D. Dubin, "Switchable Mirrors based on nickel-magnesium films," *Applied Physics Letters,* vol. 78, no. 20, p. 3047, 2001.

[120] G. Irvine and S. Celik, "Thermal Comparison of Reflective and Non-Reflective Roofs with Thin-Film Solar Panels," *Green Technologies Conference 2012,* pp. 1-3, 2012.

[121] I. P. Jain, C. Lal and A. Jain, "Hydrogen Storage in Mg: A promising material," *International Journal of Hydrogen Energy,* vol. 35, no. 10, pp. 5133-5144, May 2010.

[122] M. U. Niemann, S. S. Srinivasa, A. R. Phani, A. Kumar, D. Goswami and E. K. Stefanakos, "Nanomaterials for Hydrogen Storage Applications: A Review," *Journal Of Nanomaterials,* vol. 2008, p. 950967, 2008.

[123] H. I. Karunadasa, C. J. Chang and J. R. Long, "A molecular molybdenum-oxo

catalyst for generating hydrogen from water," *Nature,* vol. 464, no. 7293, pp. 1329-1333.

[124] A. Pundt, C. Sachs, M. Winter, M. Reetz, D. Fritsch and R. Kirchheim, "Hydrogen sorption in elastically soft stabilized Pd-clusters," *Journal of Alloys and Compounds,* vol. 293, pp. 480-483, December 1999.

[125] B. H. Liu, D. M. Kim, K. Y. Lee and J. Y. Lee, "Hydrogen storage properties of TiMn2-based alloys," *Journal of Alloys and Compounds,* vol. 240, no. 1-2, pp. 214-218, 1996.

[126] X. B. Yu, B. J. Xia, Z. Wu and N. X. Xu, "Phase structure and hydrogen sorption performance of Ti-Mn-based alloys," *MATERIALS SCIENCE AND ENGINEERING A-STRUCTURAL MATERIALS PROPERTIES MICROSTRUCTURE AND PROCESSING,* vol. 373, no. 1-2, pp. 303-308, May 2004.

[127] H. Fritzsche, E. Poirier, J. Haagsma, C. Ophus, E. Luber, C. T. Harrower and D. Mitlin, "A systematic neutron reflectometry study on hydrogen absorption in thin Mg1-xALx alloy films," *Canadian Journal of Physics,* vol. 88, pp. 1-6, 2010.

[128] W. Lohstroh, R. J. Westerwaal, A. C. Lokhorst, J. L. M., B. Dam and R. Griessen, "Double layer formation in Mg-TM switchable mirrors (TM : Ni, Co, Fe)," *Journal of Alloys and Compounds,* vol. 404, pp. 490-493, 2005.

[129] F. J. den Broeder, S. J. van der Molen, M. Kremers, J. N. Nuiberts, D. G. Nagengast, A. T. Gogh, W. H. Huisman, N. J. Koeman, B. Dam, J. H. Rector, S. Plota, M. Haaksma, R. M. Hanzen, R. M. Jungblut, P. A. Duine and R. Griessen, "Visualization

of hydrogen migration in solids using switchable mirrors," *Letters to Nature,* vol. 394, pp. 656-658, 13 August 1998.

[130] P. van der Sluis, M. Ouwerkerk and P. A. Duine, "Optical switches based on magnesium lanthanide alloy hydrides," *Applied Physics Letters,* vol. 70, pp. 3356-3359, 1997.

[131] M. Slaman, B. Dam, D. M. Borsa, H. Schreuders, J. H. Rector and R. Griessen, "Fiber optic hydrogen detectors containing Mg-based metal hydrides," *Sensors and Actuators B: Chemical,* vol. 123, no. 1, pp. 538-545, 2007.

[132] M. Slaman, B. Dam, H. Schreuders and R. Griessen, "Optimization of Mg-based fiber optic hydrogen detectors by alloying the catalysts," *International journal of Hydrogen Energy,* vol. 33, pp. 1084-1089, 2008.

[133] D. Unruh, K. Pabst and G. Schaub, "Fischer−Tropsch Synfuels from Biomass: Maximizing Carbon Efficiency and Hydrocarbon Yield," *Energy Fuels,* vol. 24, no. 4, pp. 2634-2641, 2010.

[134] J. D. Eshelby, "THE DETERMINATION OF THE ELASTIC FIELD OF AN ELLIPSOIDAL INCLUSION, AND RELATED PROBLEMS," *PROCEEDINGS OF THE ROYAL SOCIETY OF LONDON SERIES A-MATHEMATICAL AND PHYSICAL SCIENCES,* vol. 241, no. 1226, pp. 376-396.

[135] J. D. Eshelby, " THE CONTINUUM THEORY OF LATTICE DEFECTS," *SOLID STATE PHYSICS-ADVANCES IN RESEARCH AND APPLICATIONS,* vol. 3, pp. 79-144, 1956.

[136] J. D. Eshelby, " ANISOTROPIC ELASTICITY WITH APPLICATIONS TO DISLOCATION THEORY," *ACTA METALLURGICA,* vol. 1, no. 3, pp. 251-259, 1953.

[137] L. Mooj and D. Bernard, "Nucleation and growth mechanisms of nano magnesium hydride from the hydrogen sorption kinetics," *Physical Chem. Chem. Phys,* vol. 15, pp. 11501-11510, 2013.